PHASES AT COMPLEX TEMPERATURE : SPIRAL CORRELATION FUNCTIONS AND REGIONS OF FISHER ZEROS FOR ISING MODELS

Felicitas Beichert

A Thesis Submitted for the Degree of PhD
at the
University of St Andrews

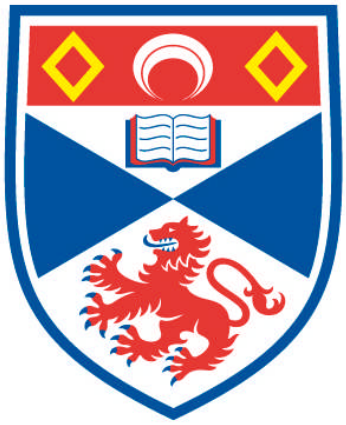

2013

PHASES AT COMPLEX TEMPERATURE: SPIRAL CORRELATION FUNCTIONS AND REGIONS OF FISHER ZEROS FOR ISING MODELS

Felicitas Beichert

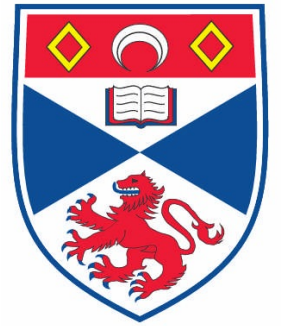

This thesis is submitted for the degree of PhD
at the
University of St Andrews

March 2013

1. Candidate's declarations:

I, Felicitas Beichert, hereby certify that this thesis, which is approximately 23 000 words in length, has been written by me, that it is the record of work carried out by me and that it has not been submitted in any previous application for a higher degree.

I was admitted as a research student in September 2009 and as a candidate for the degree of PhD in September 2009; the higher study for which this is a record was carried out in the University of St Andrews between 2009 and 2013.

Date signature of candidate

2. Supervisor's declaration:

I hereby certify that the candidate has fulfilled the conditions of the Resolution and Regulations appropriate for the degree of PhD in the University of St Andrews and that the candidate is qualified to submit this thesis in application for that degree.

Date ..... signature of supervisor

3. Permission for electronic publication: (*to be signed by both candidate and supervisor*)

In submitting this thesis to the University of St Andrews I understand that I am giving permission for it to be made available for use in accordance with the regulations of the University Library for the time being in force, subject to any copyright vested in the work not being affected thereby. I also understand that the title and the abstract will be published, and that a copy of the work may be made and supplied to any bona fide library or research worker, that my thesis will be electronically accessible for personal or research use unless exempt by award of an embargo as requested below, and that the library has the right to migrate my thesis into new electronic forms as required to ensure continued access to the thesis. I have obtained any third-party copyright permissions that may be required in order to allow such access and migration, or have requested the appropriate embargo below.

The following is an agreed request by candidate and supervisor regarding the electronic publication of this thesis:

(i) Access to printed copy and electronic publication of thesis through the University of St Andrews.

Date signature of candidate signature of supervisor

A supporting statement for a request for an embargo must be included with the submission of the draft copy of the thesis. Where part of a thesis is to be embargoed, please specify the part and the reasons.

Abstract

In this thesis we analyse the Fisher zeros for various Ising models. We show that there is long-range spiral order on the contours of zeros for classical one-dimensional Ising chains and that there is an imaginary "latent heat" associated with crossing those contours. Then we can see how areas of Fisher zeros fill in as we turn the Ising chain into Ising ladders of different widths, which seems to contradict the standard analysis presented in the literature and can be attributed to a different approach to the thermodynamic limit. Finally, we report results on frustrated two-dimensional classical Ising lattices, in particular the triangular and the kagomé lattice, and the quantum Ising problem.

Acknowledgements

I have met so many inspiring people during the course of this project, that if I thanked them all here, this thesis would vastly exceed its maximum length. That being said, there are some people who were an integral part of this project.

First of all, I could not have imagined having a better supervisor than Chris Hooley. Whenever I went into a meeting being thoroughly depressed about my work and my life as a PhD student, I would come out of it with new confidence, energy, and an abundance of new ideas and insights.

While having a great supervisor to work with is amazing, having a collaboration to work in is even better. It was inspiring to work with Roderich Moessner and Vadim Oganesyan during the course of this project and to realise what academia is all about.

I was in the lucky position to be part of the Doctoral Training Centre in Condensed Matter, which offered many new opportunities and sources of inspiration. I would like to thank EPSRC for the funding of the Centre and thank Andy Mackenzie, Christine Edwards and Julie Massey for all the hard work they put into it.

Work is important, but I need to be happy outside of my work environment in order to work well. Therefore my thanks also goes to those people who have made my PhD into a truly enjoyable experience and a happy time. For that I would in particular like to thank Jess, Kirsty, Saskia, Sebastian, Symke and Yann.

Finally, I would like to thank my family for their unconditional love and support without which I would not be who I am now.

Für Mama und Papa

Contents

Conferences and Publications

Conferences

- March Meeting of the American Physical Society (APS) in Portland, OR, USA (2010)
- Canadian Institute for Advanced Research (CIFAR) Conference and Summer School on Quantum Materials in Montreal, Canada (2010)
- Physics by the lake, Graduate Summer School in Ambleside, UK, Poster Presentation (2010)
- XV Training Course in the Physics of Strongly Correlated Systems in Vietri sul Mare, Italy (2010)
- Condensed Matter and Materials Physics (CMMP) Conference of the Institute of Physics (IOP) in Warwick, UK, Poster Presentation (2010)
- International Conference on Frustration in Condensed Matter (ICFCM), Sendai, Japan (2011)
- International Conference on Strongly Correlated Electron Systems (SCES) in Cambridge, UK, Poster Presentation (2011)
- CMMP Conference of the IOP in Manchester, UK, Oral Presentation (2011)
- APS March Meeting in Boston, MA, USA, Oral Presentation (2012)
- Workshop on Frontiers of quantum condensed matter physics: light, matter and unusual devices out of equilibrium in New York, NY, USA (2012)

Publications

- F. Beichert, C.A. Hooley, V. Oganesyan and R. Moessner,
  Correlations and phase structure of Ising models at complex temperature
  arXiv:1304.6314 (cond-mat.str-el) (2013)

List of symbols

Here is a list of the most commonly used symbols. Some symbols stand for several different entities throughout this thesis, but I have tried to minimise overlap as much as possible. It should be clear from the context which of the several meanings applies.

$\mathbf{A}$	Kasteleyn matrices in compact form for different lattice structures
a_i	coefficients of a series expansion
C	specific heat
C_j	$= \langle\langle \hat{S}_0 \hat{S}_j \rangle\rangle$; correlation function
c_i	fermion annihilation operator
d	spatial dimensionality of the system or distance from $z = 1$
D	=d+z
$\mathbf{D}$	diagonalising matrix
E	internal energy
E'	shift of the energy zero in the Migdal-Kadanoff approach
F	free energy
f	free energy density
G	Gibbs free energy
$G(r)$	cumulative distribution function of partition function zeros or correlation function
g	dimensionless coupling to a transverse field
$g(r)$	density of partition function zeros
H	external magnetic field
$\mathbf{H}$	field matrix
$\mathcal{H}$	Hamiltonian
h	$= \beta H$; reduced field
J	Ising bond strength
K	$= \beta J$
K^*	bond strength on the bonds that get introduced on L^E
k	wavenumber

L	system size and original lattice
L^E	extended lattice
L^Δ	dimer lattice
$\mathcal{L}$	Lagrangian
M	magnetisation or number of bonds that get introduced on L^E
m	$= \frac{M}{N}$
N	number of particles or length of the Ising chain/ladder
N_L	width (i.e. number of legs) of an Ising ladder
P	pressure
$P(C)$	probability of a configuration C
r	distance from the critical point or non-thermal control parameter (its critical value is labelled r_c)
r_{YL}	distance between the critical point and the edge of the distribution of partition function zeros
S	entropy or action
S_i	spin on lattice site i
$\mathbf{T}$	transfer matrix
T	temperature
T_c	critical temperature
$\mathbf{T}_H$	$= \mathbf{H}^{1/2}\mathbf{T}\mathbf{H}^{1/2}$; transfer matrix for the 1d Ising chain in a longitudinal field
t	$= \frac{T-T_c}{T_c}$; dimensionless measure for the distance to the critical point
V	volume
W	transition rate
w	$= e^{-2\beta J}$ or unsigned bond weight on a lattice
Z	partition function
z	$= \tanh K = Re^{i\theta}$ or dynamical critical exponent
α	specific heat critical exponent or mixing coefficient for subdominant eigenvalues
β	$= \frac{1}{k_B T}$ or critical exponent of the magnetisation ($t \to 0$)
$\Gamma(L)$	allowed polygon configurations on lattice L
γ	critical exponent of the susceptibility
γ_k	Bogoliubov annihilation operator

Δ	dimer generating function or critical exponent of the r_{YL}
δ	critical exponent of the magnetisation ($h \to 0$)
ϵ_k	energy spectrum of the quantum Ising model
ζ	ratio of eigenvalues of $\mathbf{T}_H$
η	order parameter or critical exponent of the correlation function
θ_n	$= \frac{\pi}{N}(2n+1)$; locations of the partition function zeros of the Ising chain on the unit circle
$\tilde{\theta}_n$	$= \frac{2\pi}{N}n$; points halfway between the zeros of the Ising chain
Λ	thermal de Broglie wavelength
$\mathbf{\Lambda}$	diagonalised transfer matrix
λ_i	i^{th} eigenvalue of the transfer matrix
μ	chemical potential
ν	correlation length critical exponent
ξ	spatial correlation length
σ_i	spin on lattice site i
τ_c	correlation time/temporal correlation length
Υ	generating function for allowed polygon configurations
ϕ	order parameter field
χ	magnetic susceptibility
ψ	angle at which a contour of partition function zeros impacts onto the real axis at the critical point
ω	allowed wavevectors due to Bloch's theorem
$\hbar\omega_q$	energy scale of quantum fluctuations

Chapter 1

Theoretical background

Everyone experiences phase transitions on a daily basis, be it boiling teawater, melting ice cubes in a glass of water or even frying an egg. Phase transitions are very common in nature and all areas of natural science. This reaches from the folding of proteins to population dynamics and from the synthesis of materials to astronomy; even the universe itself is believed to have undergone several phase transitions as it cooled down from the Big Bang. Generally at the interface of two stable phases of matter, collective behaviour becomes important. But what exactly happens to the materials when they undergo a phase transition? Is there a way that we can tailor a material so that we can control its phases of matter? [1, 2]

In order to design materials according to one's requirements, one first needs to understand the theoretical principles that control their behaviour. The difficulty when trying to formulate a theory of phase transitions is that the number of atoms involved is of the order of 10^{23} and yet they all show collective behaviour. Hence, phase transitions and their description have puzzled scientists for most of the 20th and the 21st centuries. Although a theory of classical phase transitions was established in the 1970s, there were soon found compounds with critical behaviour that did not comply with the theory. Then a new puzzle emerged: that of quantum phase transitions. Even though these transitions take place at 0K and seem like highly theoretical entities, they are believed to have a profound influence on large parts of the phase diagram of many unconventional superconductors. There is a general hope that a more profound understanding of quantum criticality and its consequences will lead to an understanding of many of the unsolved puzzles in physics today.

In this thesis we want to explore what a phase transition means if we allow one of the parameters to be complex, which is a technique originated by Lee and Yang in 1952 [3, 4]. In order to do that, we will first briefly review the theory of classical phase transitions (CPTs) in Section 1.1. In Section 1.2 we will then move on to explain an area in which there are still a lot of theoretical puzzles, but where there are very interesting experimental results: that of quantum phase transitions (QPTs). Then, we will review the fundamental theory of partition function zeros – the technique we will be using for the remainder of this thesis – in Section 1.3 and some applications in Section 1.4. Finally, we will give an overview of the following chapters

and future directions in Section 1.5.

1.1 Classical phase transitions

We distinguish between two kinds of phase transitions depending on the thermodynamic quantity in which a discontinuity occurs. Let us, for example, look at the derivatives of the Gibbs free energy [5, 6] G, where

$$dG = -S\,dT + V\,dP \quad \text{for a fluid or gas} \tag{1.1}$$

$$\text{or} \quad = -S\,dT - M\,dH \quad \text{for magnetic systems,} \tag{1.2}$$

and classify the phase transitions from there. Here S is the entropy, T is the temperature, V is the volume, P is the pressure, M is the magnetisation, and H is the external field.

1. First order transitions

   At a first order transition, there is a discontinuous jump in the first derivative of a thermodynamic potential, such as the Gibbs free energy. In general, this allows for the coexistence of two different phases. If the transition is temperature-driven, then it involves a non-zero latent heat. As an example, let us look at the liquid-gas phase transition, which can be described by (1.1). At the critical temperature, the volume (which is the first derivative of the free energy with respect to pressure, i.e. $V = \left(\frac{\partial G}{\partial P}\right)_T$) undergoes a discontinuous jump.

2. Continuous transitions

   At a continuous phase transition, a higher derivative of a thermodynamic potential is discontinuous at the critical control parameter. Usually this is a second derivative and therefore the transition is second order, but higher order transitions are possible and fall within the class of continuous transitions. At a continuous phase transition, it is not possible for two phases to coexist since the transition is accompanied by diverging length scales. As an example, let us look at the ferromagnetic phase transition in the Ising model, which can be described by (1.2). Here, the first derivative of a potential (in this example the magnetisation $M = -\left(\frac{\partial G}{\partial H}\right)_T$) changes continuously, whereas the second derivative (here the magnetic susceptibility $\chi = \left(\frac{\partial M}{\partial H}\right)_T = -\left(\frac{\partial^2 G}{\partial H^2}\right)_T$) exhibits a discontinuity at the transition point and diverges along with the correlation length.

The point at which a continuous phase transition takes place is usually called the "critical point". An example of a critical point can be seen in Fig 1.1 which shows the phase diagram of water. Since continuous phase transitions are much better understood theoretically, I will concentrate the following literature review on these transitions. Therefore I will use the term "phase transition" synonymously for continuous phase transition. In those places where I speak about first order transitions, I will indicate this explicitly.

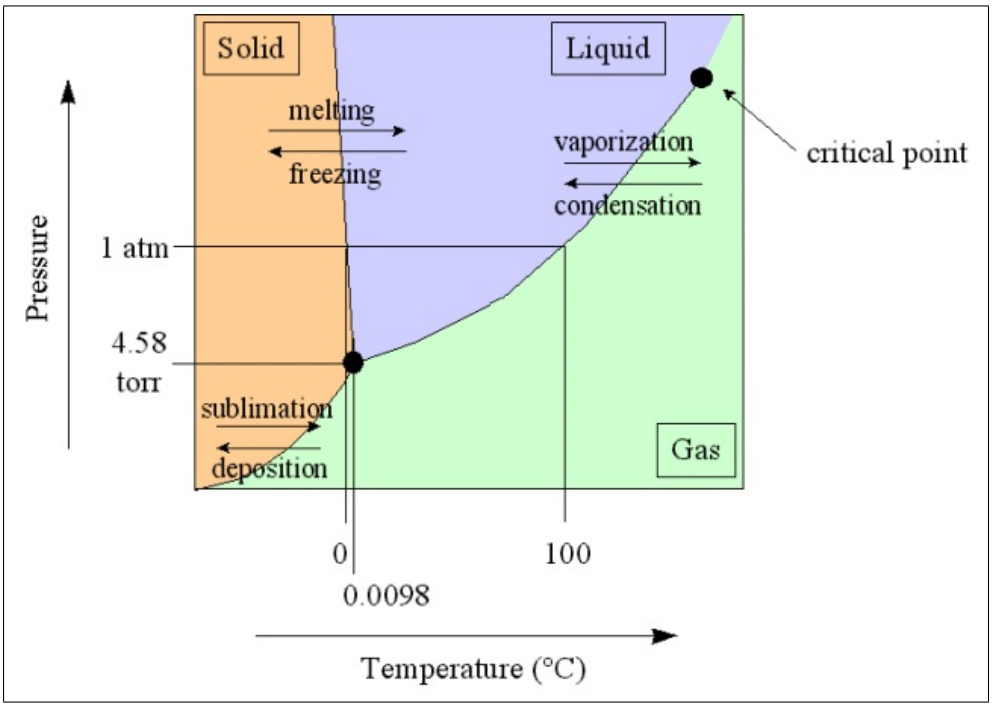

Figure 1.1: Phase diagram of water. (Figure reproduced from [7].)

The theory of continuous phase transitions is generally developed in terms of an order parameter, which is a quantity that is zero in the disordered phase and non-zero in the ordered phase. In some systems the choice of order parameter is obvious, for example for ferromagnetic phase transitions one usually chooses the magnetisation. In other cases the choice of order parameter is more difficult, for example for the Mott transition [1].

At the critical point, the correlation length ξ, which is the size of a typical ordered cluster within the sample, diverges and scales as

$$\xi(t) \sim |t|^{-\nu} \tag{1.3}$$

where t is a dimensionless measure for the distance from the critical point in terms of temperature, i.e. $t = \frac{T-T_c}{T_c}$. There are also divergences in the correlation length in terms of other tuning parameters such as pressure, external field, doping, etc. ν is called the correlation length critical exponent. A diverging correlation length essentially means that the system no longer depends on any intrinsic length scale and therefore becomes scale invariant. A set of critical exponents can completely characterise the behaviour at the phase transition independent of the microscopic properties by describing the scaling behaviour of the order parameter and its correlations depending on the distance from the critical point. The definitions of some critical exponents can be seen in Table 1.1.

These critical exponents only depend on the fundamental symmetries of the system at the critical point and on the spatial dimensionality of the system. Consequently all systems fall into

	exponent	definition	conditions
specific heat	α	$C(t) \propto \lvert t\rvert^{-\alpha}$	$t \to 0, h = 0$
magnetisation	β	$m(t) \propto \lvert t\rvert^{\beta}$	$t \to 0$ from below, $h = 0$
	δ	$m(h) \propto h^{1/\delta}$	$h \to 0, t = 0$
susceptibility	γ	$\chi(t) \propto \lvert t\rvert^{-\gamma}$	$t \to 0, h = 0$
correlation length	ν	$\xi(t) \propto \lvert t\rvert^{-\nu}$	$t \to 0, h = 0$
correlation function	η	$G(r) \propto \lvert r\rvert^{-d+2-\eta}$	$h = 0, t = 0$
dynamic	z	$\tau_c \propto \xi^z$	$h \to 0, t = 0$

Table 1.1: Table of critical exponents. [6, 8]

so-called universality classes depending on their fundamental symmetries. All the systems in a given universality class exhibit the same behaviour at criticality. For example the exponents of the liquid-gas transition are independent of the chemical composition of the fluid. Moreover, it has the same exponents as the ferromagnetic transition in uniaxial magnets. Consequently all these transitions lie in the same universality class.

The critical exponents are not all independent of each other. Instead they are related through the four scaling relations given below

$$\nu d = 2 - \alpha, \tag{1.4}$$
$$2\beta + \gamma = 2 - \alpha, \tag{1.5}$$
$$\beta\,(\delta - 1) = \gamma, \tag{1.6}$$
$$\nu\,(2 - \eta) = \gamma. \tag{1.7}$$

The theory of phase transitions is well-developed for classical phase transitions. Starting with approaches from Landau theory up to the Landau-Ginzburg-Wilson theory, there are many routes one can take to calculate the properties of a phase transition in a classical system, often with very well-fitting results. However, when quantum fluctuations are involved, the theoretical approach gets more complicated since we have to solve for the statics and the dynamics simultaneously. We will give a short introduction into the current state of the theory of quantum phase transitions in Section 1.2.

1.1.1 Landau theory

The first attempt at a general theory of second order phase transitions was done by Landau in 1937 [9]. He assumed that the free energy f of a system can be written as a series expansion in

terms of the order parameter η (i.e. that f is analytic) and that it obeys the symmetry of the Hamiltonian. Hence the Landau free energy would be of the form

$$f(T,\eta) = f_0 + a_2(T)\eta^2 + a_4(T)\eta^4 + \text{higher order terms.} \tag{1.8}$$

Here $a_2(T)$ is chosen such that f is minimised only for $\eta = 0$ as $T \geqslant T_c$ and for $|\eta| > 0$ as $T < T_c$. $a_4(T)$ always needs to be positive in order to ensure stability. If the order parameter is magnetic, this expansion of the free energy cannot include odd-order terms due to symmetry under time reversal (this can change if an external field is applied which changes the symmetry) [10].

As an example, let us look at the free energy of the Ising model which is of the form

$$f = tm^2 + um^4 - hm \tag{1.9}$$

with m (the magnetisation) being the order parameter, $t = \frac{T}{T-T_c}$ being the reduced temperature, and $h = \beta H$ being the external magnetic field. A plot of the free energy can be seen in Fig 1.2.

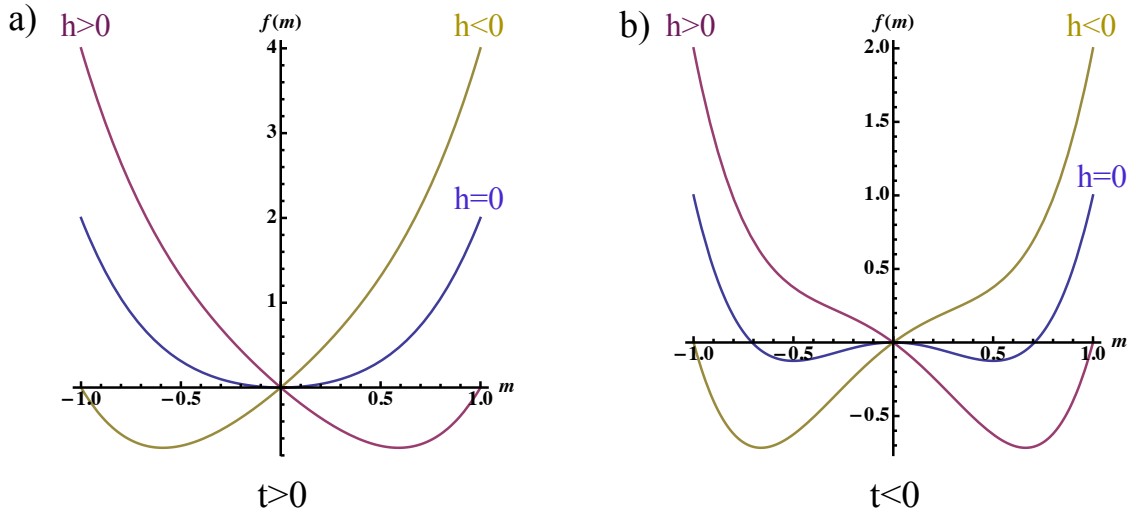

Figure 1.2: Diagram of the mean-field Landau free energy [11].

Here the behaviour needs to be described for two separate cases:

1. for $t > 0$ the quartic term can be ignored for small m and the free energy has a minimum at $\frac{h}{2t}$.

2. for $t < 0$, the quartic term cannot be ignored for stability reasons and the free energy has two degenerate minima. For an external field $h \neq 0$, the symmetry of the free energy is

broken and one minimum has a lower free energy than the other minimum and will be preferred by the system [11].

From this form of the free energy we can calculate the critical exponents of the system and determine the scaling behaviour.

Landau theory is effectively a mean-field theory that does not allow for fluctuations. To incorporate these, this theory was further developed and expanded together with Vitaly Ginzburg and Kenneth Wilson. For Ginzburg-Landau theory the free energy density[1], for instance for a magnetic order parameter, takes the form:

$$f = tm^2 + um^4 - hm + s\left(\nabla m\right)^2, \tag{1.10}$$

where the gradient terms encode the fluctuations of the order parameter. Note here that these fluctuations are purely spatial. Since the system is in equilibrium there is no time associated with it. By allowing fluctuations of the order parameter, one essentially introduces an upper and a lower critical dimension for the system. Below the lower critical dimension the fluctuations are so strong that no long-range order can emerge. Above the upper critical dimension Landau theory is valid and the system behaves in a mean-field like way. Between the upper and the lower critical dimension, the scaling exponents are not mean-field like and the scaling becomes nontrivial [11]. Similarly to Landau theory the free energy of the system has to be guessed on the basis of symmetry arguments or found via a renormalisation group approach, which is a powerful technique introduced by Wilson in 1971 [12].

1.1.2 Renormalisation group

The renormalisation group approach removes degrees of freedom by changing the lengthscale of the system. The properties of the system will only remain unaltered at the fixed points of the transformation, one of which is the critical point [13].

Basically this means that the approach tries to coarse grain the system into larger and larger slabs of the material. The aim of this is to gradually eliminate all microscopic degrees of freedom the length scales of which are smaller than the correlation length ξ. Once the system has been coarse-grained, all length scales have to be changed by the graining factor. Afterwards the relative size of the fluctuations needs to be renormalised. According to Kadanoff the new system is statistically similar to the old system. In particular, critical points are preserved when renormalised since they are fixed points of the rescaling due to the infinite correlation length. If the system is not close to criticality however, the renormalisation takes it further away from criticality because the renormalised correlation length will be smaller [14].

After having obtained the fixed points of the renormalisation scheme, one needs to find out which fixed points are stable or unstable. From there it is possible to draw a flow diagram and

[1] In order to obtain the free energy, we would have to take the integral of the free energy density over the sample.

to obtain the critical exponents.

An example of the procedure is the Migdal-Kadanoff transformation [15], which can be applied to the two-dimensional Ising model. The Migdal-Kadanoff approach is not exact, but it is a simple transformation that preserves the topology of the lattice. In the following analysis, let us call the spin on the nth site of the mth row $S_{m,n}$.

The different steps of the transformation are shown in Figure 1.3. The first step in the transformation is to move half of the bonds of the lattice (shown in green in panel a)) so that the remaining bonds have double the strength (see panel b)). This means that a quarter of the sites (shown in red in panel b)) are no longer attached to any bonds and consequently do not contribute to the partition function. Hence we can disregard them.

The next step is to integrate out, i.e. explicitly do the sum over, every second site. The sites that are integrated out are shown in purple in panel c) of Figure 1.3. Let us look for example at doing the explicit sum over $S_{1,2}$, which has bonds with $S_{1,1}$ and $S_{1,3}$. This results in

$$\sum_{S_{1,2}=\pm 1} e^{2KS_{1,1}S_{1,2}} e^{2KS_{1,2}S_{1,3}} = e^{2KS_{1,1}} e^{2KS_{1,3}} + e^{-2KS_{1,1}} e^{-2KS_{1,3}} \tag{1.11}$$

$$= 2\cosh\left(2K\left(S_{1,1}+S_{1,3}\right)\right), \tag{1.12}$$

where $K = \beta J$ as usual. For the renormalisation to work this has to obey

$$2\cosh\left(2K\left(S_{1,1}+S_{1,3}\right)\right) \equiv e^{K'S_{1,1}S_{1,3}-\beta E'}. \tag{1.13}$$

where E' is a physically unimportant shift of the energy zero. Introducing this energy offset to the Hamiltonian is necessary to allow for a general solution to equation (1.13).

Since the spins are only allowed two different states each, (1.13) only has to be satisfied for $S_{1,1} = S_{1,3}$ and $S_{1,1} = -S_{1,3}$. Let us look at these cases separately:

$$S_{1,1} = S_{1,3} : \qquad 2\cosh(4K) = e^{K'} e^{-\beta E'} \tag{1.14}$$

$$S_{1,1} = -S_{1,3} : \qquad 2 = e^{-K'} e^{-\beta E'}. \tag{1.15}$$

Dividing the two gives

$$\cosh(4K) = e^{2K'}, \tag{1.16}$$

which is called the "flow equation" (or "renormalisation group equation"). (1.16) can also be written as

$$x' = \frac{2x^2}{1+x^4}, \tag{1.17}$$

where $x \equiv e^{-2K}$ and $x' \equiv e^{-2K'}$. We are choosing to use this representation rather than using $x = e^{2K}$ so that the fixed points are all lying in a finite interval rather than at infinity. The physical fixed points of this equation, i.e. where $x' = x$ for real values of x, are those points at

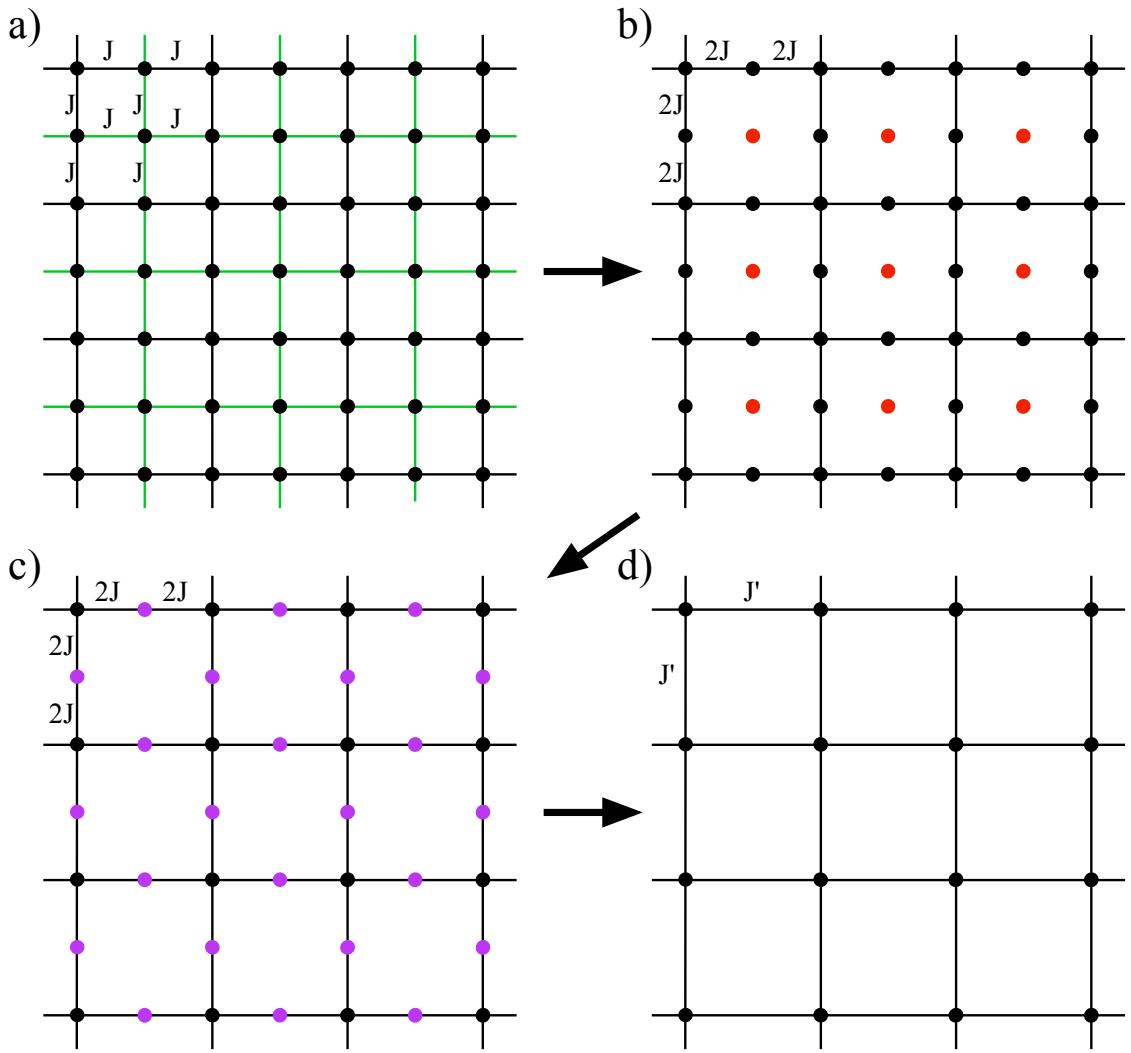

Figure 1.3: The original square lattice with bond strength J is given in panel a). The green bonds correspond to those bonds that get moved. Panel b) shows the "new" square lattice with double the bond strength on the bonds that remain. The red lattice points can now be deleted since they are no longer attached to any bonds. Panel c) shows the lattice sites that can be integrated out in purple, which leads to the renormalised lattice in panel d) [15].

which the system is invariant under a scale change. They lie at $x = 1$, $x = 0$ and $x \approx 0.54369$. The critical point corresponds to the fixed point $x \approx 0.54369$, which is the only nontrivial fixed point. This leads to a critical temperature of $K \approx 0.30469$, which is an approximation of the exact transition temperature $K \to 0.44069$.

1.2 Quantum criticality

How do quantum critical points (QCPs) differ from classical phase transitions (CPTs)? First, it should be mentioned, that QCPs are always second order transitions with diverging correlation lengths, which corresponds to a specific case of a continuous phase transition. The essential feature of QCPs is that they take place at zero temperature. The temperature of the system is not changed to make it undergo a transition, but some non-thermal control parameter such as pressure, doping or applied field is used. Sometimes even the coupling parameter in the Hamiltonian is taken as a "control parameter", even though it is only experimentally accessible by varying a physical parameter, such as indirectly controlling the hopping parameter by applying pressure [16]. One can generally approach the QCP either by keeping the temperature T constant and varying the non-thermal control parameter r or by varying T and keeping the r constant. Approaching the critical point from the different directions can give different scaling behaviour. Generally one can say that an approach via the non-thermal control parameter leads to a diverging spatial correlation length, while the temporal correlation length is already infinite, whereas doing so via temperature reduction leads to the temporal and the spatial correlation length diverging together with

$$\tau_c \sim \xi^z, \tag{1.18}$$

where z is the so-called dynamical critical exponent, τ_c is the correlation time/temporal correlation length and ξ is the spatial correlation length. It turns out that for QCPs the scaling exponents are more conveniently defined in terms of thermodynamic ratios such as the Grüneisen ratio which is defined as the ratio of thermal expansion to specific heat [17]. The reason behind this is that the Grüneisen ratio does not contain the effects of the third law of thermodynamics, which hide the effects of the QCP when we are only looking at one thermodynamic quantity.

Even though all finite temperature transitions are denoted as "classical", this does not mean that quantum effects are generally unimportant for these transitions. Hence transitions in systems such as superfluid helium or superconductors would be considered classically even though the system is highly quantum mechanical. The mechanisms involved to stabilise the phases are unimportant for the classification of quantum and classical phase transitions. The only factor taken into consideration is whether the instability is due to thermal or quantum fluctuations. At all finite (i.e. non-zero) temperatures thermal fluctuations are present. These cannot destroy long-range order for QCPs at zero temperature.

In general, quantum fluctuations are important as long as their typical energy scale is larger than the typical energy scale of thermal fluctuations, i.e. $\hbar\omega_q \geqslant k_B T$. Quantum mechanics

will be unimportant for any transition at some finite transition temperature T_c such that $|t| < T_c^{\frac{1}{\nu z}}$, i.e. asymptotically close to the transition the behaviour will be entirely classical [18]. Therefore all finite temperature transitions classify as CPTs. The macroscopic scales are entirely dominated by classical thermal fluctuations. This is shown in Fig 1.4 b) as the classical critical region. In this region the Ginzburg-Landau theory of criticality applies. All transitions at zero temperature however classify as QCPs. Even though the regions close to the phase transition at finite temperature are entirely classical, there are still large parts of the phase diagram that are affected by quantum fluctuations. One can roughly distinguish between three different regions (see Fig 1.4 a)):

1. The thermally disordered region. In this region order is destroyed by thermal fluctuations.
2. The quantum disordered region in which order is generally destroyed by quantum fluctuations.
3. The quantum critical region which lies between regions 1 and 2. The thermal as well as the quantum fluctuations are important and the system "looks" critical with respect to the parameter r but cannot establish long range order, because order is destroyed by the thermal fluctuations. The boundaries of this region are determined by the condition $k_B T > \hbar\omega_c \propto |r - r_c|^{\nu z}$. [1]

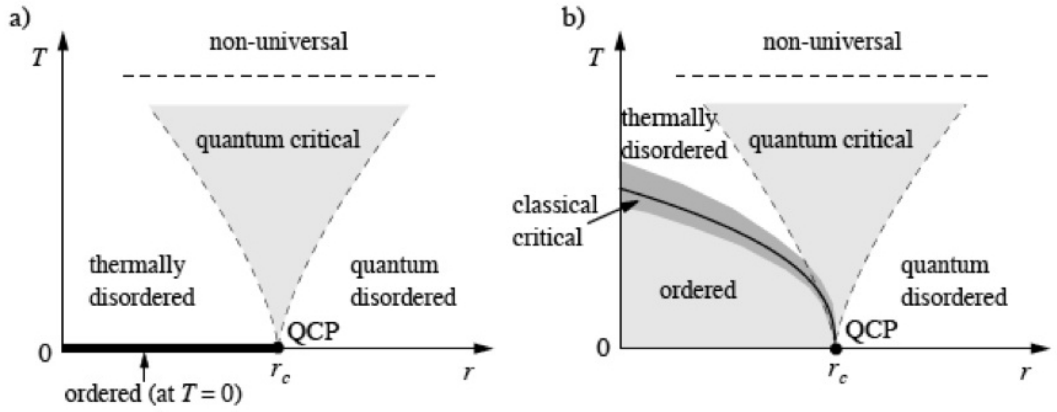

Figure 1.4: Two phase diagrams with the control parameters being temperature and a non-thermal paramter r. a) Phase diagram of a system that can only be in the ordered state at $T = 0$. b) Phase diagram of a system that has an ordered state at finite temperature. (Figure reproduced from [1].)

If long-range order is possible at finite temperature then two more regions are possible: the ordered region and the classical critical region shown above. A typical phase diagram can be seen in Fig 1.4 b). This phase diagram would also have a "classical critical region" in which we can describe the phase transition by Ginzburg-Landau theory.

The difficulty that comes in for a theoretical model of QCPs is that in a quantum mechanical system, the static and the dynamic parts of the Hamiltonian do not commute. To illustrate this point, let us first look at the classical case in which the potential and kinetic energy terms of the Hamitonian $\mathcal{H}$ commute. Therefore the partition function,

$$Z = \mathrm{Tr}\left(e^{-\beta\mathcal{H}}\right) \tag{1.19}$$

can be factorised into a kinetic and a potential energy part. This means that the static and the dynamic behaviour of the system decouple and can be solved for independently. As a result, the dynamic critical exponent z is completely independent of the static critical exponents. In contrast, for quantum partition functions one needs to explicitly take the trace over all states, since the kinetic and the potential energy part cannot be factorised in the partition function. As a consequence, the dynamical critical exponent z is no longer independent of the static exponents since the correlation time τ_c diverges together with the correlation length ξ. The divergences are related by

$$\tau_c \sim \xi^z \sim |t|^{-\nu z}. \tag{1.20}$$

From a theoretical standpoint there is work by Chakravarty, Halperin and Nelson [19] (for QCPs in insulators) and by Hertz and Millis [18, 20] (for QCPs in metals) which indicates that there exists a quantum-classical mapping according to which a QCP of d spatial dimensions corresponds to a CPT of dimension $D = d + z$. Consequently a lot of the classical results are still applicable to QCPs, for example that they would still show mean-field like critical exponents above an upper critical dimension (above which fluctuations can be neglected). This is in itself a remarkable result. It corresponds to a kind of "relativity for criticality", as one can still apply the classical results as long as one uses the dimensions of space and time together [21]. The difference is that for relativity, time only ever corresponds to one extra dimension, whereas for quantum critical points, z can have values other than one. The way the mapping works is that we write down a field theory for the action S such that

$$S = \int_0^\beta d\tau \int_{-\infty}^{\infty} d^d x \, \mathcal{L}\left[\phi\right], \tag{1.21}$$

where ϕ is the order parameter field and $\mathcal{L}$ is the Lagrangian. The τ-integral vanishes in the classical limit $\beta \to 0$ and enters the action in a similar way to the spatial integral in the quantum limit $\beta \to \infty$ such that the action of a quantum problem looks like the $d+1$ version of the action of a classical problem. The exact value of z depends on the way that the time variable enters the Lagrangian of the problem. Examples are the antiferromagnetic transition for which $z = 1$ and the liquid gas transition for which $z = 2$ [18].

There are, however, some problems with this approach, in particular when it comes to quantum criticality in metals. It has been shown [22, 23, 24, 25], that one of the underlying assumptions of Hertz-Millis theory, namely that several thermodynamic quantities such as the

specific heat and the static spin susceptibility are analytic in the order parameter, is not true for subleading terms. In addition, the theory shows signs of not being internally consistent and has been shown to make false predictions for several materials. Unfortunately, some of the most interresting puzzles in contemporary condensed matter physics are thought to arise from QCPs in metals. Some of these problems include rare-earth magnetic insulators [26, 27], heavy-fermion compounds [28, 29, 30], high temperature superconductors [31], and two-dimensional electron gases [32]. Consequently the question is, and has been for at least 15 years, whether the theory itself is still rescuable and can be altered to overcome these difficulties, or whether it needs to be completely abandoned.

It is therefore desirable to attempt an independent approach to the problem of quantum criticality, for instance an analysis of the partition function zeros for a model with a QCP. We begin this project in Chapter 5.

1.3 Partition function zeros

1.3.1 Lee-Yang theory

When we are talking about phase transitions, we are, as we have seen above, always talking about divergences in some derivative of the free energy. If we consider the free energy as the logarithm of the partition function, those divergences translate into zeros of the N-particle partition function Z_N. In fact, if the partition function is an entire function of some parameter, the zeros are the only analytic feature needed to fully determine the analytic structure of all thermodynamic quantities in the $N \to \infty$ limit.

It was first pointed out by Lee and Yang in 1952 [3, 4] that the zeros of the partition function in complex parameter space are intimately connected to the occurrence of phase transitions. Lee and Yang specifically looked at a fluid of classical particles with hardcore repulsion in a lattice approximation. From this they calculated the zeros of the partition function of this model in the fugacity plane, which they defined as

$$z = \Lambda^{-d} e^{-\frac{\mu}{k_B T}}. \tag{1.22}$$

Here, d is the dimensionality of the system, μ is the chemical potential and Λ is the thermal de Broglie wavelength defined as

$$\Lambda = \frac{\hbar}{(2mk_BT)^{1/2}}. \tag{1.23}$$

All physically accessible values of z are real and positive. Lee and Yang could prove that looking at the partition function at complex values of z in the vicinity of the real axis can give information about phase transitions taking place. We can differentiate between two possibilities:

- There are no zeros of the partition function in the complex neighbourhood of a real value of z. This causes all thermodynamic functions to be analytic for all physical values of this

z. Consequently it is not possible for a phase transition to occur.

- The zeros accumulate around a physical value of z in the thermodynamic limit and get infinitely close to the real axis. This means that nonanalyticities in thermodynamic quantities may occur which cause a phase transition to take place at the physical value of z around which the zeros accumulate.

Lee and Yang then proceeded to show that the results from the lattice gas are equivalent to a spin-$\frac{1}{2}$ Ising model [4]. The standard argument to extend the lattice gas results to general magnetic systems goes as follows [33]:

Imagine a system of N spins in which the temperature is fixed to some constant value. Then suppose that the partition function $Z_N(T, H)$ is an analytic function of a reduced field $h = \beta H = h' + ih''$ around some neighbourhood of the real h axis. As mentioned above, the zeros then are the only analytic feature of $Z_N(T, H)$ which fully determine the analytic behaviour of the thermodynamic quantities.

- For spin models in which the spin length is allowed to be arbitrarily large, $Z_N(T, H)$ is analytic around some neighbourhood of the real h axis if the integral defining $Z_N(T, H)$ uniformly converges for all h in the given neighbourhood.

- For spin models in which the magnitude of the spins is bounded, this is true if $Z_N(T, H)$ is an entire function of h provided that the Hamiltonian of the system is bounded from below.

Applying these results to any sample model means that if it is shown that there exists some region of complex h including the real axis which does not contain any zeros of $Z_N(T, H)$, then no phase transition can occur in that region. This restricts the values of a parameter h (or T) for which phase transitions may occur.

Examples of this are finite-size Ising models (see section 2) for which there is always a finite region around the real axis that is devoid of partition function zeros. Hence, there is always a finite gap between the real axis and the zero closest to it and the free energy is analytic around any physical values of h and T and no phase transition may occur.

Lee and Yang then went on to prove that all zeros of the lattice gas model with hard core repulsions lie on the unit circle in the complex fugacity plane. They then proceeded to show that the lattice gas model is equivalent to the Ising model. In the case of the Ising model, the zeros of the partition function are analysed in the complex "activity" plane rather than the complex fugacity plane, where the activity is defined as $z = e^{-2\beta H}$ with H being the applied magnetic field. The corresponding theorem is usually referred to as the "Lee-Yang circle theorem" in the literature. In the complex magnetic field plane, this means that all zeros lie on the imaginary field axis. Consequently there can only be a phase transition at zero real field for any given temperature.

The Lee-Yang theory has been significantly extended in the following decades. One of the first extensions, which has opened up new areas, was the work by Fisher [34] showing that the

results can also be applied to complex temperature. Historically the partition function zeros in the complex activity/magnetic field plane have therefore been called "Lee-Yang zeros" and zeros in the complex temperature/β plane have been called "Fisher zeros". The work in this thesis has been mainly focused around Fisher zeros and we will therefore not go into too much detail reviewing the work done on Lee-Yang zeros.

The literature following the original papers of Lee and Yang can be divided into several areas:

1. Work which tries to relax the conditions on the original Lee-Yang theorem while keeping the result that all zeros lie on the imaginary h axis. Examples of this are extensions to higher spin models [35, 36, 37, 38, 39] or the inclusion of many-spin interactions [40, 41, 42].

2. Finding the zeros or regions of the complex plane that are free of zeros for more general Ising models or other types of models. These models include the Potts model [43, 44], the Blume-Capel model [45, 44], n-vector models [46], and field theoretical models [47].

3. Further analysis of partition function zeros and their densities in order to obtain more information about the physical phase transition. We will review these results in sections 1.3.2 and 1.3.3.

4. An extension of the partition function analysis to nonequilibrium systems and quantum quenched systems. An overview of this is given in section 1.4.

The above literature mainly focuses on line contours of zeros. It has been established fairly early on that lines of partition function zeros are the most "natural" way for zeros to arise. The arguments for the focus on line densities have been summarised by Grossmann [48]. According to Grossmann, there are two main reasons for the focus on line distributions and densities of zeros:

- There are not enough zeros, even in the thermodynamic limit, to fill an unbounded two-dimensional area up to infinity.

- A one dimensional line or system of arcs on which the zeros of the partition function lie are sufficient for the descriptions of the temperature dependence of the system by a power law and we can deduce all physical quantities of the phase transition by studying the impact angles onto the real axis and the density of the zeros on the line around the point where it crosses the real axis. Consequently a two-dimensional distribution of zeros would contain more information than necessary to describe the equilibrium thermodynamics, i.e. the physics on the real-T line.

However, as we will show in Chapter 3, we have results which show that two-dimensional distributions occur even in the isotropic Ising model as we approach the thermodynamic limit.

1.3.2 Order and strength of the transition

The order of the phase transition is intimately connected to the analytic behaviour of the free energy. Since

$$-\beta F = \log Z_N, \tag{1.24}$$

we know that it is a holomorphic function of T and H except at the zeros of Z_N due to a theorem by Kneser and Lelong [48]. Therefore βF is a piecewise holomorphic function in which each region of holomorphy corresponds to a "phase" of the system. These different "phases" are thought to be separated by the lines of partition function zeros. In chapters 2 to 4 we will explore further what these complex "phases" mean in terms of physical order of the system. We will further argue, that in the case of the two-dimensional Ising model, the complex ordered "phase" fills in with partition function zeros as the thermodynamic limit is approached.

The information about the order of the phase transition must be completely contained in the behaviour of the partition function zeros since there is a way of taking the thermodynamic limit in which the free energy behaves analytically everywhere else in the complex plane. Let us, for the moment, only review the literature and consider only lines of partition function zeros. In that case, any information about the order of the phase transition must be contained in the behaviour of the lines close to the real axis, i.e. in their angle of impact onto the real axis ψ and the density of zeros near the critical point. The following results were originally derived for Lee-Yang zeros in the complex fugacity plane, but can just as well be applied to the zeros of any other complex parameter.

Let us call the density $g(r)$, where r is the distance from the critical point. Following the analysis by Abe [49, 50, 51, 52, 53], let us assume that the zeros in the complex fugacity plane lie on a line for large enough L and can be parametrized by

$$z = z_c + re^{i\psi}, \tag{1.25}$$

where ψ is the angle of impact onto the real axis. The definition of the angle ψ is shown in figure 1.5.

The zeros are then located at the points

$$z_j = z_c + r_j e^{i\psi} \tag{1.26}$$

and their density for a finite system of size L can be written as

$$g_L(r) = L^{-d} \sum_j \delta\left(r - r_j(L)\right). \tag{1.27}$$

Similarly, we can define a cumulative distribution function [53]

$$G_L(r) = \int_0^r g_L(s) ds. \tag{1.28}$$

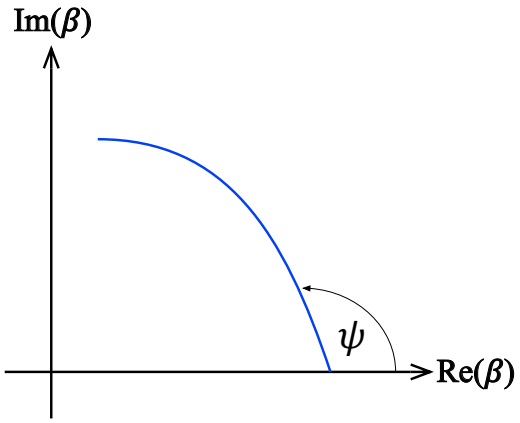

Figure 1.5: Definition of the angle ψ as the impact angle onto the real line. In the figure, the blue line represents an example of a contour of zeros close to the real line [48]

.

For a finite size system this is a sum of step functions with

$$G_L(r) = \frac{j}{L^d} \qquad \text{if} \quad r \in (r_j, r_{j+1})\,. \tag{1.29}$$

At the zeros, we assume that the cumulative density is given by the average [53, 3, 4, 54]

$$G_L(r_j) = \frac{2j-1}{2L^d}. \tag{1.30}$$

It was already shown by Lee and Yang [3, 4] that the density of zeros at the critical point has to be non-zero for a first order transition. For an infinite system the density can then be written as

$$g_\infty(r) = g_\infty(0) + ar^b + \ldots. \tag{1.31}$$

Additionally it was shown by Grossmann [48] that for a first order transition the contour of zeros has to cross the critical point perpendicular to the real axis such that $\psi \equiv \frac{\pi}{2}$.

At a second order phase transition, $g_\infty(0) = 0$ and $b = 1 - \alpha$ in order to ensure the leading critical behaviour of the specific heat to have $C \sim t^{-\alpha}$ (see [49, 50, 51, 52, 55, 56, 57]). At this point, it should be pointed out that the special case of $\alpha = 0$ corresponds to a first order transition for which the density is directly proportional to the latent heat. The corresponding cumulative distribution for a second order transition is then

$$G_\infty(r) \propto r^{2-\alpha} \tag{1.32}$$

The critical exponents of higher order transitions relate to the scaling of the density and the

impact angle of the contour as

$$\alpha = 1 - b \tag{1.33}$$

$$\gamma = \tan\left(\psi - \frac{\pi}{2}\right). \tag{1.34}$$

In addition, one can use finite-size scaling of the lowest temperature zero to extract ν [58] since the imaginary part of the lowest zero scales with lattice extent as

$$\Im(z_j) \sim L^{-1/\nu}. \tag{1.35}$$

1.3.3 Scaling relations

We have seen in the previous subsection that the location and density of the partition function zeros in the complex plane can reliably tell us the location, the order, and the strength of a phase transition. Additionally, it is possible to rederive the scaling relations (1.4)-(1.7) as well as a second set of scaling relations that connect logarithmic corrections to critical exponents [8, 59].

Let us define the exponents that characterise logarithmic corrections to the scaling of the thermodynamic quantities shown in Table 1.1 as well as the exponents for the scaling of r_{YL}, which is the distance between the critical point and the edge of the distribution of Yang-Lee zeros:

$$\text{specific heat} \quad C_\infty(t) \sim |t|^{-\alpha} |\ln|t||^{\hat{\alpha}} \tag{1.36}$$

$$\text{magnetisation} \quad m_\infty(t) \sim |t|^{\beta} |\ln|t||^{\hat{\beta}} \quad \text{for } t < 0 \tag{1.37}$$

$$m_\infty(h) \sim |h|^{1/\delta} |\ln|h||^{\hat{\delta}} \quad \text{for } t = 0 \tag{1.38}$$

$$\text{susceptibility} \quad \chi_\infty(t) \sim |t|^{-\gamma} |\ln|t||^{\hat{\gamma}} \tag{1.39}$$

$$\text{correlation length} \quad \xi_\infty(t) \sim |t|^{-\nu} |\ln|t||^{\hat{\nu}} \tag{1.40}$$

$$\text{Yang-Lee edge} \quad r_{YL}(t) \sim |t|^{\Delta} |\ln|t||^{\hat{\Delta}} \quad \text{for } t > 0. \tag{1.41}$$

The critical exponent of r_{YL} is related to the remaining critical exponents via [8]

$$\Delta = \frac{\delta\gamma}{\delta - 1} = \delta\beta = \beta + \gamma. \tag{1.42}$$

Kenna, Johnston and Janke [8, 59] from there derived the thermodynamic limit of the free energy as

$$f_\infty(t, h) = 2\Re\left(\int_{r_{YL}}^{R} \ln[h - h(r,t)] g_\infty(r,t) dr\right), \tag{1.43}$$

where the $g_\infty(r,t)$ is the density of partition function zeros at the position $h(r,t) = r\exp[i\phi(r,t)]$ and R is some cutoff. Under the assumptions that the small-t critical behaviour is dominated by

the zeros closest to the critical point and that the position of the zeros $\phi(r,t)$ can be approximated by a constant ϕ, Kenna, Johnston and Janke proceed to derive the following scaling relations for the logarithmic corrections:

$$\hat{\Delta} = \hat{\beta} - \hat{\gamma}, \tag{1.44}$$

$$\hat{\beta}(\delta - 1) = \delta\hat{\delta} - \hat{\gamma}, \tag{1.45}$$

$$\hat{\alpha} = 2\hat{\beta} - \hat{\gamma}, \qquad \text{and} \tag{1.46}$$

$$\hat{q} = \hat{\nu} + \frac{\nu\hat{\alpha}}{2 - \alpha}. \tag{1.47}$$

In the last scaling relation $\hat{q}$ is related to the correlation length $\xi_L(0)$ of a finite system at $t = 0$ via

$$\xi_L(0) \sim L(\ln L)^{\hat{q}}. \tag{1.48}$$

Their derivation applies the Widom scaling ansatz to the free energy in (1.43) and uses appropriate derivatives and substitutions to rederive both the normal scaling equations (1.4) to (1.7) and those for logarithmic corrections. Apart from (1.47), the scaling relations can be derived via conventional methods.

As an example, let us look at the derivation of (1.42) and (1.44). By differentiating (1.43) twice with respect to h and then setting $h = 0$ and substituting $r = xr_{YL}(t)$, we can obtain the magnetic susceptibility

$$\chi_\infty(t) = -\frac{2\cos(2\phi)}{r_{YL}(t)} \int_1^{R/r_{YL}(t)} \frac{g_\infty(xr_{YL}, t)}{x^2} dx \tag{1.49}$$

from which we can in turn derive an expression for the density of zeros by expanding about $r_{YL}(t)/R = 0$ up to additive corrections, such that

$$g_\infty(r,t) = \chi(t) r_{YL}(t) \Phi\left(\frac{r}{r_{YL}}\right), \tag{1.50}$$

where Φ is an undetermined function. Similarly, we can find

$$m_\infty(t,h) = \xi_\infty(t) r_{YL}(t) \Psi_\phi\left(\frac{h}{r_{YL}(t)}\right), \tag{1.51}$$

where

$$\Psi_\phi\left(\frac{h}{r_{YL}(t)}\right) = 2\Re\left(\int_1^\infty \frac{\Phi(x)}{h/r_{YL}(t) - xe^{i\phi}} dx\right). \tag{1.52}$$

Letting $h \to 0$ and inserting the expressions (1.39) and (1.41) into (1.51) gives

$$m_\infty(t) \sim |t|^{\Delta - \gamma} |\ln|t||^{\hat{\gamma} + \hat{\delta}}. \tag{1.53}$$

When we compare this to (1.37), we obtain the scaling relations (1.42) and (1.44).

1.4 Nonequilibrium transitions and partition function zeros

True equilibrium is an idealised concept that never fully applies in nature. However, most systems, especially those without an external driving force, can still be characterised rather well by equilibrium statistical mechanics. For the description of other systems, such as glasses, we require a different approach, specific to nonequilibrium systems. Since one cannot calculate a partition function for nonequilibrium systems in terms of thermodynamic state variables, it seems as if the method of analysing partition function zeros does not apply here. However, it has been shown that there is still some relevance for nonequilibrium steady states as well as for quantum quenches.

1.4.1 Nonequilibrium steady states

Nonequilibrium steady states are those that allow for a flow of for example mass or energy. Hence it leads to a circulation of probability within the space of microscopic configurations. It has been shown [60] that such systems can exhibit phase transitions. After having looked at Lee-Yang theory, one may wonder whether there is a normalisation quantity in systems that carry nonequilibrium steady states, like the partition function in equilibrium systems, to which the Lee-Yang analysis can still be applied.

Blythe and Evans [61, 62, 63, 60] found such a quantity. They define a quantity Z, which is the sum over all un-normalised steady state weights. These correspond to the un-normalised probabilities of the different configurations C. Hence, let us write

$$Z = \sum_C f(C). \tag{1.54}$$

The normalised probability for each configuration is then

$$P(C) = \frac{f(C)}{Z}. \tag{1.55}$$

For a nonequilibrium steady state system, the steady state weights are implied by the transition rates between the configurations $W(C \to C')$, which have the requirement that the total inflow into each state must equal the total outflow away from each state. This normalisation can then be treated as a nonequilibrium "partition function". As in the case of Lee-Yang or Fisher zeros, the zeros accumulate around the real axis if a phase transition occurs. Therefore they show the location of the critical point.

With the example of an asymmetric simple exclusion process, which exhibits a nonequilibrium phase transition, they showed that a first-order transition is characterised by a nonzero density of zeros of Z at the critical point, whereas for a second-order transition, the density of zeros decays as a power law. This corresponds to the behaviour of the partition function zeros in equilibrium models mentioned in section 1.3.2. This procedure has been used to study other systems, such as dynamics in the East model [64].

1.4.2 Quantum quenches

A second case has caused a lot of interest in the last decade or so [65], which is that of a system which undergoes a quantum quench, i.e. in which one parameter of the Hamiltonian is discontinuously changed so that the system is pushed out of equilibrium. This means that the system is usually prepared in the ground state of the Hamiltonian and then one of the parameters of the Hamiltonian is changed discontinuously. The time evolution is then driven by the fact that the eigenstates before the quench are not the same as those after the quench and the initial state of the system is now a non-thermal superposition of the eigenstates of the Hamiltonian after the quench. The interest in quantum quenches originates in experimental work on cold atomic gas systems, such as the work by Greiner *et al.* in 2002 [66, 67]. These systems can be modelled as isolated quantum systems which display dynamics and nonequilibrium behaviour. In particular those quenches that make the system cross a quantum critical point are of interest.

In a recent paper by Heyl, Polkovnikov and Kehrein [68], it has been shown that for some systems that undergo a quantum quench, with the example of the quantum Ising model, the corresponding dynamical phase transition is in close connection with the form of the Fisher zeros of the model considered in equilibrium. In particular, they examined the zeros of a "boundary partition function" $Z(z)$. Here, $Z(z)$ is defined as

$$Z(z) = \langle \Psi_i | e^{-z\mathcal{H}} | \Psi_i \rangle. \tag{1.56}$$

For $z = it$, the boundary partition function corresponds to the overlap amplitude of some time-evolved initial quantum state $|\Psi_i\rangle$ with itself. If z is real, i.e. $z = R$, the boundary partition function can be interpreted as the partition function of the field theory described by $\mathcal{H}$ with boundaries described by boundary states $|\Psi_i\rangle$ separated by R, which is acting as an inverse temperature. To do the quantum quench, the initial state of the system is prepared in the ground state of $\mathcal{H}$ for a given transverse field, while the time evolution is driven with a Hamiltonian of a different transverse field.

They then proceed to show that the zeros of the partition function in the complex plane form a family of lines, the form of which depends on whether the system is quenched within the same phase or across a quantum critical point. In particular, for the case of a quench across a quantum critical point, the zeros cut the time axis, giving rise to nonanalytic behaviour at times t_n^*. The zeros can then be used to determine the nonanalytic behaviour of the rate functions for return amplitude and probability at certain times t_n^*. Another closely related quantity is the work distribution function of a double quench experiment in which after the initial quench, a second quench takes place which returns the system to the original ground state Hamiltonian.

1.5 Overview

We have seen in this chapter, that from the Fisher or Lee-Yang zeros of a particular model, a lot of information about the phase transition can be extracted.

In the following chapters, we will first have a closer look at the one-dimensional Ising model and notice that the ordered state of the system lies on the contour of zeros (see chapter 2). We will also notice, that it is a "spiral order" that continuously connects the ferromagnetic and the antiferromagnetic side of the real-temperature line.

We will then move on to Ising ladders in chapter 3. In these, the number of legs determines how many contours of zeros there are. We will notice, that a similar spiral order exists along the contours of Fisher zeros. After studying differently sized ladders, we will argue that there is a finite region, which fills with zeros as the two-dimensional limit is approached. We can see evidence that, along with the zeros, the region is filled with spiral long-range order.

In chapter 4, we will look at the Kasteleyn method of deriving partition functions for the two-dimensional Ising model on different lattices. We will then use it to compute the zeros of the two-dimensional Ising model on frustrated lattices, in particular on the triangular and the kagomé lattices.

Finally, in chapter 5, we will briefly look at some results concerning Fisher zeros of the one-dimensional Ising model in a transverse field, which contains quantum fluctuations.

Chapter 2

The 1d Ising model

The one-dimensional Ising model is one of the easiest imaginable models. It was first developed by Wilhelm Lenz in 1920 [69], who gave it to his student Ernst Ising to solve. Ising then solved the one-dimensional model in 1925 [70]. The idea behind it is that we imagine a one-dimensional lattice of spins which are coupled to their nearest neighbours. Each spin can either point up or down and the coupling between the spins can be ferromagnetic or antiferromagnetic. If the coupling is ferromagnetic, then parallel alignment of each spin with its nearest neighbours is favoured, whereas antiferromagnetic coupling leads to antiparallel alignment of the spins. An Ising spin-chain with antiferromagnetic order can be seen in Fig. 2.1.

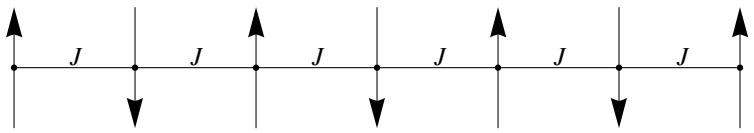

Figure 2.1: Example of a seven-site Ising chain ordered antiferromagnetically, where J denotes the strength of the coupling.

The Hamiltonian $\mathcal{H}$ of the model with N sites can be written as

$$\mathcal{H} = -J \sum_{i=1}^{N} \sigma_i \sigma_{i+1}, \tag{2.1}$$

where a positive coupling constant J corresponds to ferromagnetic coupling and negative J corresponds to antiferromagnetic coupling and σ_i denotes the spin on lattice site i which takes values ± 1 depending on whether the spin is in the "up" state or the "down" state. The larger the value of $|J|$, the stronger the correlation between each spin and its neighbours at non-zero temperature. The sum runs up to $i = N$ for periodic boundary conditions, such that $\sigma_{N+1} = \sigma_1$. If the boundary conditions are open, the sum would only run up to $i = N - 1$ in order to remove

the bond between $i = N$ and $i = 1$. For convenience purposes we can then define

$$-\beta\mathcal{H} = \sum_{i=1}^{N} K\sigma_i\sigma_{i+1}, \tag{2.2}$$

where $\beta = \frac{1}{k_B T}$ is the inverse temperature and $K = \beta J$.

Physically, this model has a phase transition at zero temperature, where the correlation length diverges. At any finite (i.e. non-zero) temperature, the spin chain is disordered and the correlation length is finite. At infinite temperature the behaviour of each spin is independent of the behaviour of the remaining spins. Consequently the correlation length is zero and the spins point up or down at random. This phase corresponds to a paramagnetic phase in which the spins only align subject to an external magnetic field. It is only at exactly zero temperature that we reach an infinite correlation length such that the region of ferromagnetic or antiferromagnetic alignment reaches from one edge of the system to the other.

2.1 Transfer matrix solution and boundary conditions

Classical Ising models in one and two dimensions can be solved via a transfer matrix approach. This includes Ising "ladders" of different sizes, which we will come back to in Chapter 3. The idea behind this approach is to find a matrix notation for the problem to be solved, such that the diagonalisation of the transfer matrix leads to a complete solution of the model. In order to do that, we have to associate different vectors with different states of the system which can pick out the corresponding matrix elements giving the Boltzmann weight $e^{-\beta E}$ of a certain configuration.

Let us now find a matrix notation for the one-dimensional problem without an external field given by the Hamiltonian in (2.1). Let us associate the vector $(1, 0)$ with $\sigma = 1$ (i.e. the spin pointing "up") and the vector $(0, 1)$ with $\sigma = -1$ (i.e. the spin pointing "down"). We can then introduce a transfer matrix $\mathbf{T}$, the elements of which are given by

$$[\mathbf{T}]_{\sigma\sigma'} \equiv e^{K\sigma\sigma'}. \tag{2.3}$$

Using the above representation, we can obtain

$$\mathbf{T} = \begin{array}{c} \\ \uparrow \\ \downarrow \end{array} \begin{array}{c} \begin{array}{cc} \uparrow & \downarrow \end{array} \\ \begin{pmatrix} e^{K} & e^{-K} \\ e^{-K} & e^{K} \end{pmatrix} \end{array}. \tag{2.4}$$

It is convenient to directly compute the eigenvalues and eigenvectors of the transfer matrix and construct the diagonalising matrix. The eigenvalues λ_1 and λ_2 can easily be found to be

$$\lambda_{1,2} = e^{K} \pm e^{-K}. \tag{2.5}$$

The eigenvector belonging to $\lambda_1 = 2\cosh K$ is given by $\left(\frac{1}{\sqrt{2}}, \frac{1}{\sqrt{2}}\right)$ and the eigenvector belonging to $\lambda_2 = 2\sinh K$ is given by $\left(\frac{1}{\sqrt{2}}, -\frac{1}{\sqrt{2}}\right)$. Consequently the matrix $\mathbf{D}$, which diagonalises $\mathbf{T}$, i.e. such that

$$\mathbf{D}^{-1}\mathbf{T}\mathbf{D} = \mathbf{\Lambda} = \begin{pmatrix} \lambda_1 & 0 \\ 0 & \lambda_2 \end{pmatrix}, \tag{2.6}$$

is given by

$$\mathbf{D} = \frac{1}{\sqrt{2}} \begin{pmatrix} 1 & 1 \\ 1 & -1 \end{pmatrix}. \tag{2.7}$$

Note that $\mathbf{D}^{-1} = \mathbf{D}$.

The exact expression of the partition function of a lattice with N sites depends on the boundary conditions of the problem. For clarity reasons, let us take a brief discourse into the solutions for different possible boundary conditions, namely open, periodic and pinned boundary conditions, in order to motivate our concentration on periodic boundary conditions for the following chapters.

- Periodic boundary conditions:

  The partition function in the transfer matrix approach for periodic boundary conditions can be computed by taking the trace of the Nth power of the transfer matrix. This means that there is one extra bond for periodic boundary conditions since site 1 is coupled to site N. The partition function can be written as

$$\begin{aligned} Z_N^p &= \sum_{\sigma_1,\sigma_2,\ldots,\sigma_N} [\mathbf{T}]_{\sigma_1\sigma_2} [\mathbf{T}]_{\sigma_2\sigma_3} \ldots [\mathbf{T}]_{\sigma_N\sigma_1} && (2.8)\\ &= \sum_{\sigma_1} \left[\mathbf{T}^N\right]_{\sigma_1\sigma_1} && (2.9)\\ &= \mathrm{Tr}(\mathbf{T}^N) && (2.10)\\ &= \mathrm{Tr}(\mathbf{D}\mathbf{\Lambda}^N\mathbf{D}^{-1}) && (2.11)\\ &= \mathrm{Tr}(\mathbf{\Lambda}^N) && (2.12)\\ &= \lambda_1^N + \lambda_2^N && (2.13)\\ &= 2^N \cosh^N K + 2^N \sinh^N K. && (2.14) \end{aligned}$$

- Open boundary conditions:

  For open boundary conditions, the restriction to get back to the same state after N sites is lifted and we have to trace over all combinations of states. Consequently, we need to

sum over all entries of the transfer matrix and write Z as

$$\begin{aligned} Z_N^o &= \sum_{\sigma_1,\sigma_2,\ldots,\sigma_N} [\mathbf{T}]_{\sigma_1\sigma_2} [\mathbf{T}]_{\sigma_2\sigma_3} \ldots [\mathbf{T}]_{\sigma_{N-1}\sigma_N} && (2.15)\\ & && (2.16)\\ &= \sum_{\sigma_1,\sigma_N} \left[\mathbf{T}^{N-1}\right]_{\sigma_1\sigma_N} && (2.17)\\ &= \sum_{i=1}^{2}\sum_{j=1}^{2} \left[\mathbf{T}^{N-1}\right]_{i,j} && (2.18)\\ &= \sum_{i=1}^{2}\sum_{j=1}^{2} \left[\mathbf{D}\mathbf{\Lambda}^{N-1}\mathbf{D}^{-1}\right]_{i,j} && (2.19)\\ &= 2^N \cosh^{N-1} K. && (2.20) \end{aligned}$$

- Pinned boundary conditions:

  Finally, let us look at pinned boundary conditions. This means that we fix the sites on the ends of the chain to be in a certain state. Here we have four choices for the combination of $|1\rangle$ and $|N\rangle$: $|\uparrow\uparrow\rangle$, $|\uparrow\downarrow\rangle$, $|\downarrow\uparrow\rangle$, and $|\downarrow\downarrow\rangle$. Since $\mathbf{T}^N$ is symmetric, pinning the ends of the chain to $|\uparrow\uparrow\rangle$ should give the same result as pinning the ends of the chain to $|\downarrow\downarrow\rangle$. Similarly, $|\uparrow\downarrow\rangle$ and $|\downarrow\uparrow\rangle$ should give the same partition function. Therefore we can write down two partition functions:

$$\begin{aligned} Z_N^{\uparrow\uparrow} = Z_N^{\downarrow\downarrow} &= \left[\mathbf{T}^{N-1}\right]_{1,1} = \left[\mathbf{T}^{N-1}\right]_{2,2} && (2.21)\\ &= \left[\mathbf{D}\mathbf{\Lambda}^{N-1}\mathbf{D}^{-1}\right]_{1,1} = \left[\mathbf{D}\mathbf{\Lambda}^{N-1}\mathbf{D}^{-1}\right]_{2,2} && (2.22)\\ &= 2^{N-2}\cosh^{N-1} K + 2^{N-2}\sinh^{N-1} K && (2.23) \end{aligned}$$

  and

$$\begin{aligned} Z_N^{\uparrow\downarrow} = Z_N^{\downarrow\uparrow} &= \left[\mathbf{T}^{N-1}\right]_{1,2} = \left[\mathbf{T}^{N-1}\right]_{2,1} && (2.24)\\ &= \left[\mathbf{D}\mathbf{\Lambda}^{N-1}\mathbf{D}^{-1}\right]_{1,2} = \left[\mathbf{D}\mathbf{\Lambda}^{N-1}\mathbf{D}^{-1}\right]_{2,1} && (2.25)\\ &= 2^{N-2}\cosh^{N-1} K - 2^{N-2}\sinh^{N-1} K. && (2.26) \end{aligned}$$

We could also examine twisted or antiperiodic boundary conditions, but they do not seem to be very physical for this system and we will refrain here from doing that. In the cases examined, both eigenvalues are present in pinned and periodic boundary conditions, whereas open boundary conditions are disparate in the sense that in the course of doing the summation, one of the eigenvalues gets "dropped". As we will see, this will lead to a pathological structure of Fisher zeros which sensitively depends on the way we take the thermodynamic limit (see Section 2.2). Similar pathologies will appear in the Ising ladders of Chapter 3. We can, however, show (see Section 2.3) that the physical behaviour, such as the correlation functions, is robust when

it comes to changing the boundary conditions. Consequently, we will solely deal with periodic boundary conditions in most of the examples given.

2.2 Fisher zeros of the model

Following from (2.13), we can write down the partition function as

$$Z_N = 2^N \cosh^N K + 2^N \sinh^N K. \tag{2.27}$$

Hence, we can easily find the zeros of this model as the points where

$$\frac{\lambda_2^N}{\lambda_1^N} = \tanh^N K = -1 = e^{i\pi(2n+1)} \tag{2.28}$$

for n being an integer. Rewriting the condition gives

$$\tanh K = e^{\frac{i\pi}{N}(2n+1)} \tag{2.29}$$

Consequently all the zeros lie on the unit circle in the complex $\tanh K$-plane. Let us rename $\tanh K$ to z, since we will be using the corresponding complex plane in this chapter as well as future chapters quite frequently. A plot of these zeros in the complex z-plane can be seen in Fig. 2.2.

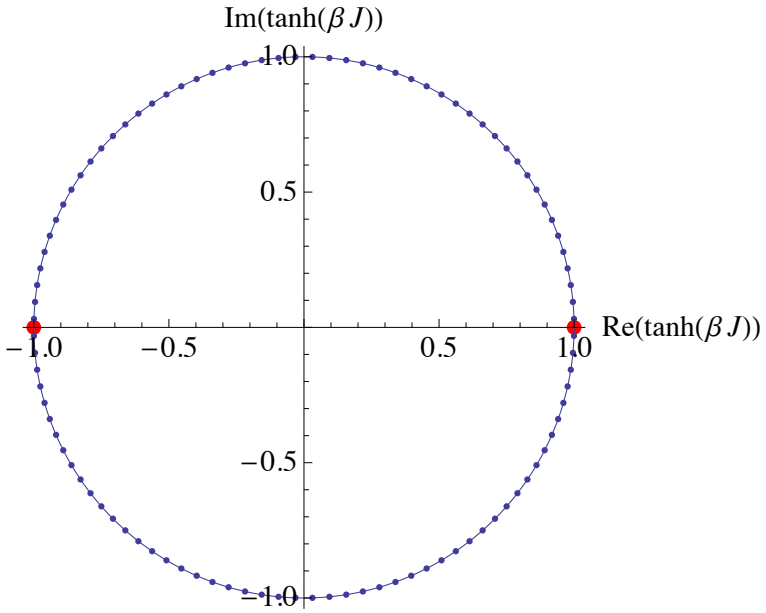

Figure 2.2: Locations of the first $N = 100$ zeros (blue dots) in the complex $\tanh(\beta J)$-plane. The red dots indicate where the $T = 0$ point maps to in this representation.

Note that the zeros lie on the contour on which the moduli of $\lambda_1 = 2\cosh K$ and $\lambda_2 = 2\sinh K$ become degenerate. Everywhere inside of the circle, λ_1 is the dominant eigenvalue and λ_2 can be

neglected in the thermodynamic limit, whereas on the outside of the circle, λ_2 is the dominant eigenvalue and λ_1 can be neglected in the thermodynamic limit. We will show in Chapter 3 and Chapter 4 that eigenvalue crossings or eigenvalue degeneracies in general correspond to zeros of the partition function.

In the case of finite N, each zero is an infinite-order zero. Due to the many-to-one nature of the mapping $K \to \tanh K$, the zeros "pile up" on top of each other once the first N zeros are distributed evenly over the circle. We will focus on the first branch such that the zeros are all first-order zeros. Approaching the thermodynamic limit ($N \to \infty$), the zeros turn into a continuous contour with constant density. This contour crosses the real axis at $z = \pm 1$, which are the two points which $T = 0$ maps to with positive and negative coupling J respectively. They can be physically interpreted to be the points of ferromagnetic and antiferromagnetic order with the positive z point being the point of ferromagnetic order and the negative one being the antiferromagnetic point. For any finite N, the $z = 1$ point always lies between two zeros, whereas there is an even-odd effect involved for the $z = -1$ point. For an even number of sites, the $z = -1$ point will always lie halfway between two zeros, whereas for an odd number of sites, it will coincide with a zero. This is due to the fact that the antiferromagnetic ground state does not obey periodic boundary conditions for an odd number of lattice sites.

In order to illustrate the point made in Section 2.1, let us now look at the locations of the zeros for open boundary conditions. From (2.20) we can derive the condition for the location of zeros, namely

$$\cosh^{N-1} K = 0. \tag{2.30}$$

The solutions correspond to the solutions of $\cosh K = 0$ and the zeros occur at

$$K = \frac{i\pi}{2} + in\pi \qquad \text{where} \qquad n \in \mathbb{Z}. \tag{2.31}$$

Hence all the zeros lie on the complex-K axis with constant spacing between the zeros. If we transform these into the $\tanh K$-plane, the zeros still all lie on the imaginary axis, although they are now all located at complex infinity according to the mapping $K \to \tanh K$.

Similarly, we can imagine changing between the different boundary conditions by introducing a parameter α which has different values for the different boundary conditions. We then write the general partition function as

$$Z_\alpha^N = 2^N \cosh^{N-1} K + 2^N \alpha \sinh^{N-1} K, \tag{2.32}$$

which has zeros at

$$z = \left(\frac{1}{\alpha}\right)^{\frac{1}{N}} e^{i\theta_n}, \tag{2.33}$$

where $\theta_n = \frac{\pi}{N}(2n+1)$.

We can then go from one set of boundary conditions to another by taking the limits $\alpha \to 0$,

$\alpha \to 1$, and $\alpha \to -1$ for open, periodic/pinned-$\uparrow\uparrow$, and pinned-$\uparrow\downarrow$ respectively. [1]

Especially in the case of open boundary conditions, we can see that the result depends sensitively on the order in which we take the two limits $\alpha \to 0$ and the thermodynamic limit $N \to \infty$. If we first take the limit of $\alpha \to 0$, all the zeros will be distributed over a circle of infinite radius, whereas if we first take the thermodynamic limit, the zeros will be distributed over the unit circle.

2.3 Correlation functions at complex temperature

In order to shed more light on the location of the different "phases" in the complex z-plane, we will analyse the behaviour of the correlation functions in different regions of the complex plane. As a result of that, we will see that the correlation function exponentially decays anywhere but on the contour of zeros. On that contour, we can see long-range order developing.

A measure of that long-range order is the correlation function and the corresponding correlation length of the system. The correlation function is given by

$$\langle\langle \hat{S}_i \hat{S}_j \rangle\rangle = \langle \hat{S}_i \hat{S}_j \rangle - \langle \hat{S}_i \rangle \langle \hat{S}_j \rangle. \tag{2.34}$$

Here, $\langle \hat{S}_i \rangle$ is the expectation value of a spin at position i. In the case of periodic boundary conditions, we can call the position i the "beginning" of the chain without loss of generality, i.e. fix the position to be zero.

Consequently, we want to calculate both the single-spin expectation value and the two-spin correlator. Let us name the sites on the lattice by the parameter j. The single-spin expectation value is then given by

$$\langle \hat{S}_j \rangle = \frac{\sum_{\mu\nu} c_{\mu\nu} \left(\mathbf{T}^j \boldsymbol{\sigma}_z \mathbf{T}^{N-j} \right)_{\mu\nu}}{\sum_{\mu\nu} c_{\mu\nu} \left(\mathbf{T}^N \right)_{\mu\nu}} \tag{2.35}$$

and

$$\langle \hat{S}_0 \hat{S}_j \rangle = \frac{\sum_{\mu\nu} c_{\mu\nu} \left(\boldsymbol{\sigma}_z \mathbf{T}^j \boldsymbol{\sigma}_z \mathbf{T}^{N-j} \right)_{\mu\nu}}{\sum_{\mu\nu} c_{\mu\nu} \left(\mathbf{T}^N \right)_{\mu\nu}}, \tag{2.36}$$

where the matrix $c_{\mu\nu}$ determines the elements to be summed over for a particular set of boundary conditions. For periodic boundary conditions, we sum over the diagonal entries such that $c_{\mu\nu} = \begin{pmatrix} 1 & 0 \\ 0 & 1 \end{pmatrix}$, whereas for open boundary conditions we need to sum over all entries such that $c_{\mu\nu} = \begin{pmatrix} 1 & 1 \\ 1 & 1 \end{pmatrix}$. That leaves pinned boundary conditions, for which we only sum over one of the entries depending on the nature of the pinning. Let us look at the least pathological case, the case of periodic boundary conditions, in more detail.

[1] The pinned boundary conditions differ from open and periodic boundary conditions by a factor of 2. This does not have any implications of the zeros and can be disregarded in the following analysis.

We want to look at

$$\begin{aligned}
\langle\langle \hat{S}_0 \hat{S}_j \rangle\rangle_p &= \langle \hat{S}_0 \hat{S}_j \rangle - \langle \hat{S}_0 \rangle \langle \hat{S}_j \rangle && (2.37)\\
&= \frac{\mathrm{Tr}\left(\boldsymbol{\sigma}_z \mathbf{T}^j \boldsymbol{\sigma}_z \mathbf{T}^{N-j}\right)}{\mathrm{Tr}\left(\mathbf{T}^N\right)} - \left(\frac{\mathrm{Tr}\left(\boldsymbol{\sigma}_z \mathbf{T}^N\right)}{\mathrm{Tr}\left(\mathbf{T}^N\right)}\right)^2 && (2.38)\\
&= \frac{\mathrm{Tr}\left(\mathbf{D}^{-1}\boldsymbol{\sigma}_z \mathbf{D}\boldsymbol{\Lambda}^j \mathbf{D}^{-1}\boldsymbol{\sigma}_z \mathbf{D}\boldsymbol{\Lambda}^{N-j}\right)}{\mathrm{Tr}\left(\boldsymbol{\Lambda}^N\right)} - \left(\frac{\mathrm{Tr}\left(\mathbf{D}^{-1}\boldsymbol{\sigma}_z \mathbf{D}\boldsymbol{\Lambda}^N\right)}{\mathrm{Tr}\left(\boldsymbol{\Lambda}^N\right)}\right)^2, && (2.39)
\end{aligned}$$

where $\boldsymbol{\sigma}_z = \begin{pmatrix} 1 & 0 \\ 0 & -1 \end{pmatrix}$ is a Pauli spin matrix. The equation (2.39) holds, even if we move on to larger systems, i.e. Ising ladders or the full two dimensional model. The size of the matrices involved, however, will vary and new $\boldsymbol{\sigma}_z$ will consist of tensor products of the Pauli $\boldsymbol{\sigma}_z$-matrix. We will also get a choice between two correlation functions: those calculated between two spins on the same leg and between two spins of different legs.

For now, let us analyse the one-dimensional correlation function and insert the expressions for the two eigenvalues. In that case, (2.39) reduces to

$$C_j = \langle\langle \hat{S}_0 \hat{S}_j \rangle\rangle = \langle \hat{S}_0 \hat{S}_j \rangle = \frac{z^j + z^{N-j}}{1 + z^N} \tag{2.40}$$

since $\langle \hat{S}_0 \rangle = 0$. We can look at different regions in the complex plane by parametrising $z = Re^{i\theta}$. (2.40) can then be rewritten as

$$C_j = \frac{R^j e^{ij\theta} + R^{N-j} e^{i(N-j)\theta}}{1 + R^N e^{iN\theta}}. \tag{2.41}$$

If we now look at the "inside region" of the contour of zeros, i.e. where $|z| < 1$ (or $R < 1$), C_j becomes

$$C_j \approx z^j = R^j e^{ij\theta} \tag{2.42}$$

for large N and reasonably small values of j. Similarly, we can analyse the behaviour in the "outside region", where $|z| > 1$ ($R > 1$) and find

$$C_j \approx z^{-j} = R^{-j} e^{-ij\theta}. \tag{2.43}$$

Looking at these two results, we can see that for a specific value of z, the amplitude of the correlation function decreases as j increases, both inside and outside of the contour. We can more easily see this by looking at the behaviour of

$$C_j = R^{-j} e^{-ij\theta}, \tag{2.44}$$

which we can rewrite as

$$C_j = e^{-j \ln R} e^{-ij\theta}. \tag{2.45}$$

We can identify $e^{-j \ln R}$ with the usual expression for the correlation function in terms of the correlation length ξ, such that

$$e^{-j \ln R} = e^{-j/\xi}. \tag{2.46}$$

We can then identify the correlation length as

$$\xi = \frac{1}{\ln R}. \tag{2.47}$$

In addition, there is a spiral aspect to the correlation functions. As we move along the chain (i.e. increase j), the correlation function picks up a phase. The sense of the spiral (i.e. the sign of the phase) changes direction as the contour of zeros is crossed and we go from the "inside region" to the "outside region". It may seem inappropriate to talk about "spiral behaviour" in an Ising model since the Ising spins are only allowed to point either up or down. Therefore they can not display spiral behaviour. But since we have effectively promoted the Z_2 symmetry of the spin variable to a $U(1)$ symmetry by allowing K to be complex, it effectively allows for a second direction in which the spiral can form, namely the imaginary $\langle \hat{S}_j \rangle$-direction.

Now let us look at what happens to the correlation function as we move along the $|z| = 1$ contour. We clearly have a problem here, since the denominator vanishes at the points $z = e^{i\theta_n}$, i.e. the locations of the zeros. We can get around this problem by considering the correlation function only at angles midway between the zeros, i.e. at locations

$$z = e^{i\tilde{\theta}_n} \qquad \text{with} \qquad \tilde{\theta}_n = \frac{2\pi}{N} n. \tag{2.48}$$

This correlation function is then well-behaved in the $N \to \infty$ limit. Substituting the above expression into (2.40) gives

$$\begin{aligned} C_j &= \frac{e^{ij\tilde{\theta}_n} + e^{i(N-j)\tilde{\theta}_n}}{1 + e^{iN\tilde{\theta}_n}} && (2.49) \\ &= \frac{e^{ij\tilde{\theta}_n} + e^{-ij\tilde{\theta}_n}}{2} && (2.50) \\ &= \cos\left(\tilde{\theta}_n j\right). && (2.51) \end{aligned}$$

This implies, that there is long-range order on the contour and in fact, that this is the only place where there is long-range order in the complex z-plane. The nature of the order is a spin-density wave with a wave vector given by $\tilde{\theta}_n$, which constitutes the superposition of the spirals on either side of the contour. The region inside the contour as well as the region outside the contour both exhibit only short-range order at the best, since the spirals decay when moving along the chain away from the "pinned" spins.

When we do the analysis for open boundary conditions, we again want to introduce a mixing

in of the second eigenvalue. We then get

$$C_j^o = \frac{\sinh^j(K)\cosh^{N-j}(K) + \alpha\cosh^j(K)\sinh^{N-j}(K)}{\cosh^N(K) + \alpha\sinh^N(K)} \tag{2.52}$$

$$= \frac{z^j + \alpha z^{N-j}}{1 + \alpha z^N} \tag{2.53}$$

$$= \frac{\left(\frac{1}{\alpha}\right)^{\frac{j}{N}} e^{ij\tilde{\theta}_n} + \alpha\left(\frac{1}{\alpha}\right)^{\frac{N-j}{N}} e^{i(N-j)\tilde{\theta}_n}}{1 + \alpha\left(\frac{1}{\alpha}\right)^{\frac{N}{N}} e^{iN\tilde{\theta}_n}} \tag{2.54}$$

$$= \frac{\left(\frac{1}{\alpha}\right)^{\frac{j}{N}} e^{ij\tilde{\theta}_n} + \left(\frac{1}{\alpha}\right)^{-\frac{j}{N}} e^{-ij\tilde{\theta}_n}}{2}. \tag{2.55}$$

As in the case where we looked at the distribution of zeros for different boundary conditions, it now matters in which order we take the limit. In order to obtain C_j, we have to both take the thermodynamic limit and the limit $\alpha \to 0$. If we take the thermodynamic limit first, C_j is well behaved and reduces to

$$C_j \sim \cos\left(\tilde{\theta}_n j\right). \tag{2.56}$$

In this case the correlation function still shows long-range order on the unit circle contour and we can say that the correlation function is robust towards a change of boundary conditions subject to the way we take the thermodynamic limit.

2.4 Heat flow and first order transitions

In order to examine phase transitions, it is useful not only to consider microscopic behaviour and long-range-order, but also thermodynamic quantities. This will, for example, enable us to determine the order of the transition in the complex plane. The thermodynamic quantity that is easiest to calculate for this model is the internal energy in the different sectors of the complex plane. It is defined as

$$E = F + \beta\frac{\partial F}{\partial \beta}, \tag{2.57}$$

where we can write F as

$$F = -\frac{N}{\beta}\ln(\lambda_{\max}). \tag{2.58}$$

Here, $\lambda_{\max}$ is the maximal eigenvalue of the transfer matrix at a given point in the complex z-plane. The explicit expression of F depends on where we are evaluating the free energy, and therefore also the internal energy, in the complex $\tanh K$-plane. If we are evaluating E inside the unit circle, the maximal eigenvalue is $2\cosh K$, which we call λ_{in}, whereas it is $2\sinh K \equiv \lambda_{\text{out}}$ outside the circle. We can derive the difference between those two internal energies as we cross the contour, which we call ΔE, by evaluating E on both sides (let us call these E_{in} and E_{out}).

Then we can derive

$$\frac{E_{\rm in}}{N} = -\frac{1}{\beta}\ln\left(\lambda_{\rm in}\right) + \beta\frac{\partial}{\partial\beta}\left(-\frac{1}{\beta}\ln\left(\lambda_{\rm in}\right)\right) \tag{2.59}$$

$$= -\frac{1}{\beta}\ln\left(\lambda_{\rm in}\right) + \frac{1}{\beta}\ln\left(\lambda_{\rm in}\right) - \frac{1}{\lambda_{\rm in}}\frac{\partial\lambda_{\rm in}}{\partial\beta} \tag{2.60}$$

$$= -\frac{1}{\lambda_{\rm in}}\frac{\partial\lambda_{\rm in}}{\partial\beta} \tag{2.61}$$

$$\text{and} \qquad \frac{E_{\rm out}}{N} = -\frac{1}{\lambda_{\rm out}}\frac{\partial\lambda_{\rm out}}{\partial\beta}. \tag{2.62}$$

We can then look at the difference between the two expressions:

$$\frac{\Delta E}{N} = \frac{E_{\rm out}}{N} - \frac{E_{\rm in}}{N} \tag{2.63}$$

$$= \lambda_{\rm in}^{-1}\frac{\partial\lambda_{\rm in}}{\partial\beta} - \lambda_{\rm out}^{-1}\frac{\partial\lambda_{\rm out}}{\partial\beta}. \tag{2.64}$$

Substituting the $\lambda_{\rm in} = 2\cosh K$ and $\lambda_{\rm out} = 2\sinh K$ for the Ising chain (2.64) gives

$$\frac{\Delta E}{N} = J\tanh K - J\tanh^{-1} K. \tag{2.65}$$

We then evaluate $\frac{\Delta E}{N}$ on the contour of zeroes, i.e. where $\tanh K = e^{i\theta}$ such that

$$\frac{\Delta E}{N} = 2iJ\sin\theta. \tag{2.66}$$

This means that there is an imaginary jump in the internal energy as we cross the contour, which can be associated with an imaginary "latent heat", which is a sign of a first order transition. As we continue the result onto the real line, the "latent heat" goes to zero and the transition becomes second order. We should note here, that the $T = 0$ phase transition to long-range order in the $d = 1$ Ising model is to some extent pathological. On the one hand the spin-spin correlation length diverges as $T \to 0$, which would normally be expected at a second-order phase transition. On the other hand, the equilibrium magnetisation jumps from zero to unity at $T = 0$, which is a sign of a first-order transition. This violates the general guideline that first order transitions do not have diverging length scales. However, it is not a contradiction as such. The same comment applies to Ising ladders considered in Chapter 3.

2.5 The 1d Ising model in a longitudinal field

In addition to the problem solved above, we can apply a field in a longitudinal direction to the spin chain, i.e. a field in the same direction in spin-space as the coupling. Let us first write

down the Hamiltonian with a longitudinal field:

$$\mathcal{H} = \sum_{i=1}^{N} \left(-J\sigma_i\sigma_{i+1} - H\sigma_i\right) \tag{2.67}$$

and hence

$$-\beta\mathcal{H} = \sum_{i=1}^{N} \left(K\sigma_i\sigma_{i+1} + h\sigma_i\right), \tag{2.68}$$

where $h = \beta H$. Following the reasoning given in [71], new transfer matrix can be written as the matrix product of the zero-field transfer matrix with a "field matrix" $\mathbf{H}$:

$$\mathbf{T}_H = \mathbf{T}\mathbf{H}, \tag{2.69}$$

where

$$\mathbf{H} = \begin{array}{c} \\ \uparrow \\ \downarrow \end{array} \begin{array}{c} \begin{array}{cc} \uparrow & \downarrow \end{array} \\ \begin{pmatrix} e^{h} & 0 \\ 0 & e^{-h} \end{pmatrix} \end{array}. \tag{2.70}$$

Since we are looking at periodic boundary conditions, we will always take the trace of the transfer matrix, which is invariant under cyclic permutations. Therefore we can write down a symmetric version of the transfer matrix, such that

$$\mathbf{T}_H = \mathbf{H}^{1/2}\mathbf{T}\mathbf{H}^{1/2} = \begin{array}{c} \\ \uparrow \\ \downarrow \end{array} \begin{array}{c} \begin{array}{cc} \uparrow & \downarrow \end{array} \\ \begin{pmatrix} e^{K+h} & e^{-K} \\ e^{-K} & e^{K-h} \end{pmatrix} \end{array}. \tag{2.71}$$

We then do an eigenvalue analysis of the new transfer matrix $\mathbf{T}_H$ and find the eigenvalues to be

$$\lambda_{\pm} = e^{K}\cosh h \pm \sqrt{e^{2K}\sinh^2 h + e^{-2K}}. \tag{2.72}$$

As a check, we can look at the limit $h \to 0$ and notice that we recover the original eigenvalues given in (2.5). The next step is to write down the partition function for periodic boundary conditions

$$Z = \lambda_+^N + \lambda_-^N \tag{2.73}$$

$$= \left(e^{K}\cosh h + \sqrt{e^{2K}\sinh^2 h + e^{-2K}}\right)^N + \left(e^{K}\cosh h - \sqrt{e^{2K}\sinh^2 h + e^{-2K}}\right)^N. \tag{2.74}$$

This partition function has zeros at

$$\left(\frac{e^{K}\cosh h - \sqrt{e^{2K}\sinh^2 h + e^{-2K}}}{e^{K}\cosh h + \sqrt{e^{2K}\sinh^2 h + e^{-2K}}}\right)^N = -1. \tag{2.75}$$

Let us call

$$\frac{e^K \cosh h - \sqrt{e^{2K} \sinh^2 h + e^{-2K}}}{e^K \cosh h + \sqrt{e^{2K} \sinh^2 h + e^{-2K}}} = \zeta \tag{2.76}$$

and write the zeros of (2.75) as located at

$$\zeta = e^{\frac{i\pi}{N}(2n+1)}. \tag{2.77}$$

We can draw these zeros in the complex ζ-plane in which they will all lie on the unit circle. Note that ζ is a function of both h and K. In the following analysis, we will fix the value of h to be some ratio of the value of K and analyse the behaviour of ζ as a function of K only. In the case of nonzero h, the real temperature axis will no longer map onto the line between $\zeta = -1$ and $\zeta = 1$. Instead, the start and end point of the line in the ζ-plane will now depend on the ratio of h and K. A non-zero external field destroys the symmetry of the mapping between the positive and the negative sides of $\Re(\zeta)$. This means that even for a small external field the contour on which the zeros lie will no longer cross the real axis at a physical value of ζ on the ferromagnetic side, even though it will still cross the real axis on the zero temperature point on the antiferromagnetic side (see figure 2.3). This happens because it is energetically favourable for the spins to align along with the field as well as satisfy all the ferromagnetic bonds. The spins can no longer undergo an ordering phase transition because the ordering has already been preempted by the field alignment.

On the antiferromagnetic side, the field has to compete with the interactions rather than reenforcing them. As long as the field is still small compared to the interaction strength K, there is still an antiferromagnetic phase transition at zero temperature. The field is not strong enough to cause flipped spin excitations out of the antiferromagnetic ground state.

As we keep increasing $|h|$, we eventually reach the point $h > 2K$ at which the field is stronger than the antiferromagnetic interactions. This leads to a change of behaviour on the antiferromagnetic side, such that the mapping of the real axis in the K-plane into the ζ-plane no longer reaches $\Re(\zeta) = -1$. Therefore the point at which the zeros would cross the real line in the thermodynamic limit no longer corresponds to a physical temperature (see figure 2.4). This means that the magnetic field is now strong enough to destroy any antiferromagnetic order that might arise, therefore there is no longer a phase transition to an antiferromagnetic state.

Let us also revisit correlation functions in a field, in particular $\langle \hat{S}_j \rangle$, the form of which we have already seen in (2.35). We can rewrite it as

$$\langle \hat{S}_j \rangle = \frac{\mathrm{Tr}\left(\mathbf{D}^{-1}\boldsymbol{\sigma}_z \mathbf{D}\boldsymbol{\Lambda}^N\right)}{\mathrm{Tr}\left(\boldsymbol{\Lambda}^N\right)}. \tag{2.78}$$

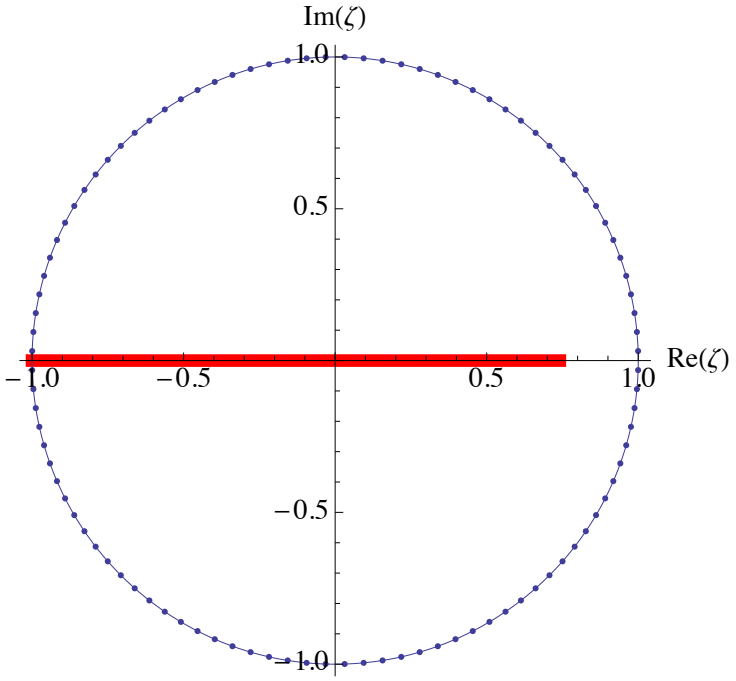

Figure 2.3: Locations of the first $N = 100$ zeros (blue dots) in the complex $\zeta(h = .1K)$-plane. The red line indicates the region to which the real temperature axis maps in this representation. As soon as h is non-zero, the circle on which the zeros lie no longer cuts the real axis at a point which maps onto a physical temperature on the ferromagnetic side. This indicates the fact, that no ferromagnetic phase transition can take place for any physical temperature since the alignment of the spins along the field pre-empts any ordering transition.

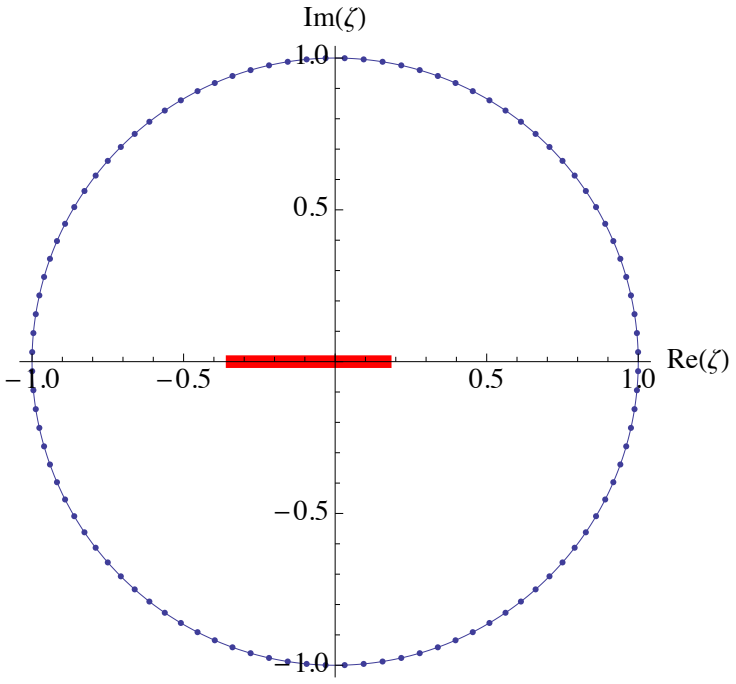

Figure 2.4: Locations of the first $N = 100$ zeros (blue dots) in the complex $\zeta(h = 2.1K)$-plane. The red line indicates the region to which the real temperature axis maps in this representation. Note that the contour on which the zeros lie now no longer crosses the real axis at any physical ζ. This means that no phase transition can take place since the external field is so strong that it destroys any ferromagnetic or antiferromagnetic order.

To calculate $\mathbf{D}$, we need the eigenvectors of the transfer matrix, which are

$$\mathbf{e}_+ = \frac{1}{\sqrt{e^{-2K} + \left(\lambda_+ - e^{K+h}\right)^2}} \begin{pmatrix} e^{-K} \\ \lambda_+ - e^{K+h} \end{pmatrix}, \text{ and} \tag{2.79}$$

$$\mathbf{e}_- = \frac{1}{\sqrt{e^{-2K} + \left(\lambda_- - e^{K+h}\right)^2}} \begin{pmatrix} e^{-K} \\ \lambda_- - e^{K+h} \end{pmatrix}. \tag{2.80}$$

In the case of non-zero field the full expressions for $\mathbf{D}$ and $\mathbf{D}^{-1}$ are still possible and, in fact, not very hard to calculate once we have the eigenvectors. It does, however, become rather tedious to do the full calculation with the explicit expressions and will most certainly not fit onto this page. Therefore let us use placeholders, such that

$$\mathbf{D} = \begin{pmatrix} a & b \\ c & d \end{pmatrix}. \tag{2.81}$$

We can then write down

$$\mathbf{D}^{-1} = \mathbf{D}^T = \begin{pmatrix} a & c \\ b & d \end{pmatrix}. \tag{2.82}$$

We have to choose a, b, c, and d such that $\mathbf{D}\mathbf{D}^{-1} = \begin{pmatrix} 1 & 0 \\ 0 & 1 \end{pmatrix}$. This means that $a^2 + c^2 \equiv 1$, $b^2 + d^2 \equiv 1$, and $ab + cd \equiv 0$. We can then further simplify

$$\mathbf{D}^{-1}\boldsymbol{\sigma}_z\mathbf{D} = \begin{pmatrix} \alpha & \gamma \\ \gamma & \beta \end{pmatrix}, \text{ where} \tag{2.83}$$

$$\alpha = a^2 - b^2, \tag{2.84}$$

$$\beta = c^2 - d^2, \text{ and} \tag{2.85}$$

$$\gamma = ac - bd. \tag{2.86}$$

Applying periodic boundary conditions, we then get

$$\langle \hat{S}_j \rangle = \frac{\alpha\lambda_+^N + \beta\lambda_-^N}{\lambda_+^N + \lambda_-^N} \tag{2.87}$$

$$= \frac{\alpha + \beta\zeta^N}{1 + \zeta^N}. \tag{2.88}$$

We can now look at the two regions inside ($|\zeta| < 1$) and outside ($|\zeta| > 1$) of the circle. The result in the thermodynamic limit is

$$\langle \hat{S}_j \rangle = \begin{cases} \alpha & \text{if } |\zeta| < 1 \\ \frac{\alpha+\beta}{2} & \text{if } |\zeta| = 1 \\ \beta & \text{if } |\zeta| > 1. \end{cases} \tag{2.89}$$

Let us now look at what α and β look like at small fields. To do that, let us first write down the explicit expressions of α and β:

$$\alpha = \frac{e^{-2K} - \left(\lambda_+ - e^{K+h}\right)^2}{e^{-2K} + \left(\lambda_+ - e^{K+h}\right)^2} \quad \text{and} \tag{2.90}$$

$$\beta = \frac{e^{-2K} - \left(\lambda_- - e^{K+h}\right)^2}{e^{-2K} + \left(\lambda_- - e^{K+h}\right)^2}. \tag{2.91}$$

Up to smallest order in h, $\lambda_\pm$ can be written as

$$\lambda_\pm = e^K \cosh h \pm \sqrt{e^{2K} \sinh^2 h + e^{-2K}}. \tag{2.92}$$

$$\approx e^K \left(1 + \frac{1}{2}h^2\right) \pm \sqrt{e^{2K} h^2 + e^{-2K}} \tag{2.93}$$

$$\approx e^K \left(1 + \frac{1}{2}h^2\right) \pm e^{-K} \left(1 + \frac{h^2}{2} e^{4K}\right). \tag{2.94}$$

Since we want to look at very small h, it is sufficient to keep terms up to linear order in h. Since the lowest order in h involved is the quadratic order, we can use

$$\lambda_\pm \approx e^K \pm e^{-K}. \tag{2.95}$$

Therefore, up to linear order, we can write

$$\alpha \approx \frac{e^{-2K} - \left(\lambda_+ - e^K (1+h)\right)^2}{e^{-2K} + \left(\lambda_+ - e^K (1+h)\right)^2} \tag{2.96}$$

$$\approx \frac{e^{-2K} - \left(e^{-K} - h e^K\right)^2}{e^{-2K} + \left(e^{-K} - h e^K\right)^2} \tag{2.97}$$

$$\approx \frac{e^{-2K} - \left(e^{-2K} - 2h\right)}{e^{-2K} + \left(e^{-2K} - 2h\right)} \tag{2.98}$$

$$= \frac{h}{e^{-2K} - h} \tag{2.99}$$

$$\approx h e^{2K} \tag{2.100}$$

and

$$\beta \approx \frac{e^{-2K} - \left(\lambda_- - e^K (1+h)\right)^2}{e^{-2K} + \left(\lambda_- - e^K (1+h)\right)^2} \tag{2.101}$$

$$\approx -h e^{2K}. \tag{2.102}$$

This means that there is a paramagnetic response to a small external magnetic field for $\zeta < 1$ and a diamagnetic response for $|\zeta| > 1$. As we approach $|\zeta| = 1$ both α and β diverge, which corresponds to a diverging linear susceptibility $\left(\frac{\partial m}{\partial h}\right)$.

Chapter 3

Ising ladders

3.1 Transfer matrices and eigenvalue crossings

As a next step, we would like to explore the two-dimensional Ising model and the behaviour of the correlation functions within the complex plane following from the distribution of Fisher zeros as they were found by Fisher in the 1960's. Fisher's result is shown in Figure 3.1. However, looking at the full solutions for the two-dimensional Ising model as described by Onsager, Kasteleyn and Fisher [72, 73, 74], we noticed that it is not so obvious to see how the behaviour of the one-dimensional Ising chain in terms of eigenvalues of transfer matrices translates to the two-dimensional model. In order to see how the one-dimensional model approaches the two-dimensional limit, we wanted to see how Ising ladders of different widths behave. From there we would like to extrapolate the limit of infinite width – the full two-dimensional model. The transfer matrices of these ladders will have the size $2^{N_L} \times 2^{N_L}$, where N_L is the number of legs, i.e. the width of the respective ladder. Hence, the Ising chain has a 2×2 transfer matrix and the full two dimensional model has a $\infty \times \infty$ transfer matrix.

Let us look at Ising ladders of different widths in this chapter. We will concentrate mainly on ladders on which we will use periodic boundary conditions in the long direction and open boundary conditions in the short direction (i.e. the width) of the ladder. In section 3.5, we will also consider ladders with periodic boundary conditions on the short direction for comparison purposes. In general, Ising ladders with periodic boundary conditions in the long and open boundary conditions in the short direction have the Hamiltonian

$$\mathcal{H} = -J \sum_{j=1}^{N} \sum_{i=1}^{N_L-1} \left(\sigma_{j,i}\sigma_{j,i+1} + \sigma_{j,i}\sigma_{j+1,i} \right), \tag{3.1}$$

where $\sigma_{N+1,i} \equiv \sigma_{1,i}$. As in the example of the Ising chain, positive J corresponds to ferromagnetic coupling and negative J corresponds to antiferromagnetic coupling.

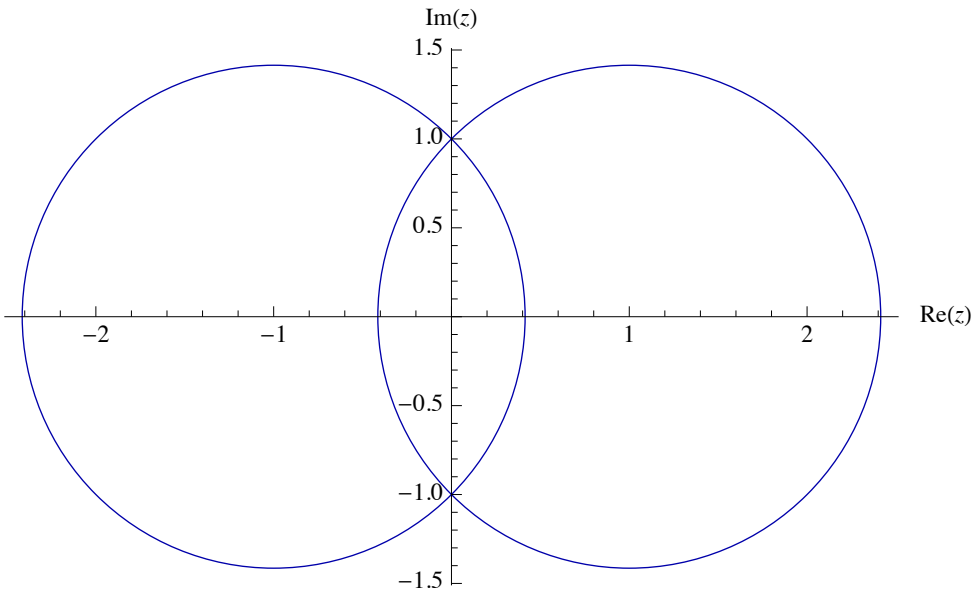

Figure 3.1: The contour of zeros for the two-dimensional square-lattice Ising model according to Fisher [72]. The derivation of this result will be revisited in Chapter 4.

3.1.1 Eigenvalue crossings

Since the size of the transfer matrix scales as 2^{N_L}, each transfer matrix will have 2^{N_L} eigenvalues. Therefore, it will quickly become impossible to evaluate the partition function zeros by setting the full partition function equal to zero and evaluating the points numerically. However, there is a way out of this by making use of the Beraha-Kahane-Weiss theorem [75, 76, 77, 78, 79]. In the transfer matrix language, there are two conditions which have to be fulfilled for the theorem to hold:

1. the partition function can be written as a sum over weighted eigenvalues to the power N
2. no two co-dominant eigenvalues (i.e. in the case where there is no unique dominant eigenvalue) are degenerate over an area of the complex domain.

If these conditions are fulfilled, then there are two possibilities for partition function zeros to occur:

1. there is a unique dominant eigenvalue λ_k at a point z and its weight α_k is zero at that point or
2. there are two or more co-dominant eigenvalues at z.

The first possibility leads to zeros at isolated points in the complex domain, even in the thermodynamic limit, whereas the second possibility can lead to curves of zeros as $N \to \infty$. It is the second possibility that leads to interesting partition function zeros with regards to phase transitions. These will be the most important features of the Beraha-Kahane-Weiss theorem

for the discussion of ladders. We will see in chapter 4, that the theorem does not apply to the 2-dimensional Ising model because two or more eigenvalues are degenerate and co-dominant over a finite region of the complex plane.

We can use this theorem to find the zeros of the different Ising ladders. This is done by ordering the eigenvalues according to the size of their absolute values. Then the difference between the two largest eigenvalues can be computed and the points at which that difference goes to zero can be found numerically by keeping only those points where the difference is below a certain threshold value. We can then plot those points to get an idea of the behaviour of zeros. Let us now look at specific examples of these Ising ladders and what their transfer matrices look like.

3.2 Zeros of the 2-leg Ising ladder

The simplest case of an "Ising ladder" is that where two Ising chains are coupled so that there are both intra- and interchain bonds. We call this the two-leg Ising ladder, which is shown in Figure 3.2.

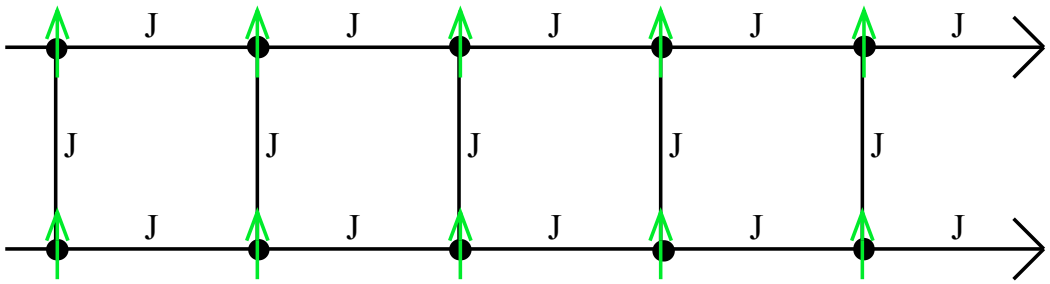

Figure 3.2: The two-leg Ising ladder in a ferromagnetic groundstate.

In order to solve this model, we have to look at the spin states on one of the rungs coupled to the next rung of the ladder in order to compute the transfer matrix. To calculate the elements of the transfer matrix, we look at the configurations of the "unit cell". Two different unit cells are shown in Figure 3.3. They consist of four sites which are coupled both horizontally and vertically. We choose to use the second, symmetric unit cell with halved coupling strength in the vertical direction. This avoids double counting and leads to a symmetric transfer matrix. Computing the transfer matrix then gives:

$$\mathbf{T}_2 = \begin{array}{c} \\ \uparrow\uparrow \\ \uparrow\downarrow \\ \downarrow\uparrow \\ \downarrow\downarrow \end{array} \begin{array}{c} \begin{array}{cccc} \uparrow\uparrow & \uparrow\downarrow & \downarrow\uparrow & \downarrow\downarrow \end{array} \\ \begin{pmatrix} e^{3K} & 1 & 1 & e^{-3K} \\ 1 & e^{K} & e^{-3K} & 1 \\ 1 & e^{-3K} & e^{K} & 1 \\ e^{-3K} & 1 & 1 & e^{3K} \end{pmatrix} \end{array}. \tag{3.2}$$

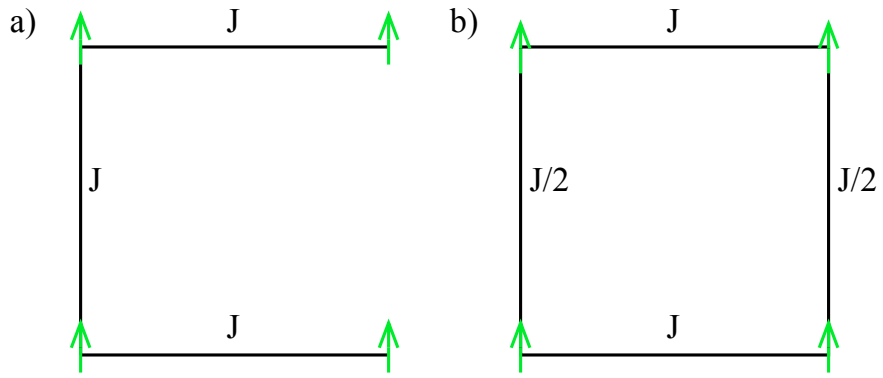

Figure 3.3: Two possible unit cells of the two-leg ladder for the generation of the transfer matrix. The unit cell in panel a) ensures that no double counting takes place, whereas the unit cell in panel b) also ensures that the transfer matrix is symmetric.

Diagonalising this matrix gives us 4 eigenvalues. Consequently

$$Z = \lambda_1^N + \lambda_2^N + \lambda_3^N + \lambda_4^N \tag{3.3}$$

with

$$\lambda_1 = 2e^{-K}\sinh(2K) \tag{3.4}$$

$$\lambda_2 = 2e^{K}\sinh(2K) \tag{3.5}$$

$$\lambda_3 = \frac{1}{2}e^{-4K}\left(e^K + e^{3K} + e^{5K} + e^{7K} - e^K\left(1+e^{2K}\right)\sqrt{1-4e^{2K}+10e^{4K}-4e^{6K}+e^{8K}}\right) \tag{3.6}$$

$$= \cosh(3K) + \cosh(K)\left(1 - 2\sqrt{\cosh^2(2K) - 2\cosh(2K) + 2}\right) \tag{3.7}$$

$$\lambda_4 = \frac{1}{2}e^{-4K}\left(e^K + e^{3K} + e^{5K} + e^{7K} + e^K\left(1+e^{2K}\right)\sqrt{1-4e^{2K}+10e^{4K}-4e^{6K}+e^{8K}}\right) \tag{3.8}$$

$$= \cosh(3K) + \cosh(K)\left(1 + 2\sqrt{\cosh^2(2K) - 2\cosh(2K) + 2}\right). \tag{3.9}$$

It is possible to numerically calculate the zeros of the two-leg ladder using the full partition function given in (3.3) rather than looking at the degeneracy conditions for the eigenvalues. The full numerical calculation also gives information about the density of the zeros, since the number of zeros is fixed to be $N * N_L$ in the calculation. The $N * N_L$ zeros are consequently distributed over the features that would make contours in the thermodynamic limit. In the case of the Ising chain, these were evenly distributed over the circle, whereas in the case of Ising ladders, the distribution shows modulations along the contours. The result for the two-leg ladder is given in Figure 3.4. In contrast, if we look at the zeros obtained by using the degeneracy condition in

Figure 3.5, we cannot gain insight about the density of zeros on the contours since the number of zeros is not fixed when computing the eigenvalue crossings. The discretisation of the zeros is due to the calculation method, which imposes a grid on the complex plane on which we evaluate the difference between the two eigenvalues at each point. Comparing Figure 3.4 to Figure 3.5, we can see that the loci of the zeros in the thermodynamic limit are expected to coincide with each other.

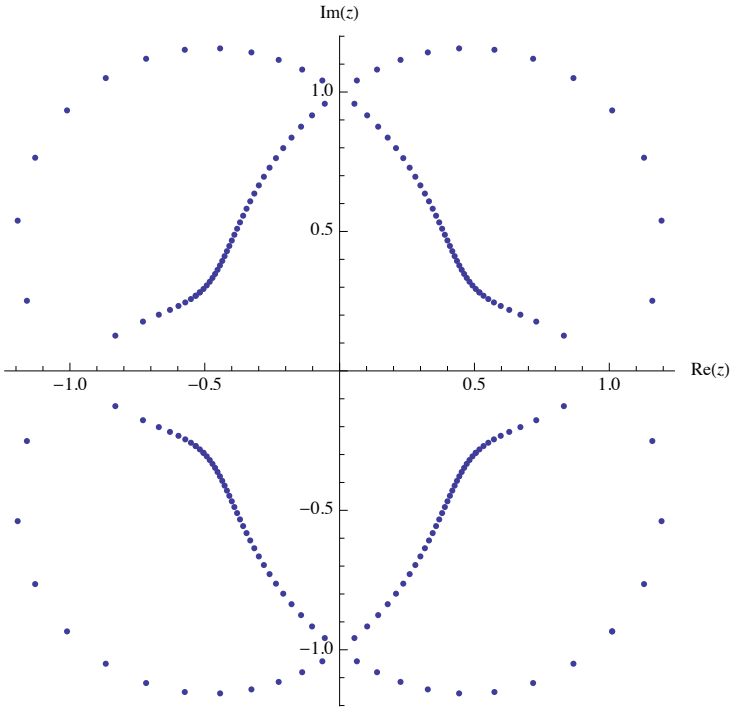

Figure 3.4: Zeros of the two-leg Ising ladder (i.e. $N_L = 2$) of length $N = 100$. These are calculated by setting the full partition function equal to zero and numerically finding the solutions of the equation.

To examine the features of Figure 3.5 more closely, we can zoom in on the crossing point on the real axis, i.e. the point $\Re(z) = 1$ and $\Im(z) = 0$, where $z = \tanh K$ as before. This can be seen in Figure 3.6. We notice that the contours come in linearly onto the real axis and we can calculate the crossing angles of the contours with the real axis. To do that, we take the zeros closest to the real axis and connect them to $z = 1$. Then we can compute the angles of impact. We find that the angles between the contours are constant, i.e. the angle between any two adjacent contours is $\frac{\pi}{2}$. The real axis halves the angle between two contours on each side and all contours impact at $\pm\frac{\pi}{4}$.

In fact, it can be shown analytically that the number of contours of zeros emanating from the point $z = 1$ is $2N_L$, which corresponds to N_L lines crossing at the point $z = 1$. The argument goes as follows:

Since the point $z = 1$ maps onto the zero temperature point, we can do a low temperature

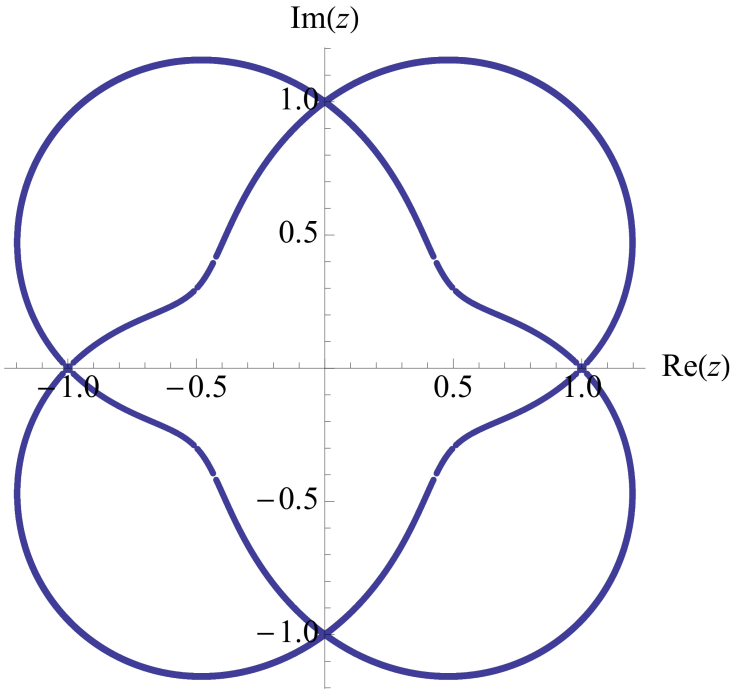

Figure 3.5: Zeros of the two-leg Ising ladder calculated via eigenvalue crossings. Notice that the number of contours ending in the critical points $z = \pm 1$ is equal to $2N_L$.

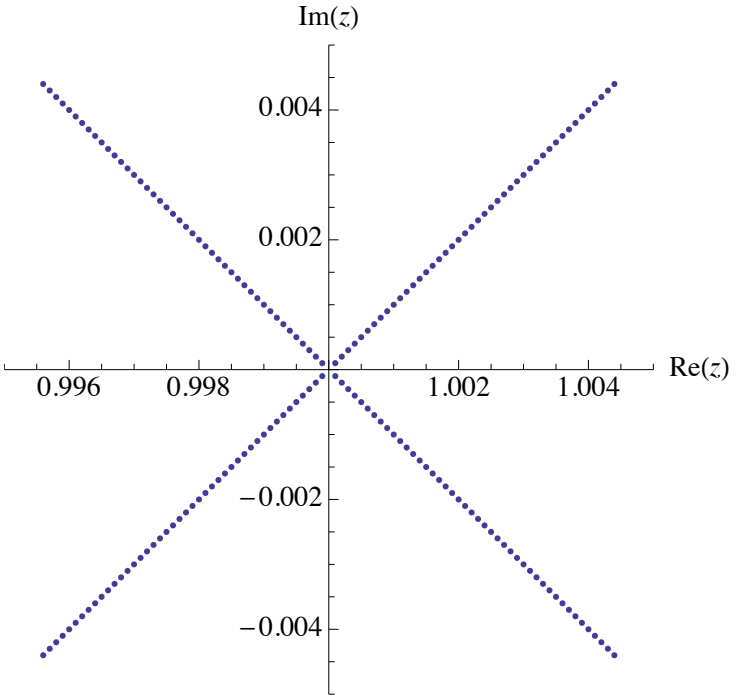

Figure 3.6: Zeros of the two-leg Ising ladder close to $z = 1$. Notice that they linearly approach the real axis at equidistant angles.

expansion of the partition function. In order to simplify the calculation, let us look at the ferromagnetic point and set the ground state energy of the ferromagnetic configuration to zero. The Hamiltonian then becomes

$$\mathcal{H} = -J \sum_{\langle ij \rangle} (\sigma_i \sigma_j - 1) \,. \tag{3.10}$$

When writing down the low-temperature partition function, we notice that the ground state adds a weight of $e^0 = 1$ to the partition function. The ground state is doubly degenerate since the configuration in which all spins point up has the same energy as the configuration in which all spins point down. The next lowest energy state which breaks the ground state degeneracy is the state which has two ferromagnetic sectors aligned in opposite directions. There are, in fact, smaller excitations to the ground state for ladders with three legs as we move away from zero temperature: single flipped spins. For example, if there is one down spin in a background of up spins, it has energy w^3 if it is located on the edge of the ladder, where $w = e^{-2\beta J}$, and w^4 if it is located within the ladder. However, we can consider these as spins that "dress" the ground state and for which we can renormalise the energy since they do not break the ground state degeneracy. The lowest energy excitation which does break the ground state degeneracy therefore corresponds to that of a domain wall separating the two ferromagnetic sectors. This domain wall has an energy of order w^{N_L}. We can therefore write

$$Z = 2 + f\left(w^{N_L}\right) \tag{3.11}$$

to first order in energy excitations. We can write down a simplified, low-temperature reduced transfer matrix, which looks like

$$\mathbf{T} = \begin{array}{c} \\ \text{FM}\uparrow \\ \text{FM}\downarrow \end{array} \begin{array}{c} \begin{array}{cc} \text{FM}\uparrow & \text{FM}\downarrow \end{array} \\ \begin{pmatrix} 1 & w^{N_L} \\ w^{N_L} & 1 \end{pmatrix} \end{array}. \tag{3.12}$$

The eigenvalues of the matrix are

$$\lambda_+ = 1 + w^{N_L} = 1 + d^{N_L} \qquad \text{and} \tag{3.13}$$

$$\lambda_- = 1 - w^{N_L} = 1 - d^{N_L}, \tag{3.14}$$

where $d = z - 1$ denotes the distance from the critical point. As we discussed above, the contours of zeros occur when $|\lambda_+| = |\lambda_-|$. To find the zeros, let us first take the absolute values of the eigenvalues, such that

$$|\lambda_+| = \left(1 + d^{N_L}\right)\left(1 + (d^*)^{N_L}\right) = 1 + |d|^{2N_L} + d^{N_L} + (d^*)^{N_L} \qquad \text{and} \tag{3.15}$$

$$|\lambda_-| = \left(1 - d^{N_L}\right)\left(1 - (d^*)^{N_L}\right) = 1 + |d|^{2N_L} - d^{N_L} - (d^*)^{N_L} \,. \tag{3.16}$$

We can equate these to obtain the condition

$$d^{N_L} + (d^*)^{N_L} = 0 \tag{3.17}$$

$$\therefore \quad d^{N_L} = -(d^*)^{N_L} \tag{3.18}$$

$$\therefore \quad \left(\frac{d}{d^*}\right)^{N_L} = -1. \tag{3.19}$$

Finally, we can identify $d = Re^{i\psi_n}$, such that

$$e^{2i\psi_n N_L} = -1 \tag{3.20}$$

$$= e^{i\pi(2n+1)} \quad \text{and} \tag{3.21}$$

$$\psi_n = \frac{\pi}{2N_L}(2n+1). \tag{3.22}$$

This means that the number of contours of zeros crossing at the $z = 1$ point is the same as the number of legs on the ladder. In addition, the angles between the contours are the same. This means that, as we increase the number of legs on the ladder, we expect the region around $z = 1$ to fill in with Fisher zeros. In fact, we will see exactly this behaviour in Sections 3.3 and 3.4.

3.3 Zeros of the 3-leg Ising ladder

Taking the calculation a small step further, we increase the number of legs of the ladder to three, as shown in Figure 3.7.

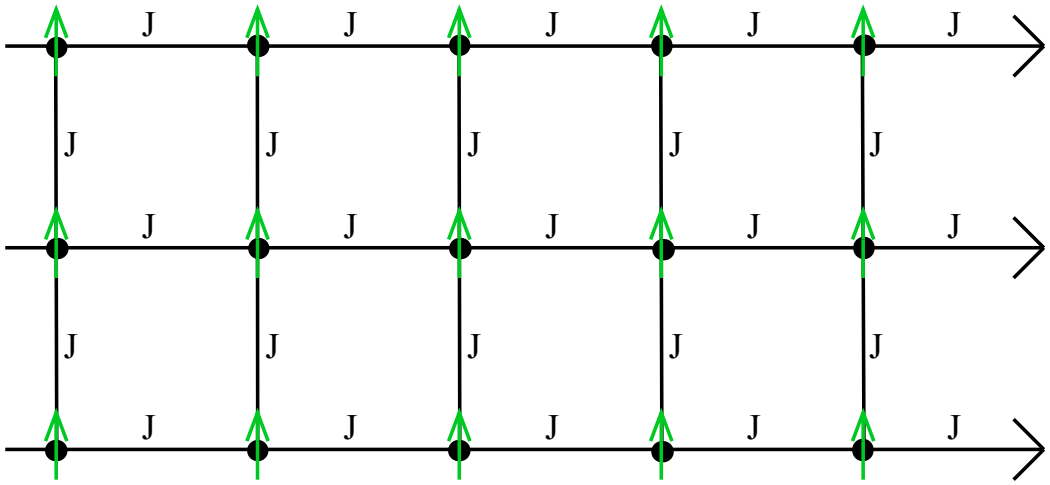

Figure 3.7: The three-leg Ising ladder in a ferromagnetic ground state.

In the 3-leg ladder, each rung is a tensor product of three single spin states and the resulting transfer matrix is 8×8. To construct the transfer matrix, we again create a symmetric unit cell with which the whole ladder can be generated. This unit cell is shown in Figure 3.8.

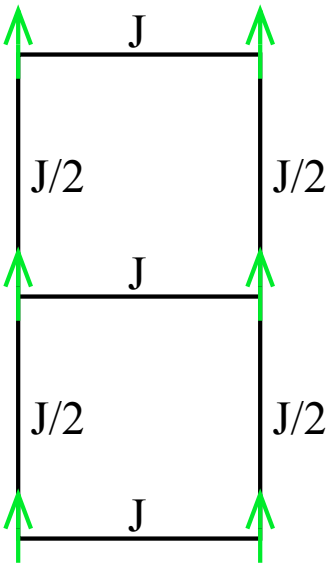

Figure 3.8: The symmetric unit cell of the three-leg ladder. Note that the coupling strength on the rungs is halved to avoid double counting.

We can then write down the transfer matrix for the three-leg ladder as

$$\mathbf{T}_3 = \begin{array}{c} \\ \uparrow\uparrow\uparrow \\ \uparrow\uparrow\downarrow \\ \uparrow\downarrow\uparrow \\ \uparrow\downarrow\downarrow \\ \downarrow\uparrow\uparrow \\ \downarrow\uparrow\downarrow \\ \downarrow\downarrow\uparrow \\ \downarrow\downarrow\downarrow \end{array} \begin{array}{c} \begin{array}{cccccccc} \uparrow\uparrow\uparrow & \uparrow\uparrow\downarrow & \uparrow\downarrow\uparrow & \uparrow\downarrow\downarrow & \downarrow\uparrow\uparrow & \downarrow\uparrow\downarrow & \downarrow\downarrow\uparrow & \downarrow\downarrow\downarrow \end{array} \\ \begin{pmatrix} e^{5K} & e^{2K} & e^{K} & 1 & e^{2K} & e^{-K} & 1 & e^{-K} \\ e^{2K} & e^{3K} & e^{-2K} & e^{K} & e^{-K} & 1 & e^{-3K} & 1 \\ e^{K} & e^{-2K} & e^{K} & 1 & e^{-2K} & e^{-5K} & 1 & e^{-K} \\ 1 & e^{K} & 1 & e^{3K} & e^{-3K} & e^{-2K} & e^{-K} & e^{2K} \\ e^{2K} & e^{-K} & e^{-2K} & e^{-3K} & e^{3K} & 1 & e^{K} & 1 \\ e^{-K} & 1 & e^{-5K} & e^{-2K} & 1 & e^{K} & e^{-2K} & e^{K} \\ 1 & e^{-3K} & 1 & e^{-K} & e^{K} & e^{-2K} & e^{3K} & e^{2K} \\ e^{-K} & 1 & e^{-K} & e^{2K} & 1 & e^{K} & e^{2K} & e^{5K} \end{pmatrix} \end{array}. \tag{3.23}$$

As for the case of the two-leg ladder, we diagonalise the matrix and compute its eigenvalues. Since the matrix has 8 eigenvalues, the partition function can be written as

$$Z = \lambda_1^N + \lambda_2^N + \lambda_3^N + \lambda_4^N + \lambda_5^N + \lambda_6^N + \lambda_7^N + \lambda_8^N. \tag{3.24}$$

The eigenvalues of the three-leg ladder are easily calculated in principle, but the algebraic expressions are unfortunately rather long and tedious. Therefore it does not seem to add any

relevant information to print them here.

In the case of the three-leg ladder we have to use the Beraha-Kahane-Weiss theorem to compute the locations of the zero contours since the number of eigenvalues makes it impossible to solve for the zero contours using the full partition function. A plot of the zeros obtained by the eigenvalue-crossing method is given in Figure 3.9.

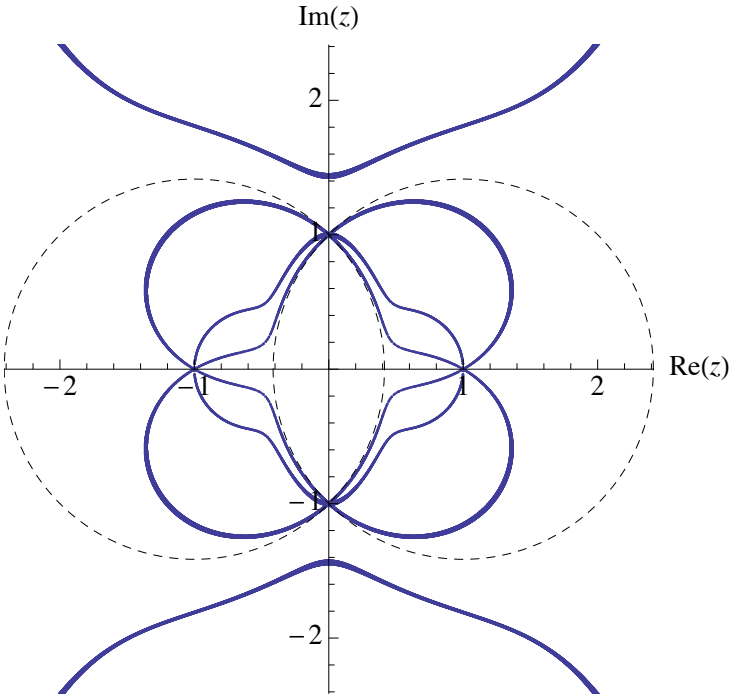

Figure 3.9: Zeros of the three-leg Ising ladder calculated via eigenvalue crossings. We added the Fisher circles from Figure 3.1 (dashed) for comparison purposes. The number of contours ending in the critical points $z = \pm 1$ is equal to $2N_L$ and the contours seem to fill in the areas inside one of the Fisher circles but not inside the other circle. There are additional features outside the Fisher circles, the meaning of which we cannot yet explain, but they are far away from the real line and are therefore not expected to significantly influence the physical behaviour. Note that the density variation does not have any meaning for numerical results obtained via eigenvalue crossings. The discretisation is due to the grid on which we are evaluating the difference between the eigenvalues.

It is interesting to further analyse the region around the zero temperature ferromagnetic point. At that point, the contours cross the real axis at equidistant angles. To further illustrate that point, let us numerically calculate zeros around the ferromagnetic point. Such a zoom-in picture around $z = 1$ is shown in Figure 3.10. We numerically analysed the impact angles onto the real axis, by calculating the slope between the zeros closest to $z = 1$ and the point $z = 1$ and found them to be approximately $\frac{\pi}{6}$, $\frac{\pi}{2}$, and $\frac{5\pi}{6}$. Interestingly, if we consider the literature and apply the criteria for transitions of different order, we notice that the middle contour represents a first order transition, according to the theory, and the other two contours represent higher order phase transitions [48].

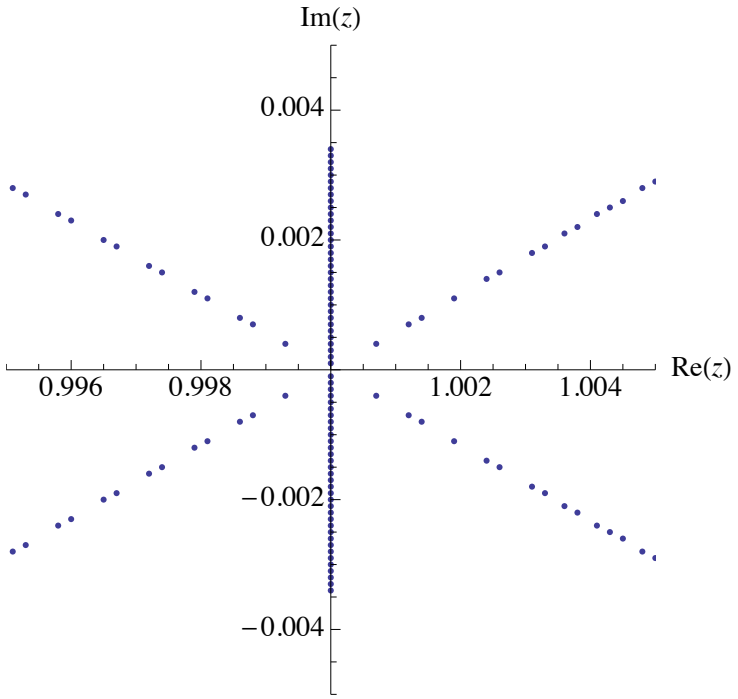

Figure 3.10: Zeros of the three-leg Ising ladder close to $z = 1$ obtained via eigenvalue crossings. The zero contours cross the real axis at angles $\frac{\pi(2n+1)}{6}$ with $n = 0, 1, 2$. The angle of impact of the middle contour onto the real axis indicates that a first order transition takes place at $z = 1$, whereas a higher order transition is implied by the impact angles of the remaining two contours.

3.4 Zeros of larger ladders

As we increase the ladder size, it is no longer useful to display the transfer matrices explicitly here since they become rather large. However, we can still follow the procedure outlined above in order to obtain the zero contours in the complex z-plane.

In this section we will show the results for larger ladders. In order to achieve a better resolution, we concentrated the zero-finding procedure onto the upper left quadrant. This does not result in any information loss, since the zeros are symmetric about both axes. Examples of differently sized ladders are shown in Figures 3.11, 3.13, and 3.15.

The angles ψ_n at which these contours cross the real axis behave as

$$\psi_n = \frac{\pi}{2N_L}(1 + 2n) \quad \text{with} \quad n = 0, \ldots, N_L - 1. \tag{3.25}$$

We have seen both analytically and numerically that the number of contours crossing at the point $z = 1$ is equal to the number of legs on the ladder. As we increase the number of legs, we fill up the space between the innermost and the outermost contour. Additionally, these two contours (i.e. the innermost and the outermost) close in on the real axis as the number of contours increases. From this we can hypothesise that in the full two-dimensional model, the contours of zeros will be infinitely close to the real axis and the zeros will fill an area in complex

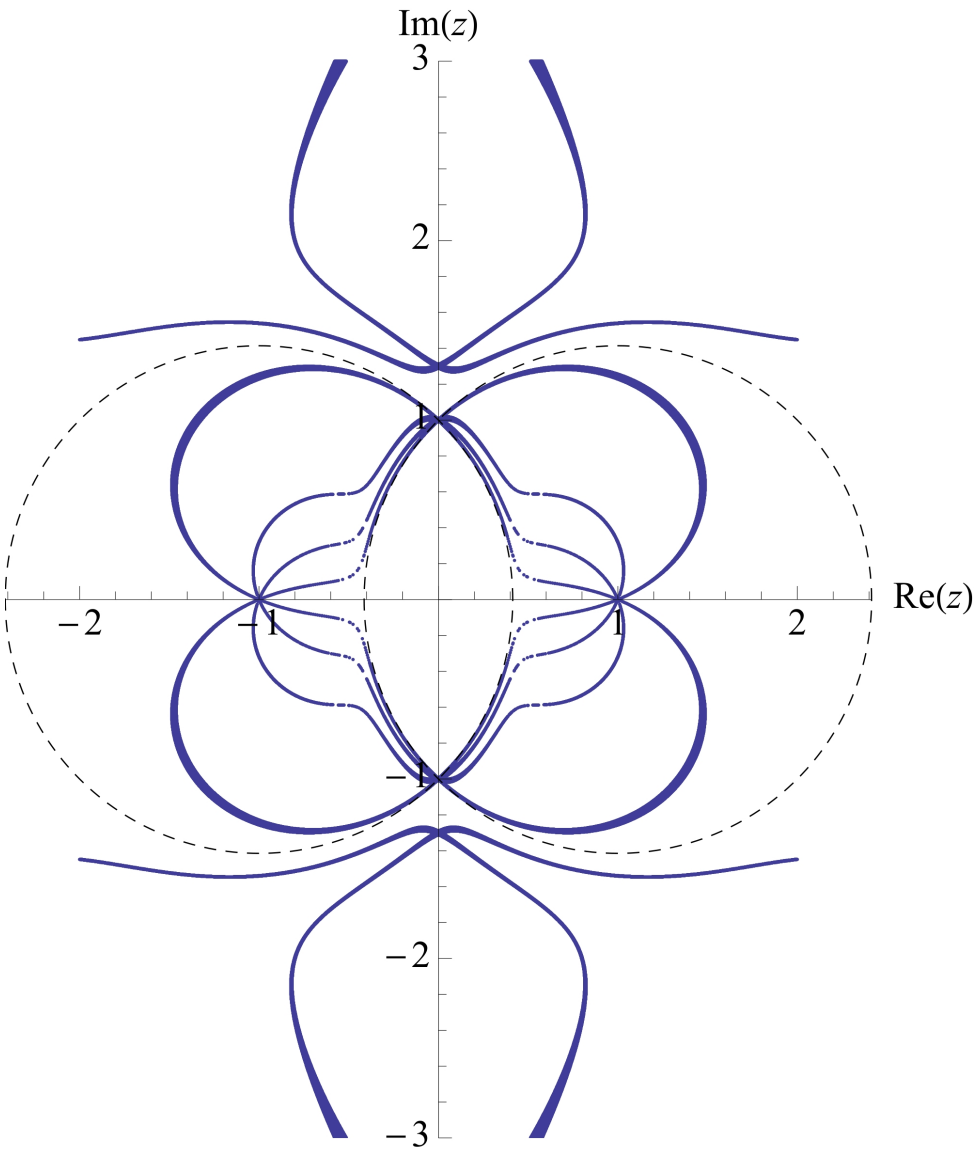

Figure 3.11: Zeros of the four-leg Ising ladder calculated via eigenvalue crossings. Due to limitations of calculation power, we calculated the zeros in the upper right quadrant and then used the symmetry properties to create the full picture after checking that they still exist at low resolution. We also added the Fisher circles (dashed) for illustration purposes. Notice again, that the number of contours ending in the critical points $z = \pm 1$ equals $2N_L$.

z-space. The area that is filled up by the zeros looks as if it will be the region that is inside one Fisher circle but not inside both Fisher circles (i.e. the symmetric difference between the two Fisher circles).

It seems as if this result would contradict Fisher's result that the only contours of Fisher zeros for the isotropic Ising model in two dimensions are the two Fisher circles. However, we think that the Fisher result arises due to a different order of taking the limits. Fisher's approach is to take the partition function in the thermodynamic limit, which only contains the maximal

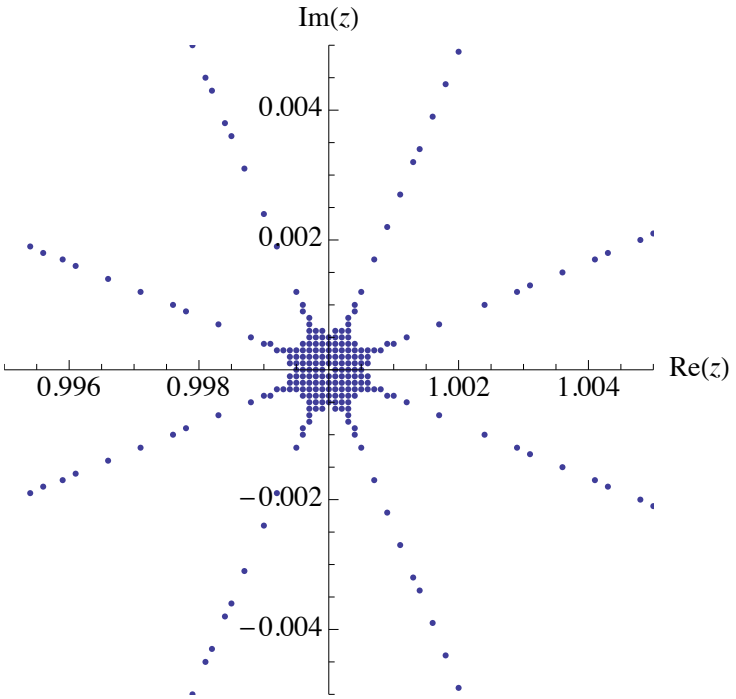

Figure 3.12: Zeros of the four-leg Ising ladder close to $z = 1$. Notice that there are $2N_L$ contours of zeros ending at the critical point $z = 1$ coming in at angles $\frac{\pi(2n+1)}{8}$. Also there is a finite area around the critical point in which the eigenvalues are degenerate, or very close to degenerate.

eigenvalues, and calculate the Fisher zeros from there. In our approach, we keep the exact partition function containing all the eigenvalues and notice a different limiting behaviour of the zeros.

This means that in the two-dimensional model, we have two different kinds of holomorphic regions: those which were already holomorphic in the quasi-one-dimensional models (i.e. the ladders) and those which became holomorphic due to the "vanishing" of the Fisher zeros in the thermodynamic limit. In those regions, we can see spiral order with a continuously evolving **q**-vector as the region is traversed. These spiral aspects can only be seen if we take the thermodynamic limit while keeping more than just the maximal eigenvalues. Therefore they cannot be seen in the Fisher treatment.

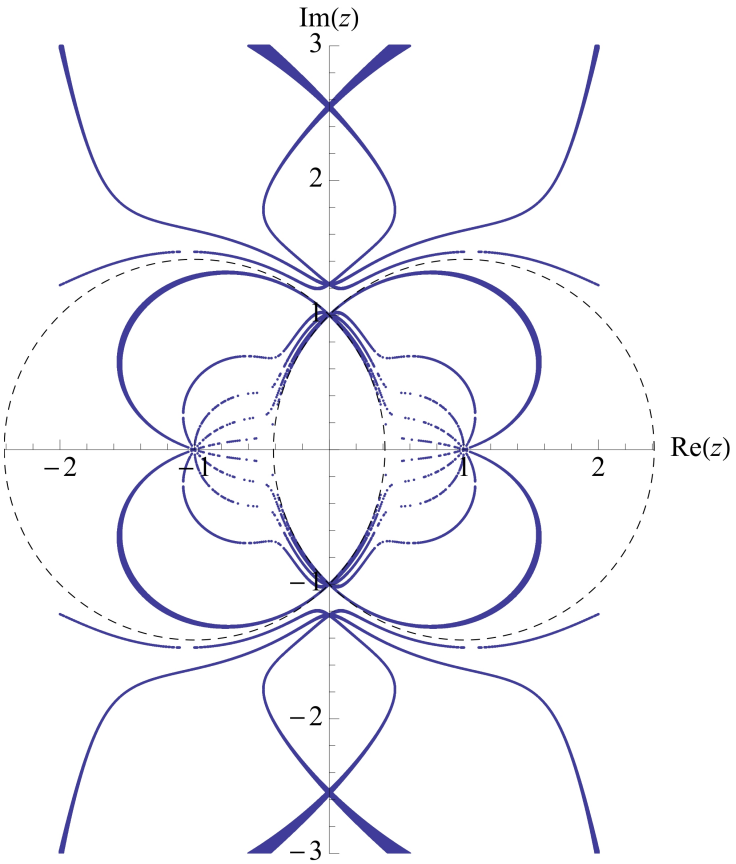

Figure 3.13: Zeros of the five-leg Ising ladder calculated via eigenvalue crossings. Due to limitations of calculation power, we calculated the zeros in the upper right quadrant and then used the symmetry properties to create the full picture. The Fisher circles are added as dashed lines. Notice again, that the number of contours ending in the critical points $z = \pm 1$ equals $2N_L$.

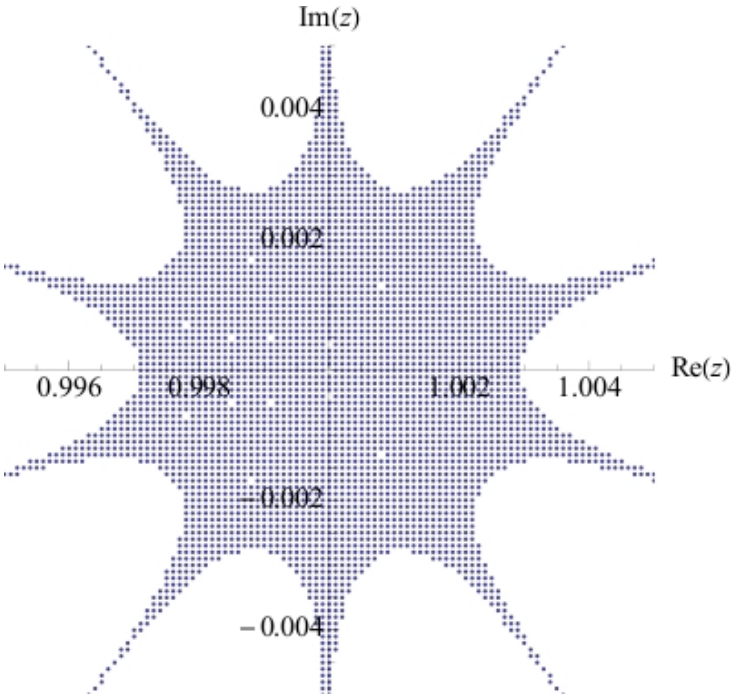

Figure 3.14: Zeros of the five-leg Ising ladder close to $z = 1$ obtained via eigenvalue crossings. Note that the square lattice pattern of discrete zeros around $z = 1$ is due to the grid of points sampled. Also note that there is a finite area between the contours in which $|\lambda_1| - |\lambda_2| \to 0$.

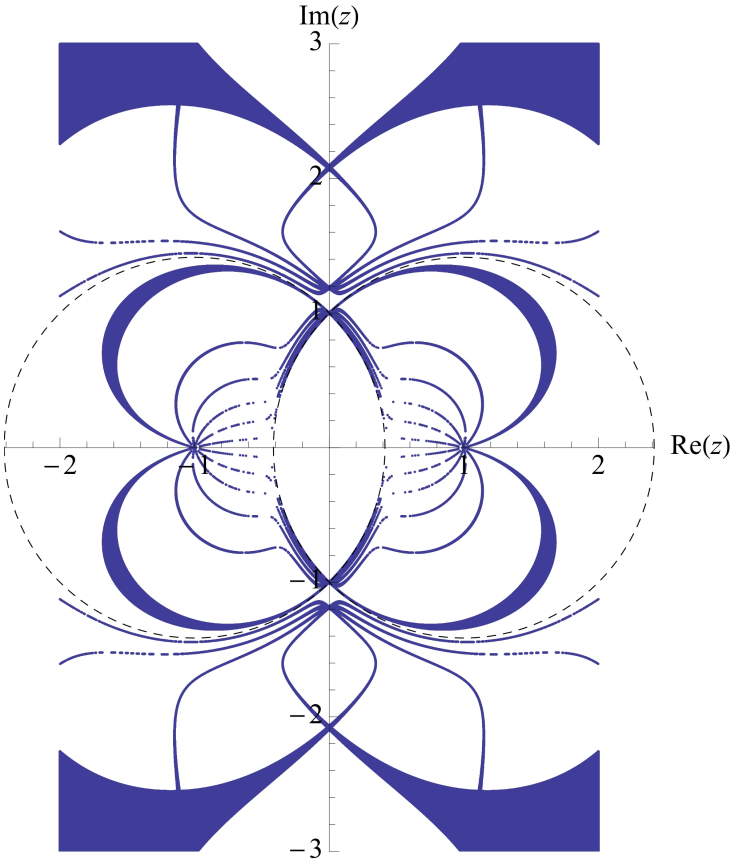

Figure 3.15: Zeros of the six-leg Ising ladder calculated via eigenvalue crossings. Due to limitations of calculation power, we calculated the zeros in the upper right quadrant and then used the symmetry properties to create the full picture. Once again, the number of contours ending in the critical points $z = \pm 1$ equals $2N_L$. The Fisher circles are added as dashed lines. Note that the features which look like there is an area of zeros around $z \approx 1.5 + 2.8i$ are not truly areas. If we reduce the cutoff value of $|\lambda_1| - |\lambda_2|$, only the edges of the area survive as contours of zeros.

3.5 Ladders with periodic boundary conditions on the rungs

As we have seen in the Ising chain, there was some boundary condition dependent variation of the Fisher zeros. The zeros are more fragile towards a change of boundary conditions the further they are away from the real axis since there is no physical reason due to which they should correspond to open boundary condition zeros. However, the analytical proof that the number of contours crossing at the point $z = 1$ is equal to the number of legs on the ladder is still valid for periodic boundary conditions since the statistical weight of a straight domain wall excitation does not change.

However, we expect the behaviour around the real axis between $z = -1$ and $z = 1$, i.e. around all those temperatures that map onto the real temperature, to be similar to the case of open boundary conditions. An exception to this is the antiferromagnetic side of the real axis for ladders with an odd number of legs. Here frustration effects play a role in the case of periodic boundary conditions: on each rung one of the bonds cannot be satisfied, even in the ground state. These speculations are confirmed by Figures 3.16 and 3.17. In Figure 3.17, the number of legs are even, therefore the behaviour of the zeros around both the ferromagnetic point and the antiferromagnetic point are similar to the case of open boundary conditions on the rung (shown in Figure 3.11), even though there are deviations in the zero patterns further away from real z. The frustration effect on ladders with an odd number of legs can clearly be seen on the antiferromagnetic side in Figure 3.16, which is no longer a symmetric image of the zeros on the ferromagnetic side.

To see whether there is any difference in the behaviour close to the real axis, we also zoomed in on the ferromagnetic critical point. The corresponding figure can be seen in Figure 3.18. As expected, the angles of impact onto the real line correspond to those in the case of open boundary conditions.

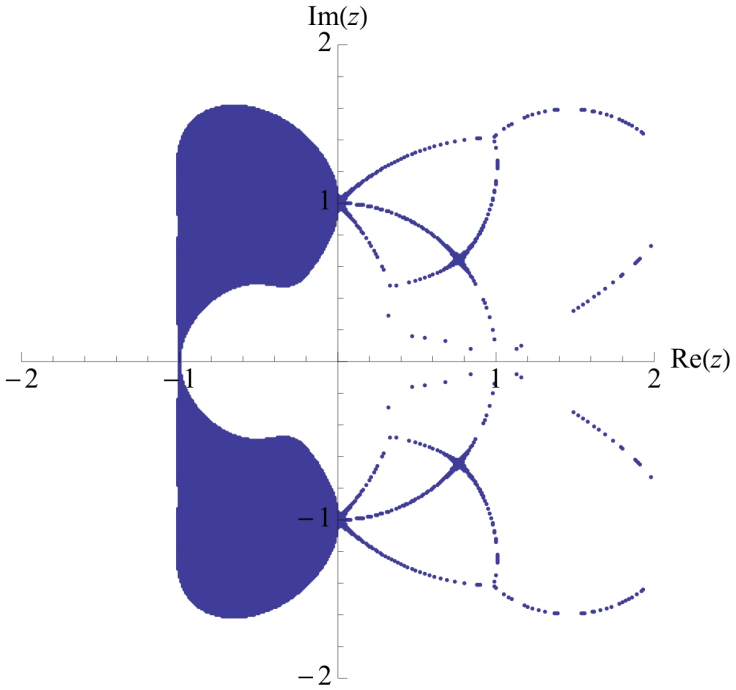

Figure 3.16: Zeros of the three-leg Ising ladder with periodic boundary conditions. The antiferromagnetic side is frustrated due to the boundary conditions, which leads to an asymmetry of the zeros about the imaginary axis. The further away we get from the real axis on the ferromagnetic side, the more the zeros change from the zeros found for open boundary conditions (see Figure 3.9). We think that this is due to frustration being introduced due to spiral correlation functions in the complex plane.

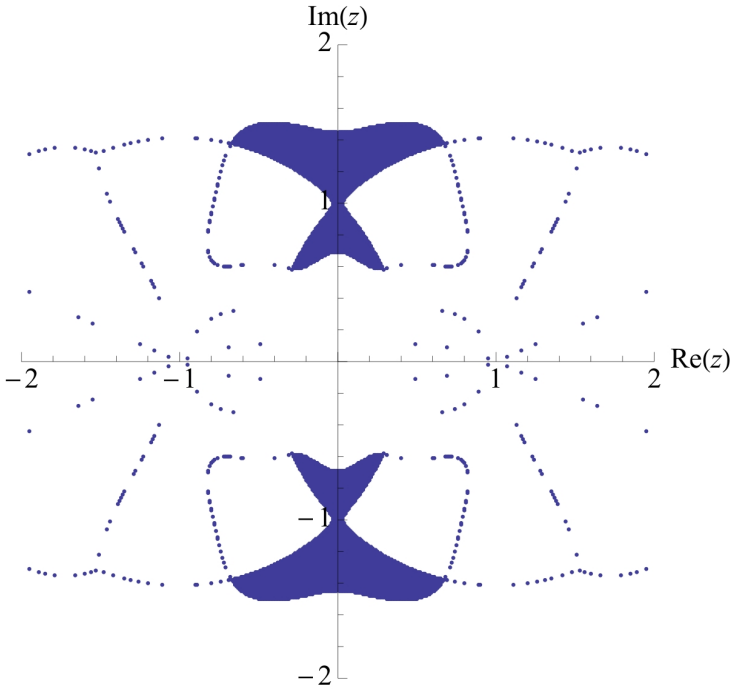

Figure 3.17: Zeros of the four-leg Ising ladder with periodic boundary conditions. Due to an even number of legs, there is no frustration effect on the antiferromagnetic side. The behaviour of the zeros close to the real axis corresponds to the behaviour close to the real axis for open boundary conditions. Once again frustration effects occur as we move away from the real axis, which results in locations of zeros that differ from those in Figure 3.11.

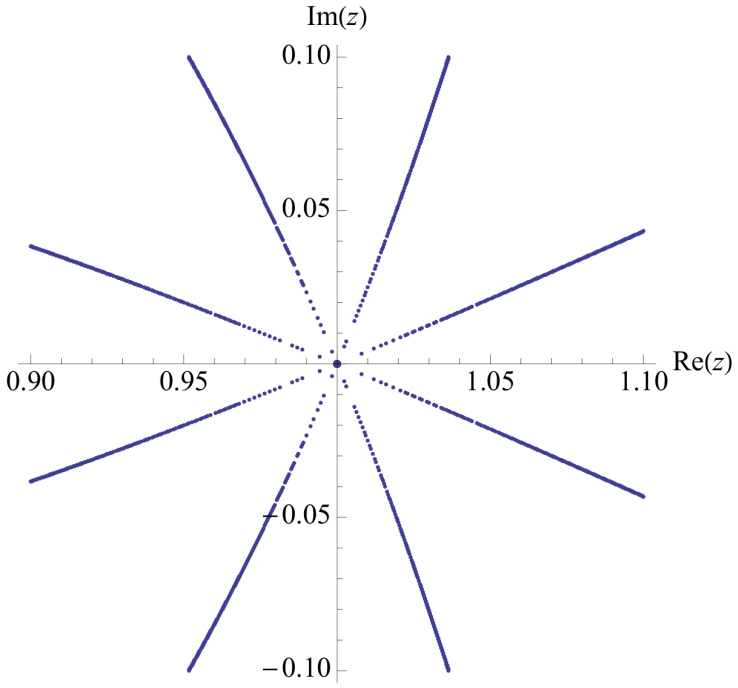

Figure 3.18: Zeros of the four-leg Ising ladder with periodic boundary conditions around the critical point. Note that the angles at which the contours cross the real axis are the same as those in Figure 3.14.

3.6 Correlation functions at complex temperature

We have seen in Section 2.3 that the correlation function C_j of the Ising chain can only display long-range density-wave order if it is evaluated at a point in the complex plane that lies on the contour containing the partition function zeros in the thermodynamic limit. If C_j is evaluated just outside that contour, we can see spiral order with a decaying amplitude. Let us now check whether the correlation function on the two-leg ladder displays similar behaviour.

Since we now have a ladder with two legs and consequently a 4×4 transfer matrix, we can no longer just use the Pauli-matrix $\boldsymbol{\sigma}_z$ to evaluate the correlation function. Instead we use the direct products of $\boldsymbol{\sigma}_z$ with the 2×2 identity matrix. The two resulting matrices correspond to fixing a spin on the upper or the lower leg of the ladder respectively such that

$$\boldsymbol{\sigma}_1 = \begin{pmatrix} 1 & 0 & 0 & 0 \\ 0 & 1 & 0 & 0 \\ 0 & 0 & -1 & 0 \\ 0 & 0 & 0 & -1 \end{pmatrix}, \tag{3.26}$$

fixes a spin on the leg that corresponds to $j = 1$ and

$$\boldsymbol{\sigma}_2 = \begin{pmatrix} 1 & 0 & 0 & 0 \\ 0 & -1 & 0 & 0 \\ 0 & 0 & 1 & 0 \\ 0 & 0 & 0 & -1 \end{pmatrix} \tag{3.27}$$

fixes a spin on leg that corresponds to $j = 2$.[1]

Let us now calculate the correlation function between two sites on the same leg of the ladder

$$C_j = \frac{\mathrm{Tr}\left(\boldsymbol{\sigma}_1 \mathbf{T}^j \boldsymbol{\sigma}_1 \mathbf{T}^{N-j}\right)}{\mathrm{Tr}\left(\mathbf{T}^N\right)} \tag{3.28}$$

and evaluate it at different points in the complex z-plane. As in the case of the Ising chain, let us choose two points in the complex z-plane on which we evaluate C_j and plot it as a function of j, one of which lies on the contour of zeros and one of which lies near the contour. These points are shown in Figure 3.20 and a plot of the real part of the correlation function as a function of j is shown in Figure 3.19. In the left panel, we can see a plot of the correlation function evaluated at a point on the inner contour of the two-leg ladder. It shows long range order as a function of lattice index j, even though the amplitude of the correlation function is less than one. On the right panel, C_j is evaluated at a point slightly away from the inner contour and we can see the real part of C_j decaying as we increase the distance between site 0 and site j. The same effect can be seen for the outer contour on the two-leg ladder. As we can see, long-range order solely exists on the contours of Fisher zeros, whereas the regions away from the contours are

[1] This choice is arbitrary, we could just as well swap the labels.

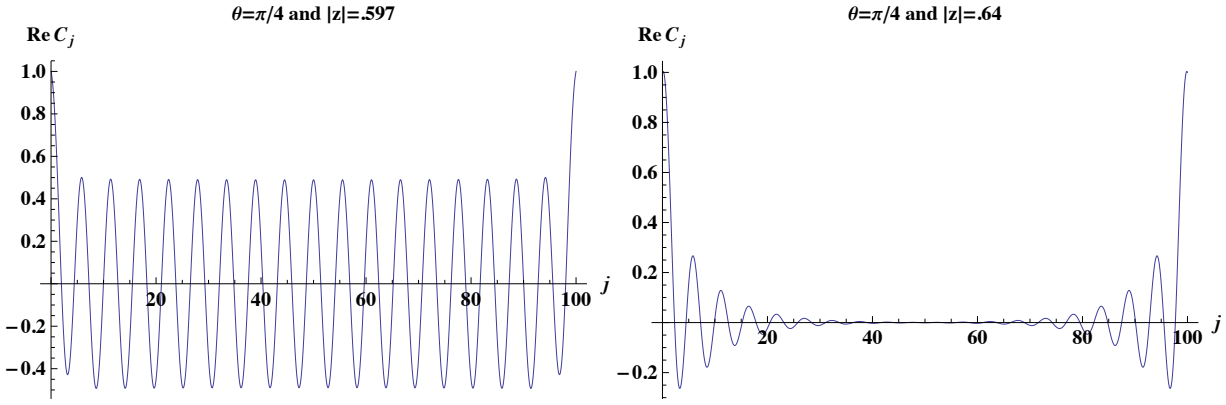

Figure 3.19: The real part of the correlation function C_j as a function of the lattice index j on the inner contour of the two-leg ladder and just above the inner contour.

characterised by decaying correlations.

This seems to stand in contradiction to the statement that the regions between contours of Fisher zeros correspond to different phases [48]. Following that statement, one would expect the region between the two contours of Fisher zeros to display the signatures of an ordered phase. Instead, the long-range order only appears on the contours themselves, which makes sense when we take the Beraha-Kahane-Weiss theorem into consideration. According to the theorem, the contours occur when the two dominant eigenvalues become degenerate. The degeneracy condition also lies at the heart of diverging correlation length. This is due to the fact that the correlation function for transfer matrix problems is of the form (with $\lambda_1 \equiv \lambda_{\max}$)

$$\langle S_0 S_j \rangle \sim a_1 \left(\frac{\lambda_2}{\lambda_{\max}} \right)^j + a_2 \left(\frac{\lambda_3}{\lambda_{\max}} \right)^j + a_3 \left(\frac{\lambda_4}{\lambda_{\max}} \right)^j \tag{3.29}$$

in the case of the two-leg ladder. These exponentially decay with j unless $\lambda_{\max}$ and any of the other eigenvalues have the same absolute value. Since this is the same condition as the Beraha-Kahane-Weiss condition for Fisher zeros, it seems natural that the long-range order should occur on the same contours on which Fisher zeros are present. So how would this affect a model in which there is a nonzero transition temperature and a real ordered phase along the real line rather than just one point of long-range order on the real line?

Our data suggests that there should be several dominant degenerate eigenvalues which cause the long-range order. In principle, following Beraha-Kahane-Weiss, this would lead to partition function zeros for lines on which the eigenvalues are degenerate. Most likely, the part of the real axis which shows long-range order and eigenvalue degeneracy can be extended into the complex plane such that there would be a finite region of degenerate eigenvalues. In this case, the Beraha-Kahane-Weiss theorem no longer applies. We think this is due to a sensitivity of taking the limits. As we have seen in the one-dimensional chain, we can take two thermodynamic limits: one in which we obtain a contour of zeros and one in which we obtain a contour of long-range order. Therefore, we believe that only the edges of such a region of zeros would show up

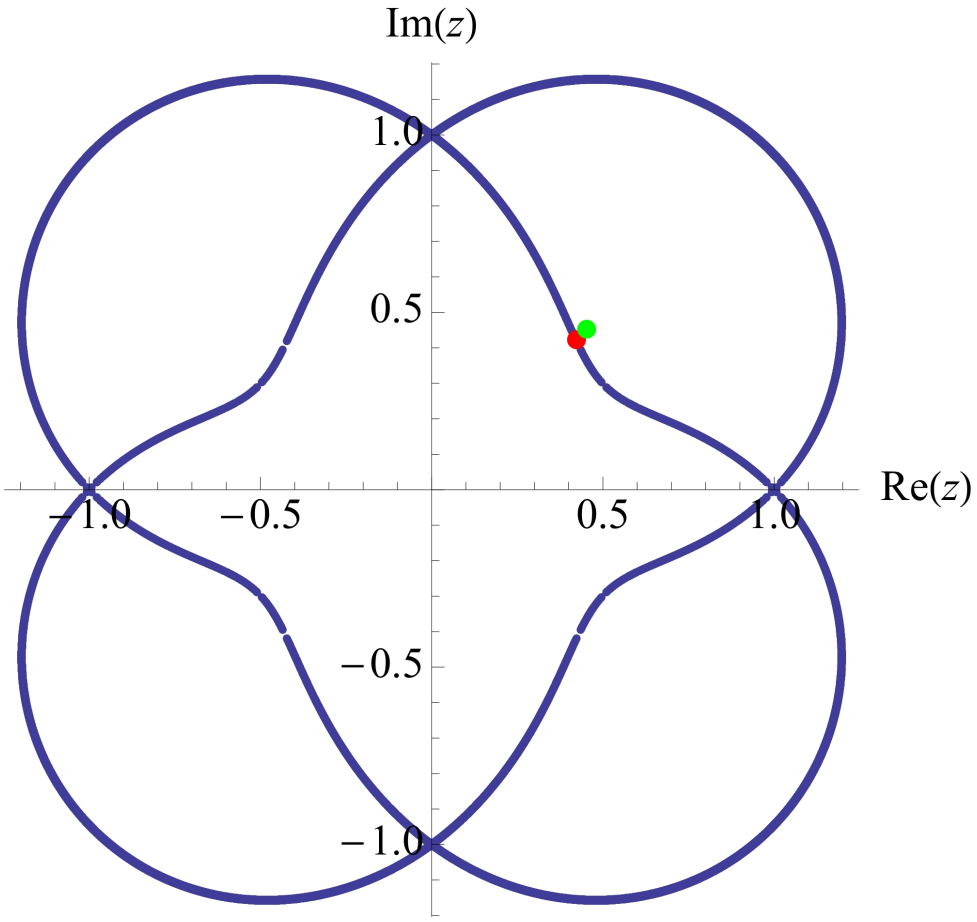

Figure 3.20: Locations where $\Re(C_j)$ is evaluated in Figure 3.19. The red point corresponds to $\theta = \frac{\pi}{4}$ and $|z| = .597$ and the green point corresponds to $\theta = \frac{\pi}{4}$ and $|z| = .64$.

in a model in which the thermodynamic limit has been taken, such as the full two-dimensional Ising model.

3.7 Heat flow and first order transitions

Let us now examine, whether there is some form of "latent heat" attached to crossing a contour in the case of an Ising ladder. In order to do that, let us return to the calculation of energy differences shown in chapter 2.4.

We can identify the dominant eigenvalue in each region and calculate $\frac{\Delta E}{N}$ on the contours using (2.64). A plot of the real and imaginary parts of $\frac{\Delta E}{N}$ can be seen in Fig. 3.22. We can see that there is indeed an internal energy jump, and therefore a latent heat, anywhere on the contour with a complex K. The transition can therefore be classified as first order. Once the contour touches the real line, the latent heat goes to zero and the transition becomes second order. Note that the real part of the latent heat remains essentially zero up to some critical angle which appears to correspond to the angle of the 'kink' in the inner contour of Fisher zeros, which is circled in red in Fig. 3.21.

We think that this behaviour is due to the ladders being quasi-one-dimensional. Close to the real axis, the zeros are still different from the two-dimensional model, but the features above the "kink" are already approaching the two-dimensional Fisher contours. Therefore the latent heat is still purely imaginary as we cross the contours below the "kink", resembling the one-dimensional behaviour, and picks up a real part as we approach those parts of the contour that resemble the two-dimensional behaviour.

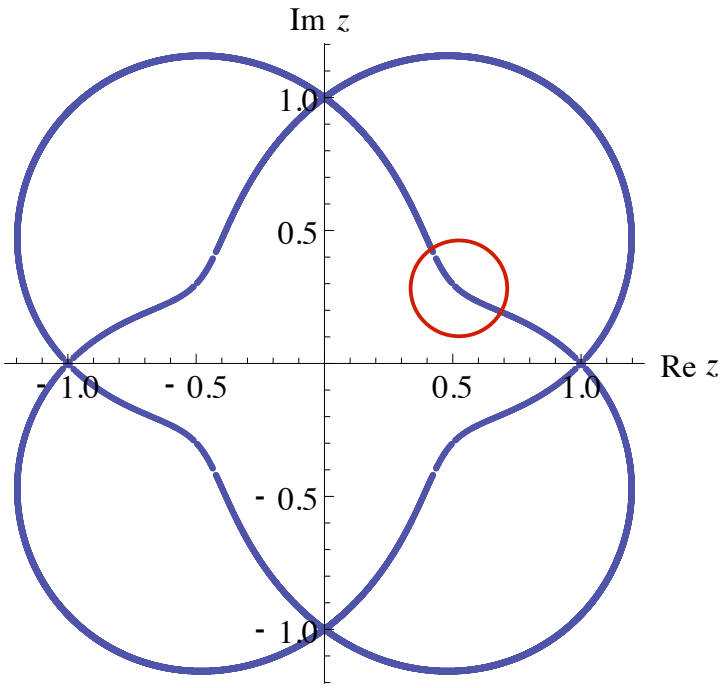

Figure 3.21: Contour of zeros of the two-leg ladder. The red circle indicates the 'kink' in the inner contour.

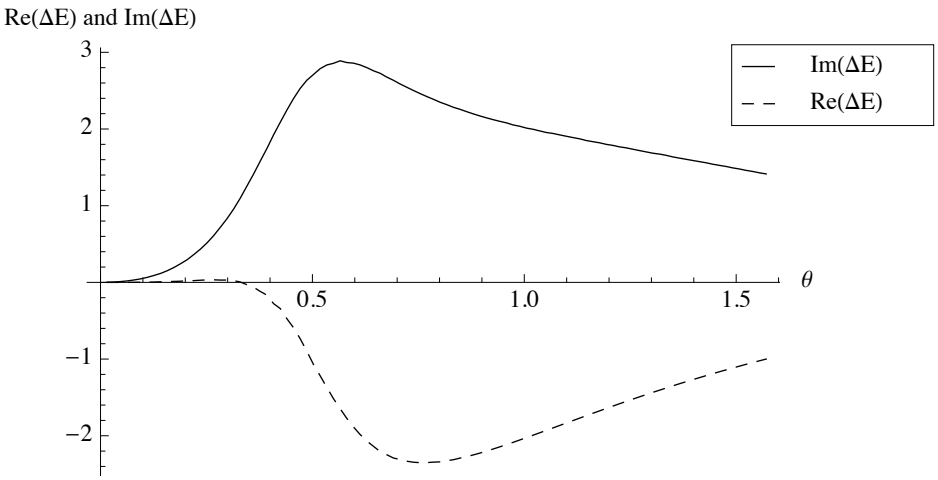

Figure 3.22: Real and imaginary parts of the jump in the internal energy as the inner contour of the two-leg ladder zeros is crossed as a function of the angle in the z-plane.

3.8 Summary of the findings and open questions

After looking at the behaviour of the partition function zeros for ladders of different widths, we have seen several indications of an area of zeros emerging in the two-dimensional Ising model. The first indication was the fact that more and more zeros seem to accumulate in the area between the Fisher circles as we increase the width of the ladder. We proved that the number of contours ending at the critical point is actually equal to twice the number of legs on the ladder, which indicates an area of co-dominant eigenvalues around the critical point in the thermodynamic limit. The second indication is that long-range order is closely connected to the locations of the zeros. In fact, we have seen that long-range order only exists along those contours on which we find the partition function zeros. We know that there is long-range order in the two-dimensional model for a stretch along the real line as well as co-dominant eigenvalues along the real axis of the two-dimensional model [80].

The question now remains why Fisher does not report zeros inside the Fisher circles or at least zeros along the part of the real axis on which there is long-range order [34]. We suggest that the problem is rather sensitive to taking the thermodynamic limit, similar to the case of the Ising chain in which the zeros disappeared if we took the thermodynamic limit of the long-range ordered points. Due to the fact that Fisher used the exact partition function after the thermodynamic limit had been taken [34], it seems probable that this is where the reason lies.

Other questions that remain and which we don't fully understand yet are

- How can we extract the order of the transition from the impact angles in the case of several contours crossing the critical point?
- How does the amplitude of the correlation function behave in the case of larger ladders? We can see that there is long-range order on the contours, but the amplitude is smaller than in the case of the Ising chain. In fact, it seems to be exactly half of the amplitude of the chain.
- What do the features of degenerate eigenvalues far away from the real axis (i.e. above $\Im(z) = 1$) mean and how do they behave in the thermodynamic limit?

Chapter 4

The 2d Ising model

4.1 Review of the Kasteleyn method

The Ising model in two dimensions is one of the most extensively studied models in statistical mechanics. This is largely due to the fact that it is one of the few exactly solvable models that display a phase transition at finite temperature $T = T_c$ [1]. The two-dimensional Ising model is defined by the interaction Hamiltonian

$$H = -\sum_{\langle ij \rangle} \left(J^v \sigma_{i,j}\sigma_{i,j+1} + J^h \sigma_{i,j}\sigma_{i+1,j} + h\sigma_{i,j} \right), \tag{4.1}$$

where we sum over the nearest neighbours on a rectangular lattice of horizontal length L^h and vertical length L^v with open boundary conditions. The coupling on the horizontal bonds is J^h and the coupling on the vertical bonds is J^v. Here, we will only consider the case of zero external field (i.e. $h = 0$) and an isotropic lattice on which $J^h = J^v = J$ and $L_h = L_v = L$, such that

$$H = -J \sum_{\langle ij \rangle} \left(\sigma_{i,j}\sigma_{i,j+1} + \sigma_{i,j}\sigma_{i+1,j} \right), \tag{4.2}$$

where we sum over the nearest neighbours on a square lattice with open boundary conditions. This is the same Hamiltonian as given in (3.1) with $N = N_L = L$, i.e. the Hamiltonian for a "ladder" with as many legs as rungs. Solving the full two-dimensional Ising model in which $L \to \infty$ by the transfer matrix method used in the previous chapters would involve diagonalising an $2^L \times 2^L$ matrix where L is infinite.

The existence of long-range order at nonzero temperature was first proven by Peierls [82] in 1936. The critical temperature of the transition was found in 1941 by Kramers and Wannier [83, 84]. Following from that, Lars Onsager [74] discovered in 1944 that exact computations can be done in the case of $h = 0$ and computed the free energy of the model for open boundary conditions.

[1] Another solvable model with a finite T_c is for example a special case of the Haldane-Shastry model [81].

In the Ising model, long-range order at $T \geq 0$ does not contradict the Mermin Wagner theorem [85, 86, 87], which claims that long-range order is not possible in systems in one or two dimensions at non-zero temperature. It only applies to models with a continuous symmetry for which the long-range ordering involves the breaking of that symmetry. The up-down symmetry of the Ising model is a discrete symmetry, which allows for long-range order at nonzero temperatures.

In addition, the Ising model has been solved in different ways, one of them using the fact that the Ising model can be reduced to a tiling problem of dimers on a decorated lattice. This was first introduced by Kasteleyn [73] in 1963 and further developed by Fisher [72] using results from dimer coverings on planar lattices [88]. We will concentrate on the dimer solution here since it is first of all much simpler than Onsager's solution and secondly it is easily adapted to different lattices and boundary conditions.

For convenience purposes we will do some relabelling. Once again, we will use

$$K = \beta J = \frac{J}{k_B T}. \tag{4.3}$$

Additionally, we shift the energy such that the energy of a single ferromagnetic bond corresponds to zero (which is the ground state for $K > 0$, but not for $K < 0$). A single bond linking two antiparallel spins then has energy $2K$. Hence, the totally aligned state $\sigma_i \equiv 1$ for all σ_i has zero energy. We can then write the partition function on an arbitrary lattice as

$$Z(T, L) = \sum_{\sigma_i = \pm 1} e^{\sum_{\langle ij \rangle}^{L} K_{ij}(\sigma_i \sigma_j - 1)}, \tag{4.4}$$

where K_{ij} is the coupling for the bond between σ_i and σ_j. We introduce this "generalised coupling" since we are going to introduce auxiliary bonds in the following procedure for which the coupling will have values other than K. The first sum runs over all values $\sigma_i = \pm 1$ for each vertex i in the lattice L and the second sum runs over all bonds in L. The identity

$$e^{K_{ij}\sigma_i\sigma_j} \equiv \cosh K_{ij} \left(1 + z_{ij}\sigma_i\sigma_j\right), \tag{4.5}$$

where $z_{ij} = \tanh K_{ij}$ holds for any $\sigma_i\sigma_j$ which only takes values ± 1. We can use this identity to rewrite the partition function as

$$Z = \sum_{\sigma_i = \pm 1} \prod_{\langle ij \rangle} e^{-K_{ij}} \cosh K_{ij} \left(1 + z_{ij}\sigma_i\sigma_j\right). \tag{4.6}$$

Let us now consider the only term that still contains the spin variables:

$$\begin{aligned} \sum_{\sigma_i = \pm 1} \prod_{\langle ij \rangle} (1 + z_{ij}\sigma_i\sigma_j) \quad &= \quad \sum_{\sigma_{i,j} = \pm 1} (1 + z\sigma_1\sigma_2 + z\sigma_1\sigma_{L+1} + z\sigma_2\sigma_3 + \ldots \\ &\quad + z^2\sigma_1\sigma_2\sigma_2\sigma_3 + \ldots), \end{aligned} \tag{4.7}$$

where the first L spins are those in the first row of the lattice and σ_{L+1} is vertically connected to σ_1.

Due to the fact that the spin can only take on values of ± 1, only terms with even powers of each σ_i contribute to the partition function. This is easily seen using the example of small powers of σ_i:

$$\begin{aligned}
\sum_{\sigma_i=\pm 1} \sigma_i &= (-1)^1 + 1^1 = 0, && (4.8)\\
\sum_{\sigma_i=\pm 1} \sigma_i^2 &= (-1)^2 + 1^2 = 2, && (4.9)\\
\sum_{\sigma_i=\pm 1} \sigma_i^3 &= (-1)^3 + 1^3 = 0, && (4.10)\\
\sum_{\sigma_i=\pm 1} \sigma_i^4 &= (-1)^4 + 1^4 = 2, && (4.11)\\
&\vdots
\end{aligned}$$

Since each index i is summed over separately, the powers of each of the σ_i in the expansion has to be even in order to add a contribution to the partition function. Even powers in all the σ_i means that these terms correspond to closed polygon loops on the lattice L. A closed polygon loop needs to have an even number of bonds r (which includes $r = 0$) meeting at each site i of the lattice, where each lattice bond $\langle ij \rangle$ within such a polygon carries weight $z_{ij} = \tanh K_{ij}$. In terms of the polygon loops, we can rewrite the partition function as

$$Z = 2^N \left(\prod_{\langle ij \rangle} e^{-K_{ij}} \cosh K_{ij} \right) \Upsilon \left(z_{ij}; L \right), \tag{4.12}$$

where N is the number of vertices on the lattice L (and therefore equal to the number of spins) and

$$\Upsilon \left(z_{ij}; L \right) = \sum_{\Gamma(L)} \prod_{(gh) \subset \Gamma} z_{gh} \tag{4.13}$$

is the generating function of all allowed polygon configurations $\Gamma(L)$. As before, $z_{gh} = \tanh K_{gh}$ is the weight of a bond within the polygon.

The reason behind considering these closed polygon loops is that there is a one-to-one mapping between the polygon loops on the lattice L and dimer coverings on a "dimer lattice" L^Δ. The corresponding combinatorial problem for dimers is rather easy to solve. In fact, the generating function of the dimer coverings can be expressed in terms of the Pfaffian of the "Kasteleyn matrix" the generation of which we will now introduce.

In order to construct the Kasteleyn matrix more easily, we are first looking for the dimer lattice L^Δ. This lattice has to satisfy three conditions:

1. L^Δ is a planar lattice (as long as the original lattice L is planar). This means that the

lattice is two-dimensional and does not have any crossing bonds. Kasteleyn's basic theorem can then be applied directly in order to construct the appropriate Pfaffian.

2. A maximum of three bonds meet on each vertex of the lattice.

3. There is a one-to-one correspondence between the polygon configurations on L and the dimer configurations on L^{Δ}.

A way to obey these conditions was shown by Fisher [72]. The corresponding lattice is produced by a two-step procedure:

1. Each vertex at which more than three bonds meet is expanded into several vertices, each of degree three. Let us call this expanded lattice L^E. The additional bonds of this lattice are assigned a parameter K^*, whereas the original bonds retain the parameter K. Once we have derived the generating function, we take $K^* \to \infty$ in order to "lock together" the two spins on that bond. Let us now write down the partition function including all bonds of the expanded lattice:

$$Z\left(T, L^E\right) = 2^N \left[\prod_{\langle ij \rangle} e^{-K_{ij}} \cosh K_{ij}\right] \Upsilon(z_{ij}, z^* = 1; L^E), \tag{4.14}$$

   where the product only runs over the bonds of the original lattice L.

2. In order to set up a one-to-one correspondence between the polygon configurations on L^E and the dimer configurations on L^{Δ}, we replace each vertex of degree two on L^E by a pair of new vertices joined by an "internal bond" and each vertex of degree three by a triplet of new vertices joined by three internal bonds. This procedure can be seen in Figure 4.1. The internal bonds in this step we parametrise with K'. Similarly to K^*, we will also "lock" these bonds by taking $K' \to \infty$ in order to obtain the right partition function for the original lattice.

   Since the presence of a polygon bond on L^E is associated with the absence of a dimer on the corresponding bond on L^{Δ}, we define a second generating function $\Delta(z^{-1}, (z^*)^{-1}, (z')^{-1}; L^{\Delta})$ for the dimer configurations on L^{Δ}. An example of all the loop configurations for each site on the square lattice and the corresponding dimer configurations on the dimer lattice is given in Figure 4.2.

The two generating functions are related by

$$\Upsilon\left(z^{-1}, (z^*)^{-1}; L\right) = (z^*)^M \left(\prod_{\langle ij \rangle}^{(L)} z\right) \Delta\left(z^{-1}, (z^*)^{-1}, 1; L^{\Delta}\right), \tag{4.15}$$

where M is the number of bonds that get introduced on L^E in addition to the bonds on the original lattice. This enables us to write down the partition function for the original lattice in

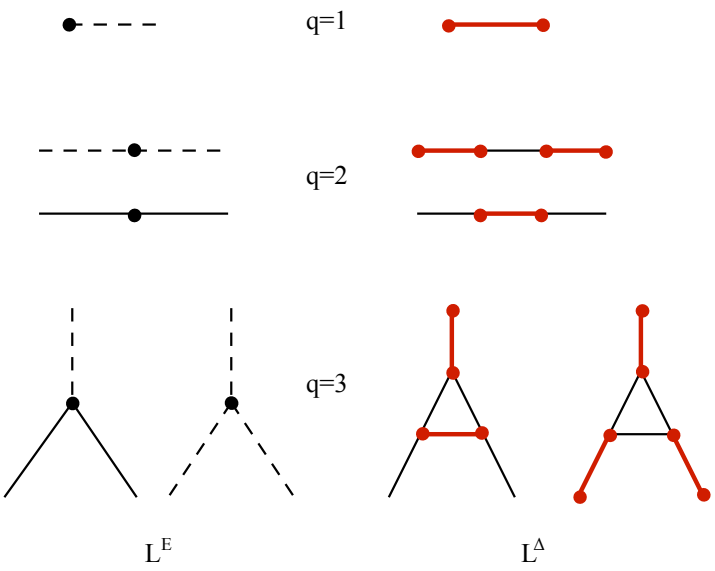

Figure 4.1: Replacement of the polygon loops on L^E by the corresponding dimer coverings for L^Δ. Notice that the presence of a dimer (in red) on a bond of L^Δ corresponds to the absence of a polygon loop on the corresponding bond of L^E [72].

terms of these functions as

$$Z\left(T,L\right)=2^N\left(\prod_{\langle ij\rangle}^{(L)}z\left(1+z\right)^{-1}\right)\Delta\left(z^{-1},1,1;L^\Delta\right). \tag{4.16}$$

The question now remains as to how we can construct the generating function Δ. It was pointed out by Kasteleyn [89] that the generating function can be expressed as the Pfaffian, i.e. the square root of the determinant, of a matrix that contains the bond weights. In order to construct that matrix, we have to orient the bonds on the lattice in order to ensure that the dimer configurations are counted correctly. A way of orienting those bonds is to follow Kasteleyn's protocol on the planar square lattice. He constructs the entries D of the matrix of which the Pfaffian is to be taken such that

$$D(i,j;i+1,j)=w \quad \text{and} \quad D(i,j;i,j+1)=(-1)^i w, \tag{4.17}$$

where w corresponds to the unsigned weight of the bond in question. Therefore a bond that is oriented from site i to site j, leads to matrix elements $a_{ij}=+w_{ij}$ and $a_{ji}=-w_{ij}$.

The above procedure only applies to planar lattices. This means, that the lattice can be drawn on a normal sheet of paper (even though it may have to be infinitely large) without any bonds crossing. This is true for any square Ising lattice with open boundary conditions. It is even true, if the boundary conditions are open in one direction and periodic in the other, which

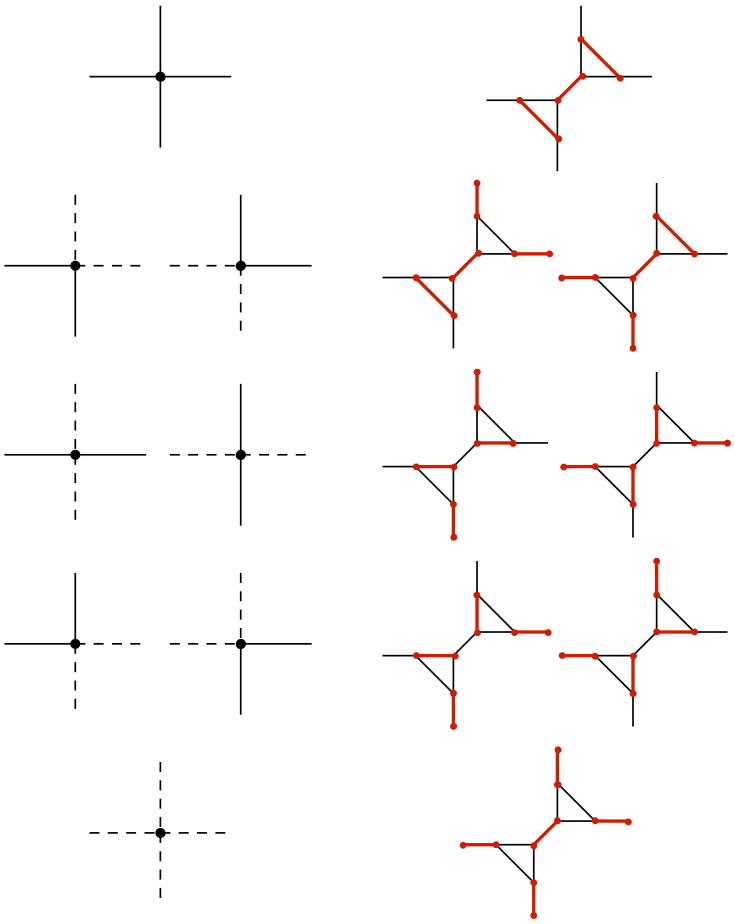

Figure 4.2: The allowed polygon bond configurations on a vertex of degree 4 on the original lattice L and the corresponding dimer configurations on the dimer lattice L^{Δ}. The dimers are shown in red. [72]

is shown in Figure 4.3 a). If we want to work with periodic boundary conditions in both the longitudinal and the vertical direction, the associated lattice is no longer planar. This means that it cannot be drawn on a sheet of paper without bonds crossing as shown in Figure 4.3 b)[2].

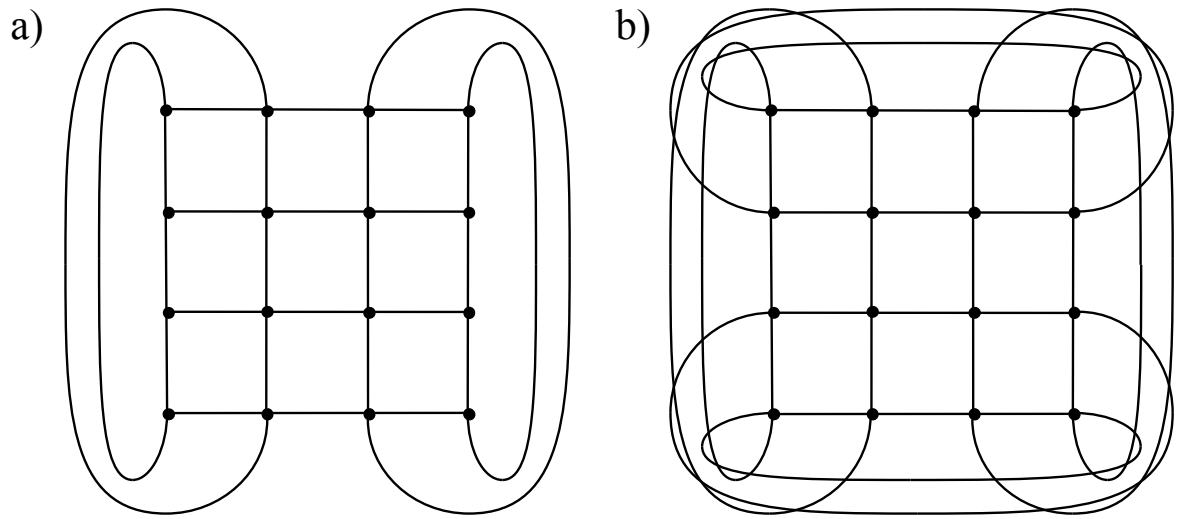

Figure 4.3: Panel a) shows a 4×4 square lattice with periodic boundary conditions in the vertical direction, which is a planar lattice. Panel b) shows the same lattice but now with periodic boundary conditions in both directions. This lattice is no longer planar, since there is no way of drawing it without bonds crossing.

In order to be able to express the generating function of a non-planar lattice in terms of Pfaffians, we have to take the sum over the Pfaffians of four different "sectors". This is due to the fact that we can split up the periodicity into four types of dimer configurations (examples can be seen in Figure 4.4):

1. The sector where an even number of dimers crosses the boundary between $\sigma_{i,N}$ and $\sigma_{i,1}$ which we will call the vertical boundary or the corresponding horizontal boundary between $\sigma_{N,j}$ and $\sigma_{1,j}$. We will call this sector the "even-even" or "(e,e)" sector. We therefore need to adjust the orientation of the dimers on the boundary. The corresponding matrix coefficients which need to be changed in this sector are

$$D_1(N, j; 1, j) = w \quad \text{and} \quad D_1(i, N; i, 1) = (-1)^i w. \tag{4.18}$$

2. The sector where an even number of dimers crosses the horizontal boundary and an odd number of dimers crosses the vertical boundary. This sector is called the "even-odd" or "(e,o)" sector. The matrix coefficients which need to be changed in this sector are

$$D_2(N, j; 1, j) = w \quad \text{and} \quad D_2(i, N; i, 1) = (-1)^{i+1} w. \tag{4.19}$$

[2]The reason behind this is that the square lattice with periodic boundary conditions drawn without crossing bonds corresponds to a torus, which is topologically different from a sheet and therefore non-planar.

3. The sector where an odd number of dimers crosses the horizontal boundary and an even number of dimers crosses the vertical boundary. This sector is called the "odd-even" or "(o,e)" sector. The matrix coefficients which need to be changed in this sector are

$$D_3(N, j; 1, j) = -w \quad \text{and} \quad D_3(i, N; i, 1) = (-1)^i w. \tag{4.20}$$

4. The sector where an odd number of dimers crosses the horizontal boundary and an odd number of dimers crosses the vertical boundary. This sector is called the "odd-odd" or "(o,o)" sector. The matrix coefficients which need to be changed in this sector are

$$D_4(N, j; 1, j) = -w \quad \text{and} \quad D_4(i, N; i, 1) = (-1)^{i+1} w. \tag{4.21}$$

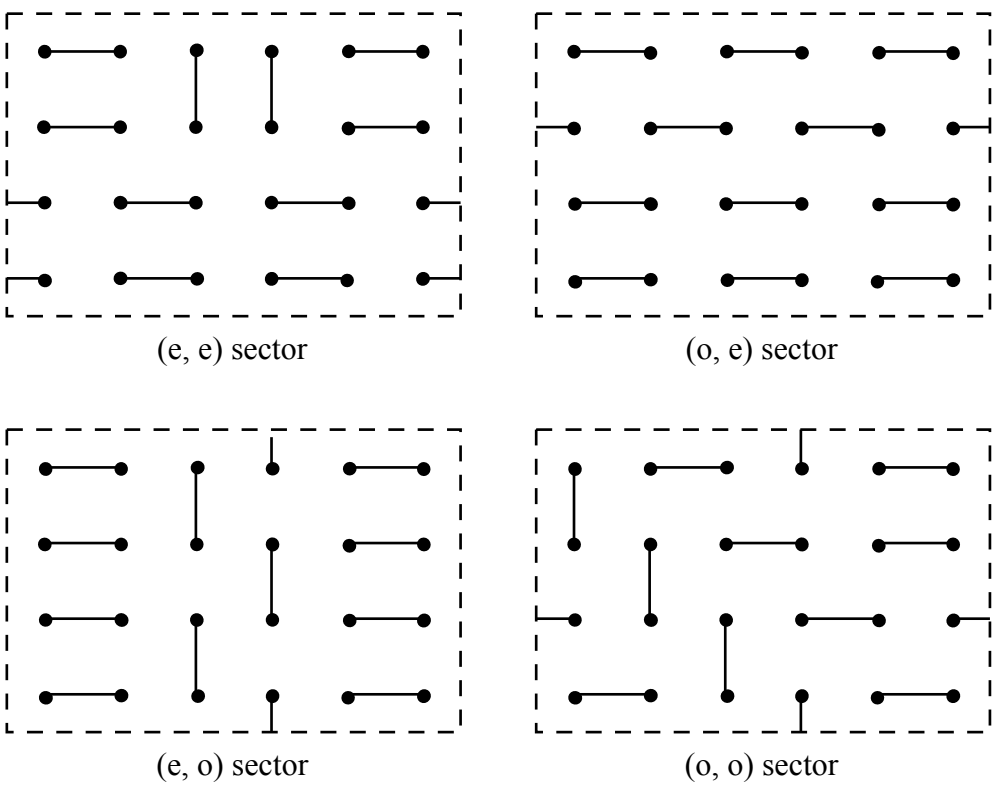

Figure 4.4: Examples of configurations in each of the four different sectors on a toroidal lattice [89].

The dimer and therefore the loop configurations generated by the Pfaffian of each sector are all of the configurations that can be created by flipping pairs of dimers from a reference state that lies within the sector. For the (e,e) sector we could for example take the reference state shown in Figure 4.5.

The Pfaffians of the different sectors count different configuration classes with different signs

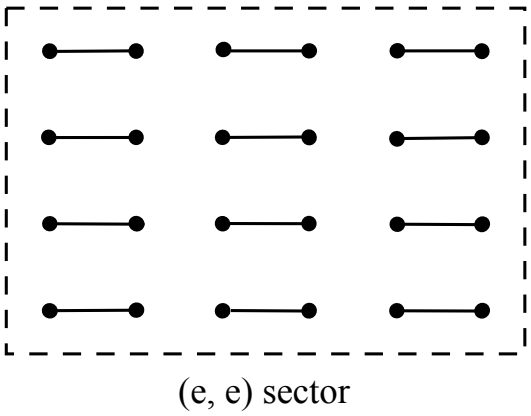

Figure 4.5: Reference state of the (e,e) sector.

according to Table 4.1. Hence we can write down the combination of Pfaffians that counts all

Class of configurations	Sign of corresponding terms in Pf D_μ			
	D_1	D_2	D_3	D_4
(e,e)	+	+	+	+
(o,e)	-	-	+	+
(e,o)	-	+	-	+
(o,o)	-	+	+	-

Table 4.1: The different sectors and the signs of the corresponding terms in their Pfaffians [89].

configurations correctly as

$$\Delta = \frac{1}{2}\left(-\operatorname{Pf} D_1 + \operatorname{Pf} D_2 + \operatorname{Pf} D_3 + \operatorname{Pf} D_4\right) \tag{4.22}$$

Unfortunately, by turning our original square lattice L into a more complicated lattice L^Δ which is fit for dimer covering, we have to define a new procedure to assign signs to the entries in the matrix. A way to do this was shown by Fisher [72] along with the introduction of his dimer lattice L^Δ. He showed that if a lattice is oriented so that an odd number of bonds on each face of the lattice is oriented clockwise, the Pfaffian of the corresponding matrix counts all dimer coverings correctly and is equal to the generating function Δ. We will obey this rule from now on.

The problem of the above treatment is that the resulting matrices have size $2^\infty \times 2^\infty$. In order to avoid having to deal with matrices of infinite size, we would like to get it into block-diagonal form. To do this we employ Bloch's theorem and introduce two phases $\omega_1 = e^{i\theta_1}$ and $\omega_2 = e^{i\theta_2}$ between the different diagonal blocks. Strictly seen, we are only allowed to use Bloch's theorem for a lattice with periodic boundary conditions which does not work for any individual sector, but we make the assumption that the boundary contributions are negligible

in the thermodynamic limit. The difference between the matrices of the different sectors then consists of sums over different values of θ_1 and θ_2. This is easily seen from the solution given by McCoy [80]. Let us list the allowed values of θ_1 and θ_2 in the different sectors:

Sector	θ_1	θ_2
(e,e)	$\frac{2\pi n_1}{L}$	$\frac{2\pi n_2}{L}$
(e,o)	$\frac{2\pi n_1}{L}$	$\frac{\pi(2n_2-1)}{L}$
(o,e)	$\frac{\pi(2n_1-1)}{L}$	$\frac{2\pi n_2}{L}$
(o,o)	$\frac{\pi(2n_1-1)}{L}$	$\frac{\pi(2n_2-1)}{L}$

Table 4.2: Allowed values of θ_1 and θ_2 [80].

4.2 Review of Fisher zeros on the square lattice

Let us now look at one of the most extensively studied lattices in connection with the two-dimensional Ising model, the square lattice. We create the dimer lattice through the procedure above and arrive at the lattice given in Figure 4.6.

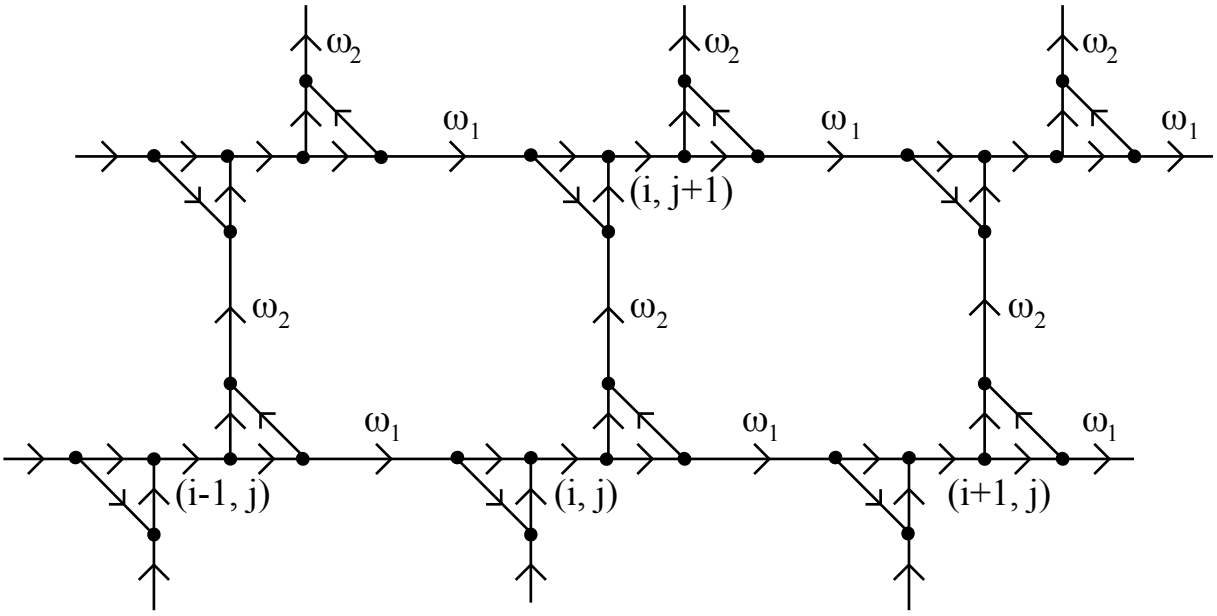

Figure 4.6: The dimer lattice of the Ising model on a square lattice with a suitable orientation of the bonds [72].

Next, we need to write down the matrix that belongs to the dimer lattice of the isotropic

square lattice, which is shown in Figure 4.6. Here we will consider the matrix for open boundary conditions. Since we take the thermodynamic limit, the difference between the results from open and periodic boundary conditions should go to zero. Open boundary conditions also mean that the finite lattice with open boundary conditions is no longer translationally invariant. However, once we take the thermodynamic limit, translational invariance is restored and we can employ Bloch's theorem once again. This matrix in its compact form was first written down by Fisher [72] and can be written as

$$\mathbf{A}_{\text{square}} = \begin{pmatrix} 0 & 1 & 1 & 0 & -z^{-1}\omega_1^* & 0 \\ -1 & 0 & 1 & 0 & 0 & -z^{-1}\omega_2^* \\ -1 & -1 & 0 & 1 & 0 & 0 \\ 0 & 0 & -1 & 0 & 1 & 1 \\ z^{-1}\omega_1 & 0 & 0 & -1 & 0 & 1 \\ 0 & z^{-1}\omega_2 & 0 & -1 & -1 & 0 \end{pmatrix}, \tag{4.23}$$

where

$$\omega_1 = e^{i\theta_1(n_1)} \qquad \text{and} \qquad \omega_2 = e^{i\theta_2(n_2)} \tag{4.24}$$

$$\theta_1(n_1) = \frac{2\pi n_1}{L} \qquad \text{and} \qquad \theta_2(n_2) = \frac{2\pi n_2}{L} \tag{4.25}$$

and $z^{-1} = (\tanh K)^{-1}$ as before. The Pfaffian of the full matrix is equal to the product over all θ_1 and θ_2 of the Pfaffian of $\mathbf{A}_{\text{square}}$. From this we can write down the partition function of the square lattice Ising model as

$$Z(T,L) = 2^N \left(\prod_{\langle ij \rangle}^{(L)} z(1+z)^{-1} \right) \prod_{\theta_1} \prod_{\theta_2} \text{Pf}\left(\mathbf{A}_{\text{square}}\right) \tag{4.26}$$

$$= \prod_{n_1=1}^{L} \prod_{n_2=1}^{L} \left(\left(\frac{1+z^2}{1-z^2} \right)^2 - \frac{2z}{1-z^2} \left(\cos\left(\frac{2\pi n_1}{L} \right) + \cos\left(\frac{2\pi n_2}{L} \right) \right) \right). \tag{4.27}$$

The corresponding free-energy density is

$$-\frac{f}{k_B T} = \lim_{L\to\infty} \frac{1}{L^2} \log Z(T,L) \tag{4.28}$$

$$= 2\log 2 + \log z^2 - 2\log(1+z) + \lim_{L\to\infty} \frac{1}{2L^2} \log \left(\prod_{\theta_1} \prod_{\theta_2} \det(\mathbf{A}_{\text{square}}) \right). \tag{4.29}$$

The zeros of the partition function are then found [34] to lie on two circles of radius $\sqrt{2}$ centred around $z = \pm 1$, i.e. at

$$z = \pm 1 + \sqrt{2} e^{i\phi}. \tag{4.30}$$

These contours of zeros are shown in Figure 4.7.

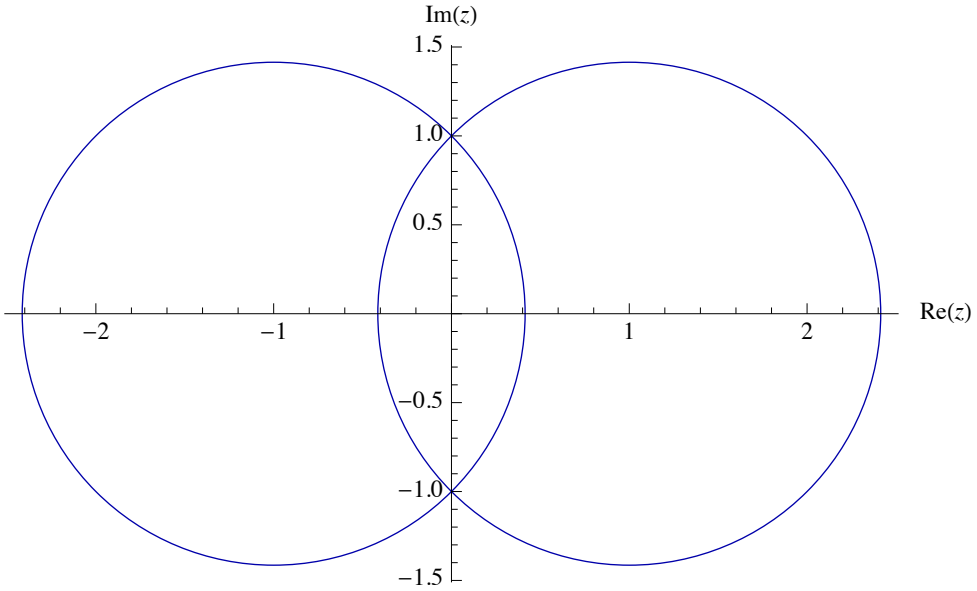

Figure 4.7: The contour of zeros for the two-dimensional square-lattice Ising model according to Fisher [72]. The critical points lie at $z = -1 + \sqrt{2}$ and $z = 1 - \sqrt{2}$.

Using Table 4.2, we can also write down the full partition function on the torus, i.e. for a lattice with periodic boundary conditions. This was first written down by Kaufman [90]. The full partition function is then given as the sum of four terms:

$$Z(T,L) = \frac{1}{2}\left(-Z_{ee}(T,L) + Z_{eo}(T,L) + Z_{oe}(T,L) + Z_{oo}(T,L)\right), \tag{4.31}$$

where

$$Z_{ee} = 2^{L^2} \prod_{n_1=1}^{L} \prod_{n_2=1}^{L} \left(\cosh^2(2K) - \sinh(2K)\left(\cos\frac{2\pi n_1}{L} + \cos\frac{2\pi n_2}{L}\right)\right)^2 \tag{4.32}$$

$$= 2^{L^2} \prod_{n_1=1}^{L} \prod_{n_2=1}^{L} \left(\left(\frac{1+z^2}{1-z^2}\right)^2 - \frac{2z}{1-z^2}\left(\cos\frac{2\pi n_1}{L} + \cos\frac{2\pi n_2}{L}\right)\right)^2, \tag{4.33}$$

$$Z_{eo} = 2^{L^2} \prod_{n_1=1}^{L} \prod_{n_2=1}^{L} \left(\left(\frac{1+z^2}{1-z^2}\right)^2 - \frac{2z}{1-z^2}\left(\cos\frac{2\pi n_1}{L} + \cos\frac{\pi(2n_2-1)}{L}\right)\right)^2, \tag{4.34}$$

$$Z_{oe} = 2^{L^2} \prod_{n_1=1}^{L} \prod_{n_2=1}^{L} \left(\left(\frac{1+z^2}{1-z^2}\right)^2 - \frac{2z}{1-z^2}\left(\cos\frac{\pi(2n_1-1)}{L} + \cos\frac{2\pi n_2}{L}\right)\right)^2, \tag{4.35}$$

$$Z_{oo} = 2^{L^2} \prod_{n_1=1}^{L} \prod_{n_2=1}^{L} \left(\left(\frac{1+z^2}{1-z^2}\right)^2 - \frac{2z}{1-z^2}\left(\cos\frac{\pi(2n_1-1)}{L} + \cos\frac{\pi(2n_2-1)}{L}\right)\right)^2. \tag{4.36}$$

The zeros of the Ising model on a torus are more difficult to calculate since, due to the sum over the different sectors, the partition function no longer factorises.

4.3 Fisher zeros on frustrated lattices

Let us now look at the distribution of Fisher zeros on lattices that are geometrically frustrated. Examples of these are the triangular and the kagomé lattice. These are shown in Figures 4.8 and 4.9.

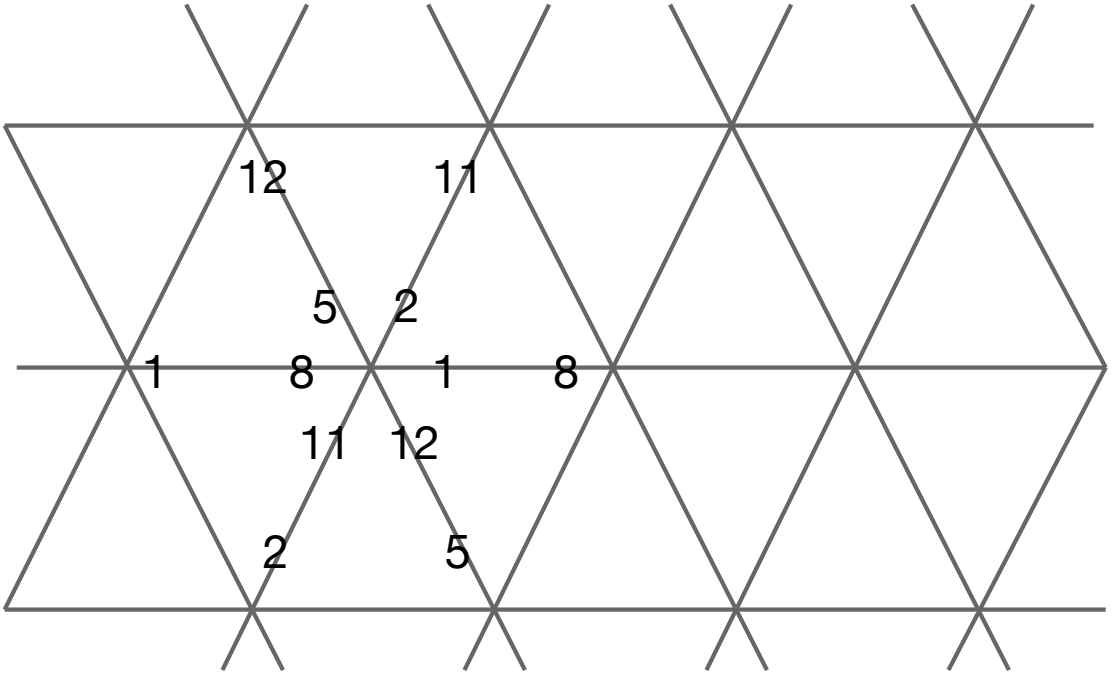

Figure 4.8: The original triangular lattice with the labelling of the vertices of the expanded lattice according to Figure 4.10.

Once again, we obey the protocol given in chapter 4.1 and expand the original lattice into a dimer lattice with appropriate weights. The dimer lattices of the triangular lattice and the kagomé lattice are given in Figures 4.10 and 4.11 respectively.

Looking at Figure 4.10 we can write down the Kasteleyn matrix in compact form for an Ising model on a triangular lattice:

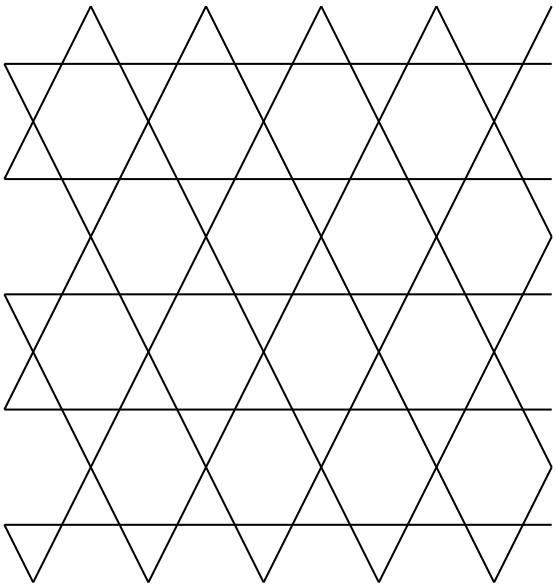

Figure 4.9: The kagomé lattice.

$$\mathbf{A}_{\rm tri} = \begin{pmatrix} 0 & 1 & 1 & 0 & 0 & 0 & 0 & -\frac{\omega_1^*}{z} & 0 & 0 & 0 & 0 \\ -1 & 0 & 1 & 0 & 0 & 0 & 0 & 0 & 0 & 0 & \frac{\omega_2^*}{z} & 0 \\ -1 & -1 & 0 & -\frac{1}{z^*} & 0 & 0 & 0 & 0 & 0 & 0 & 0 & 0 \\ 0 & 0 & \frac{1}{z^*} & 0 & 1 & 1 & 0 & 0 & 0 & 0 & 0 & 0 \\ 0 & 0 & 0 & -1 & 0 & 1 & 0 & 0 & 0 & 0 & 0 & -\frac{\omega_3^*}{z} \\ 0 & 0 & 0 & -1 & -1 & 0 & -\frac{1}{z^*} & 0 & 0 & 0 & 0 & 0 \\ 0 & 0 & 0 & 0 & 0 & \frac{1}{z^*} & 0 & 1 & 1 & 0 & 0 & 0 \\ \frac{\omega_1}{z} & 0 & 0 & 0 & 0 & 0 & -1 & 0 & 1 & 0 & 0 & 0 \\ 0 & 0 & 0 & 0 & 0 & 0 & -1 & -1 & 0 & -\frac{1}{z^*} & 0 & 0 \\ 0 & 0 & 0 & 0 & 0 & 0 & 0 & 0 & \frac{1}{z^*} & 0 & 1 & 1 \\ 0 & -\frac{\omega_2}{z} & 0 & 0 & 0 & 0 & 0 & 0 & 0 & -1 & 0 & 1 \\ 0 & 0 & 0 & 0 & \frac{\omega_3}{z} & 0 & 0 & 0 & 0 & -1 & -1 & 0 \end{pmatrix}. \tag{4.37}$$

As a next step, we can find the determinant of the matrix and from there the Pfaffian and from there the partition function of the frustrated lattice system. Let us start with the determinant

$$\begin{aligned} \det \mathbf{A}_{\rm tri} &= 1 + 3w^2 + 3w^4 + w^6 - w\left(1-w^2\right)^2\left(\omega_1 + \omega_1^{-1} - \omega_2 - \omega_2^{-1} + \omega_3 + \omega_3^{-1}\right) \\ &\quad -4w^3\left(\omega_1^{-1}\omega_2\omega_3^{-1} + \omega_1\omega_2^{-1}\omega_3\right) \qquad (4.38) \\ &= (1+z^{-2})^3 - 2z^{-1}\left(1-z^{-2}\right)^2\left(\cos\theta_1 - \cos\theta_2 + \cos(\theta_1+\theta_2)\right) \\ &\quad -8z^{-3}\cos(2\theta_1) \qquad (4.39) \end{aligned}$$

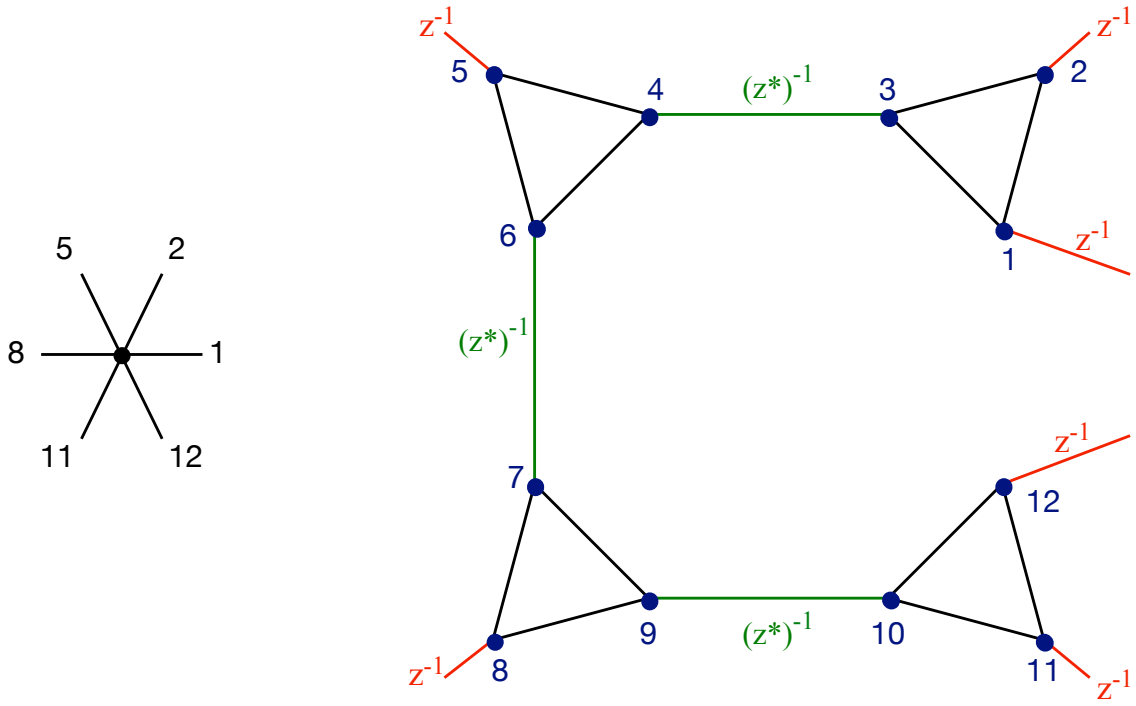

Figure 4.10: An original lattice vertex and its corresponding dimer vertices for the triangular lattice. The red bonds are the original lattice bonds that get assigned weight z^{-1} on the dimer lattice. The green bonds correspond to the additional bonds on the expanded lattice and are assigned weight $(z^*)^{-1}$. The black bonds are the bonds that get added when introducing the dimer lattice and they have weight 1 each.

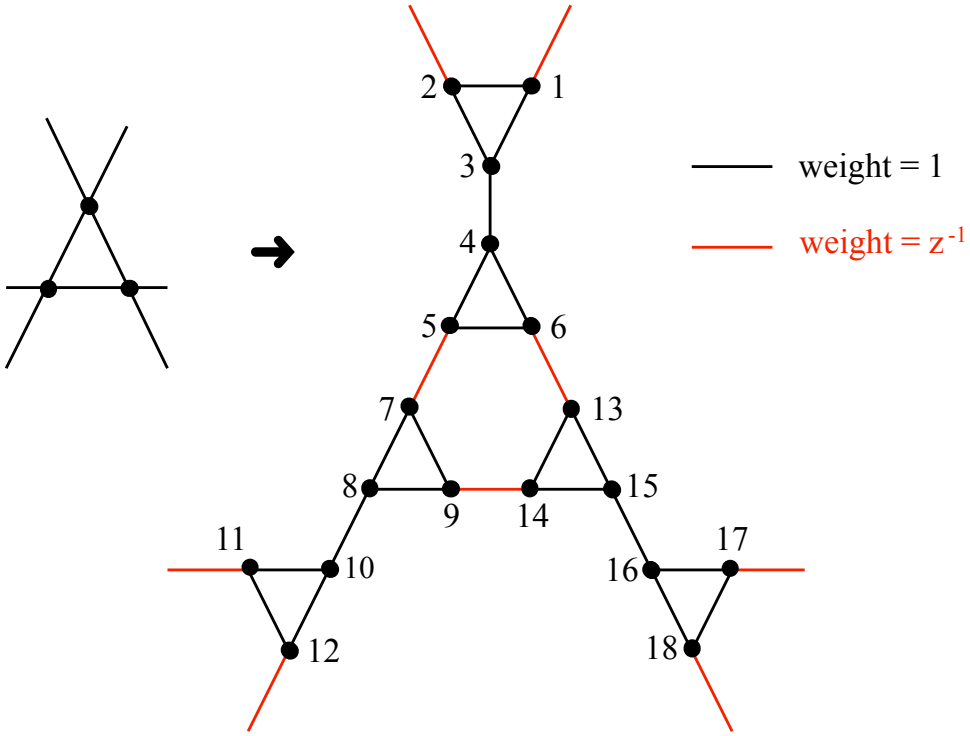

Figure 4.11: An original lattice vertex and its corresponding dimer vertices for the kagomé lattice. The red bonds are the original lattice bonds that get assigned weight z^{-1} on the dimer lattice. The black bonds are the additional bonds that get added when introducing the expanded and the dimer lattice and they have weight 1 each.

with

$$\omega_2 = e^{i\theta_2} \tag{4.40}$$

$$\omega_3 = e^{i\theta_1} \tag{4.41}$$

$$\omega_1 = e^{i\theta_1} e^{i\theta_2} = e^{i(\theta_1+\theta_2)} \tag{4.42}$$

according to Figure 4.12. Having calculated the determinant, which is the square of the Pfaffian,

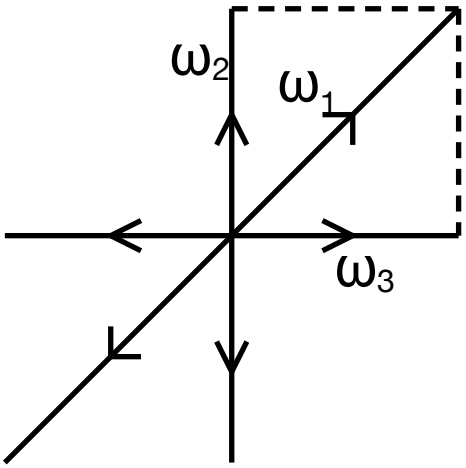

Figure 4.12: Definition of the lattice directions on the triangular and the kagomé lattices. They are similar to the square lattice but with an additional direction that goes diagonally across the unit cell of the square lattice.

we can write down the partition function

$$Z_{\text{tri}}(T, L) = 2^N \left(\prod_{\langle ij \rangle}^{(L)} z(1+z)^{-1} \right) \prod_{\theta_1} \prod_{\theta_2} \sqrt{\det\left(\mathbf{A}_{\text{tri}}\right)}. \tag{4.43}$$

Finally, we can numerically evaluate the zeros of (4.43) for different values of θ_1 and θ_2. These are plotted in Figure 4.13.

Similarly, we can write down the Kasteleyn matrix of the kagomé lattice by looking at Figure 4.11. The corresponding matrix in compact form is given in (4.44).

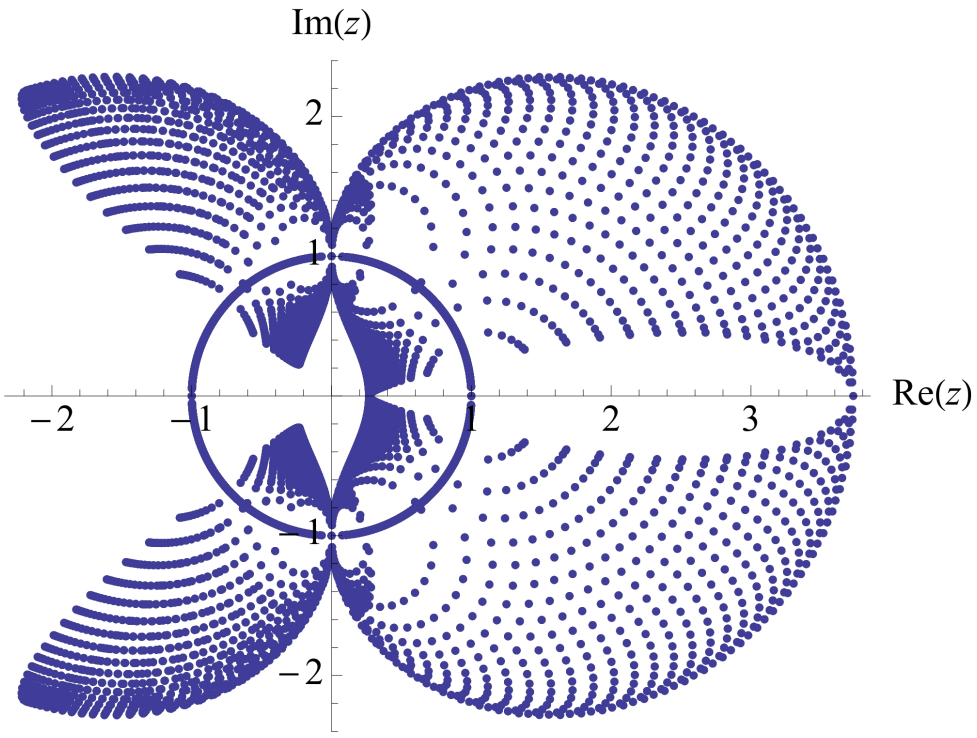

Figure 4.13: The partition function zeros of the triangular lattice for $L = 80$. Notice that there is an accumulation of zeros and therefore a phase transition at a non-zero temperature on the ferromagnetic side. This transition does not occur on the antiferromagnetic side due to geometric frustration.

$$\mathbf{A}_{\text{kag}} = \begin{pmatrix}
0 & 1 & 1 & 0 & 0 & 0 & 0 & 0 & 0 & 0 & 0 & -\frac{\omega_3^*}{z} & 0 & 0 & 0 & 0 & 0 & 0 \\
-1 & 0 & 1 & 0 & 0 & 0 & 0 & 0 & 0 & 0 & 0 & 0 & 0 & 0 & 0 & 0 & 0 & -\frac{\omega_2^*}{z} \\
-1 & -1 & 0 & 1 & 0 & 0 & 0 & 0 & 0 & 0 & 0 & 0 & 0 & 0 & 0 & 0 & 0 & 0 \\
0 & 0 & -1 & 0 & 1 & 1 & 0 & 0 & 0 & 0 & 0 & 0 & 0 & 0 & 0 & 0 & 0 & 0 \\
0 & 0 & 0 & -1 & 0 & 1 & -z^{-1} & 0 & 0 & 0 & 0 & 0 & 0 & 0 & 0 & 0 & 0 & 0 \\
0 & 0 & 0 & -1 & -1 & 0 & 0 & 0 & 0 & 0 & 0 & 0 & -z^{-1} & 0 & 0 & 0 & 0 & 0 \\
0 & 0 & 0 & 0 & z^{-1} & 0 & 0 & 1 & 1 & 0 & 0 & 0 & 0 & 0 & 0 & 0 & 0 & 0 \\
0 & 0 & 0 & 0 & 0 & 0 & -1 & 0 & 1 & 1 & 0 & 0 & 0 & 0 & 0 & 0 & 0 & 0 \\
0 & 0 & 0 & 0 & 0 & 0 & -1 & -1 & 0 & 0 & 0 & 0 & 0 & -z^{-1} & 0 & 0 & 0 & 0 \\
0 & 0 & 0 & 0 & 0 & 0 & 0 & -1 & 0 & 0 & 1 & 1 & 0 & 0 & 0 & 0 & 0 & 0 \\
0 & 0 & 0 & 0 & 0 & 0 & 0 & 0 & 0 & -1 & 0 & 1 & 0 & 0 & 0 & 0 & -\frac{\omega_1^*}{z} & 0 \\
\frac{\omega_3}{z} & 0 & 0 & 0 & 0 & 0 & 0 & 0 & 0 & -1 & -1 & 0 & 0 & 0 & 0 & 0 & 0 & 0 \\
0 & 0 & 0 & 0 & 0 & z^{-1} & 0 & 0 & 0 & 0 & 0 & 0 & 0 & 1 & 1 & 0 & 0 & 0 \\
0 & 0 & 0 & 0 & 0 & 0 & 0 & 0 & z^{-1} & 0 & 0 & 0 & -1 & 0 & 1 & 0 & 0 & 0 \\
0 & 0 & 0 & 0 & 0 & 0 & 0 & 0 & 0 & 0 & 0 & 0 & -1 & -1 & 0 & 1 & 0 & 0 \\
0 & 0 & 0 & 0 & 0 & 0 & 0 & 0 & 0 & 0 & 0 & 0 & 0 & 0 & -1 & 0 & 1 & 1 \\
0 & 0 & 0 & 0 & 0 & 0 & 0 & 0 & 0 & 0 & \frac{\omega_1}{z} & 0 & 0 & 0 & 0 & -1 & 0 & 1 \\
0 & \frac{\omega_2}{z} & 0 & 0 & 0 & 0 & 0 & 0 & 0 & 0 & 0 & 0 & 0 & 0 & 0 & -1 & -1 & 0
\end{pmatrix}. \tag{4.44}$$

The corresponding determinant can be written as

$$\begin{aligned}\det(\mathbf{A}_{\rm kag}) &= \left(1+z^{-8}\right)\left(1+z^{-4}\right) - 2z^{-2}\left(1-z^{-4}\right)^2(\cos\theta_1+\cos\theta_2) \\ &\quad +2iz^{-3}\left(1-z^{-4}\right)\left(1+z^{-2}\right)(\sin\theta_1-\sin\theta_2) - 2iz^{-2}\left(1-z^{-4}\right)^2\sin(\theta_1+\theta_2) \\ &\quad -2z^{-3}\left(1-z^{-2}\right)^3(\cos(\theta_1+\theta_2)+i\sin(2\theta_1)) + 4z^{-4}\left(1-z^{-4}\right)\cos(\theta_1-\theta_2) \\ &\quad -2iz^{-3}\left(1+z^{-2}\right)^3\sin(\theta_1-\theta_2) \\ &\quad -2z^{-3}\left(1-z^{-4}\right)^2(\cos(2\theta_1+\theta_2)-\cos\theta_1) \end{aligned} \tag{4.45}$$

Using this determinant, we can write down the partition function

$$Z_{\rm kag}(T,L) = 2^N\left(\prod_{\langle ij\rangle}^{(L)} z(1+z)^{-1}\right)\prod_{\theta_1}\prod_{\theta_2}\sqrt{\det\left(\mathbf{A}_{\rm kag}\right)}. \tag{4.46}$$

and numerically evaluate its zeros. These are shown in Figure 4.14.

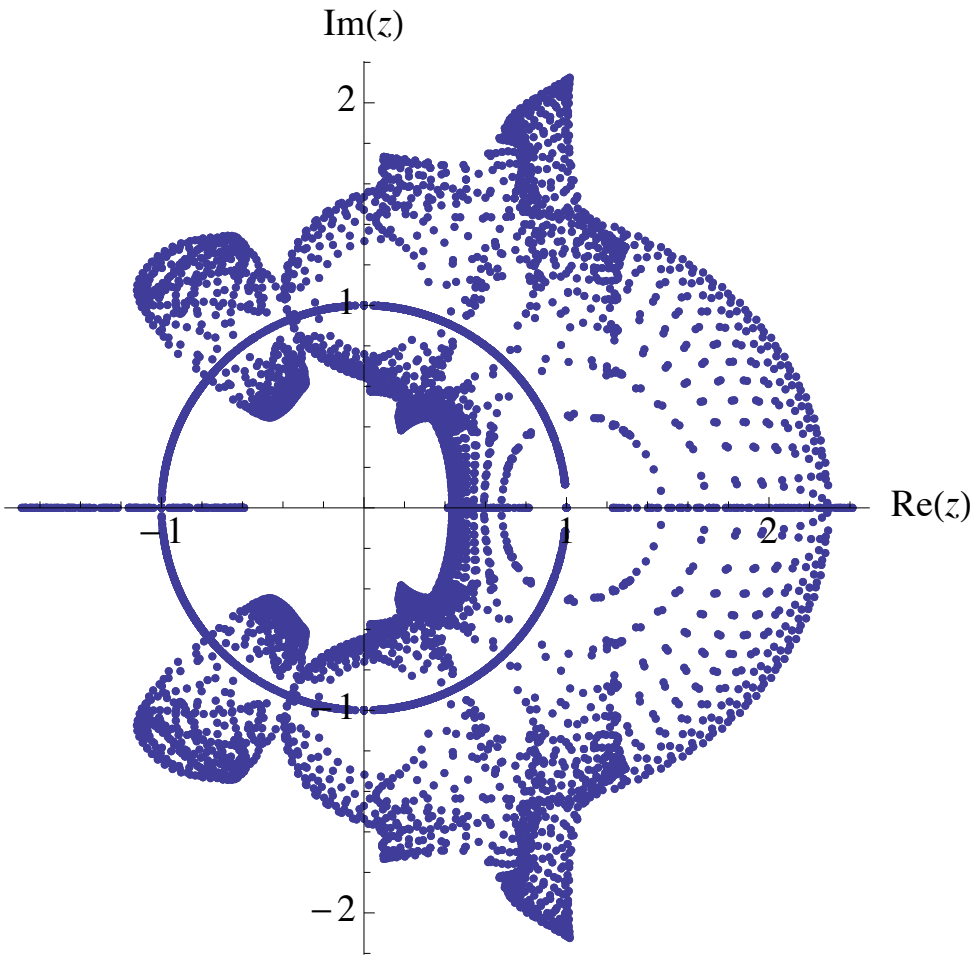

Figure 4.14: The partition function zeros of the kagomé lattice for $L = 40$. Notice that there is an accumulation of zeros and therefore a phase transition at a non-zero temperature on the ferromagnetic side. The zeros which seem to be closing in on a real z on the antiferromagnetic side lie further away from the real axis than in the case of the triangular lattice. This might be interpreted as a measure of the "amount of frustration" in the model. There appear to be zeros lying along the real line on the antiferromagnetic line. These zeros are clearly unphysical and are probably due to sign issues when taking the Pfaffians.

4.4 Comments

In this chapter we have calculated the partition function zeros for two frustrated lattices: the triangular and the kagomé lattice. However, it should be noted that the results shown are still very preliminary and should be taken with a grain of salt.

Firstly, the procedure employed here is not the same procedure that we used in order to find the partition function zeros in Chapters 2 and 3. The results here are all obtained *after* having taken the thermodynamic limit. As we have seen in Chapter 3, the structure of the zeros sensitively depends on the way we take the thermodynamic limit, which might lead to some differences in interpretation.

In addition, there may be sign issues coming in with taking the Pfaffians, which we are still working on resolving.

Chapter 5

The quantum Ising model

The quantum Ising model is one of the simplest models that displays a quantum phase transition. This means that it exhibits two symmetry-distinguished $T \to 0$ states for different values of some non-thermal tuning parameter which have different low-lying excitations and different quantum ordering properties.

5.1 Review of the exact solution

We are looking at the 1d transverse field Ising model with the Hamiltonian

$$\hat{\mathcal{H}} = -J \sum_i \left(g\hat{\sigma}_i^x + \hat{\sigma}_i^z \hat{\sigma}_{i+1}^z \right). \tag{5.1}$$

In this Hamiltonian, the second term is responsible for the alignment of the spins. J is an exchange constant, which sets the microscopic energy scale. We have already further analysed this term in the previous chapters. In the first term of the Hamiltonian g is a dimensionless coupling to an external transverse magnetic field, which will be the tuning parameter. A nonzero g allows for tunnelling between the up and the down states of the spin with an amplitude proportional to g [91].

The $\hat{\sigma}_i^x$ and $\hat{\sigma}_i^z$ correspond to the Pauli matrices. The matrices on different sites (i.e. $i \neq j$) commute with each other since they act in separate Hilbert subspaces. The eigenvalues of $\hat{\sigma}_i^z$ are ± 1 and the corresponding eigenstates can be labelled as $|\uparrow\rangle$ and $|\downarrow\rangle$.

Let us now analyse the two limiting cases of $g \gg 1$ and $g \ll 1$, which will correspond to two different types of ground states of the spin chain. These are shown in Figure 5.1.

1. In the case of $g \ll 1$, the tunnelling between the $|\uparrow\rangle$ and the $|\downarrow\rangle$ states can be neglected. This leads to a ferromagnetically ordered state in the z-direction with the Z_2 symmetry broken. The fundamental excitations away from this ground state correspond to domain walls between lines of flipped spins. For $g = 0$, each spin configuration is an eigenstate of the Hamiltonian as we have already seen in the classical Ising model. As we increase g

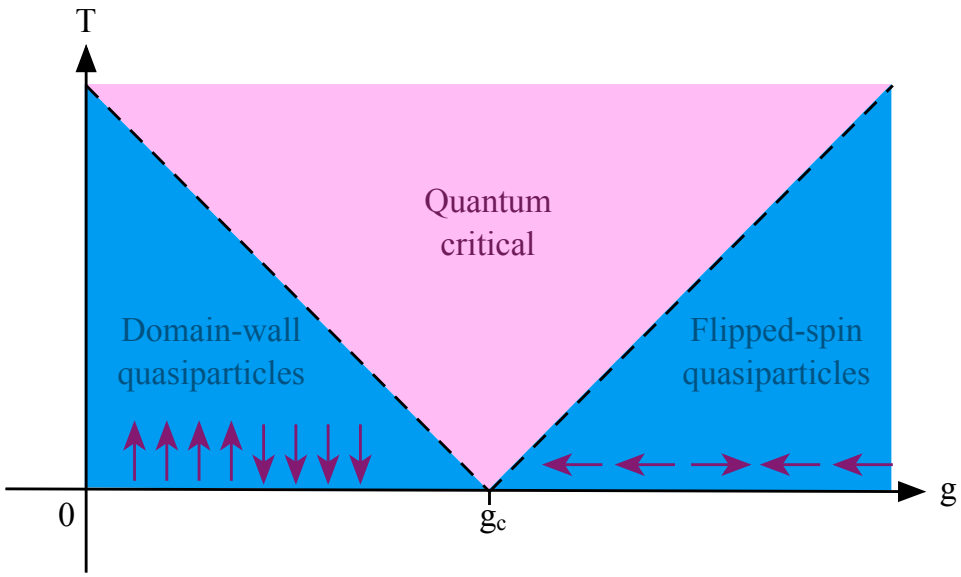

Figure 5.1: Phase diagram of the quantum Ising model. There is a quantum critical point g_c between the two phases at which the nature of the quasiparticle excitations changes. [92]

to a small but nonzero value, the domain walls become mobile even at zero temperature. This leads to the development of zero-point motion and quantum kinetics.

2. In the case of $g \gg 1$ the ground state is an eigenstate of $\hat{\sigma}_i^x$. We can define the two eigenstates of $\hat{\sigma}_i^x$ to be

$$|\rightarrow\rangle_i = \frac{1}{\sqrt{2}}\left(|\uparrow\rangle_i + |\downarrow\rangle_i\right) \qquad \text{and} \tag{5.2}$$

$$|\leftarrow\rangle_i = \frac{1}{\sqrt{2}}\left(|\uparrow\rangle_i - |\downarrow\rangle_i\right). \tag{5.3}$$

The state where all spins are aligned with the transverse field (i.e. they are all in the $|\rightarrow\rangle_i$ configuration) corresponds to the ground state of a quantum paramagnet with no spontaneously broken symmetry. The system can be excited out of the ground state by flipping spins in the direction opposite to the external field (i.e. into the $|\leftarrow\rangle_i$ configuration). These flipped spins then correspond to quasiparticles which are stationary for $g = \infty$ and develop dynamics for $g < \infty$.

The point that lies between those two symmetry-distinguished $T \rightarrow 0$ states is the quantum critical point $g = g_c = 1$. The state of the system at this critical value of g cannot be characterised by either of those two simple pictures of the collective behaviour. Instead, both types of order and both types of quasiparticles compete with each other. This leads to scale invariance of the ground state correlation function

$$\langle \hat{\sigma}_j^z \hat{\sigma}_k^z \rangle \sim \frac{1}{|j-k|^{1/4}} \tag{5.4}$$

for large $|j-k|$. As we increase the temperature and move away from the quantum critical point in the vertical direction of the phase diagram, a new timescale of order $\frac{\hbar}{k_B T}$ emerges which universally determines the relaxation rate for spin fluctuations, which is one of the fundamental properties of a QCP. The quantum-classical mapping leads to the critical point being in the same universality class as the two-dimensional Ising model on the square lattice.

Let us now calculate the exact spectrum of the model by diagonalising the Hamiltonian following the derivation in [91]. To do that, we first use a Jordan-Wigner transformation [93, 94] followed by a Bogoliubov transformation [95]. The Jordan-Wigner transformation maps the sites with spin-1/2 degrees of freedom onto sites with single orbitals that have spinless fermions hopping between the sites. Therefore a spin-up state can be associated with an empty orbital and a spin-down state with an occupied one. We can then derive the operator relation

$$\hat{\sigma}_i^z = 1 - 2c_i^\dagger c_i, \tag{5.5}$$

where the canonical fermion operator c_i annihilates a fermion on site i and $c_i^\dagger$ creates a fermion on site i.

Equation (5.5) holds for a single site model, but we have additional complications for a model with more than one site since the σ_i^z on different sites commute, whereas the c_i on different sites anticommute. Jordan and Wigner found a solution to this problem by finding a representation that satisfies both on-site and inter-site commutation relations:

$$\hat{\sigma}_i^+ = \frac{1}{2}\left(\hat{\sigma}_i^x + i\hat{\sigma}_i^y\right) = \left[\prod_{j<i}(1-2c_j^\dagger c_j)\right] c_i, \tag{5.6}$$

$$\hat{\sigma}_i^- = \frac{1}{2}\left(\hat{\sigma}_i^x - i\hat{\sigma}_i^y\right) = \left[\prod_{j<i}(1-2c_j^\dagger c_j)\right] c_i^\dagger. \tag{5.7}$$

The additional term corresponds to a series of operators which determines whether the number of occupied sites to the left of a site i is even or odd. It returns a value of 1 if there is an even number of occupied sites to the left of site i and -1 if the number of occupied sites to the left of i is odd. For the transverse field Ising model it is convenient to use a slightly different representation in which the spin axes have been rotated by 90 degrees about the y axis, such that

$$\hat{\sigma}_i^x = 1 - 2c_i^\dagger c_i \qquad \text{and} \tag{5.8}$$

$$\hat{\sigma}_i^z = -\left[\prod_{j<i}(1-2c_j^\dagger c_j)\right](c_i + c_i^\dagger). \tag{5.9}$$

We insert these expressions into the Hamiltonian given in (5.1) and rewrite it as

$$\mathcal{H} = -J \sum_i \left(c_i^\dagger c_{i+1} + c_{i+1}^\dagger c_i + c_i^\dagger c_{i+1}^\dagger + c_{i+1} c_i - 2g c_i^\dagger c_i + g \right). \tag{5.10}$$

Some terms in this Hamiltonian, such as $c_{i+1}c_i$, violate the fermion number conservation. This means that spins can be flipped and eigenstates of $\mathcal{H}$ do not have a definite fermion number. In order to diagonalise $\mathcal{H}$, we use the momentum eigenstates

$$c_k = \frac{1}{\sqrt{N}} \sum_j c_j e^{-ikj}, \tag{5.11}$$

where we choose the lattice spacing to be equal to 1 and N is the number of sites, as usual. We then get

$$\mathcal{H} = J \sum_k \left(2\left[g - \cos k \right] c_k^\dagger c_k - i \sin k \left[c_{-k}^\dagger c_k^\dagger + c_{-k} c_k \right] - g \right). \tag{5.12}$$

Finally, we want to transform these into a set of Bogoliubov operators with conserved quasi-particle number. We define these operators to be

$$\gamma_k = u_k c_k - i v_k c_{-k}^\dagger, \tag{5.13}$$

with $u_k^2 + v_k^2 = 1$, $u_{-k} = u_k$ and $v_{-k} = -v_k$. It can be shown that the γ_k have the same anticommutation relations as the c_k. We can also write down the inverse mapping such that

$$c_k = u_k \gamma_k + i v_k \gamma_{-k}^\dagger. \tag{5.14}$$

The expression (5.14) for c_k can then be inserted into (5.12). Additionally, we impose that $\mathcal{H}$ mustn't contain any terms that violate the number conservation of the γ fermions, such as $\gamma_k \gamma_{-k}$. We can do this by appropriately choosing the still undefined constants u_k and v_k. A choice that allows for number conservation for the γ fermions is $u_k = \cos(\theta_k/2)$ and $v_k = \sin(\theta_k/2)$ with

$$\tan\theta_k = \frac{\sin k}{\cos k - g}. \tag{5.15}$$

$\mathcal{H}$ then reduces to

$$\mathcal{H} = \sum_k \epsilon_k \left(\gamma_k^\dagger \gamma_k - \frac{1}{2} \right), \tag{5.16}$$

where

$$\epsilon_k = 2J \left(1 + g^2 - 2g \cos k \right)^{1/2}. \tag{5.17}$$

Here, $\epsilon_k \geq 0$ is the single particle energy of a γ fermion. The Bogoliubov transformation changes the nature of the ground state. The new ground state of $\mathcal{H}$ contains no γ fermions and the excited

states emerge when we occupy the single particle states, whereas the old ground state satisfied $c_k |gs\rangle = 0$. The excited states after the Bogoliubov transformation can be labelled by the number of occupied single γ-particle states with distinct k.

5.2 Bands of zeros

As we have shown in Section 5.1, the Hamiltonian in the continuum limit can be diagonalised to

$$\hat{H} = \frac{L}{2\pi} \int_{-\pi}^{\pi} \epsilon_k \hat{\gamma}_k^\dagger \hat{\gamma}_k \, dk, \tag{5.18}$$

where

$$\begin{aligned} \epsilon_k &= 2J\sqrt{1 - 2g\cos k + g^2} && (5.19)\\ \Rightarrow \quad k &= \arccos\left(\frac{1 + g^2 - \left(\frac{\epsilon}{2J}\right)^2}{2g}\right) && (5.20)\\ &= \arccos\left(\frac{1+g^2}{2g} - \frac{\epsilon^2}{8gJ^2}\right) && (5.21)\\ &\equiv \arccos\left(A - \alpha\right). && (5.22) \end{aligned}$$

From the dispersion relation, we can calculate the density of states

$$\begin{aligned} \frac{dn}{d\epsilon} &= \frac{dn}{dk}\frac{dk}{d\epsilon} && (5.23)\\ &= \frac{dn}{dk}\frac{dk}{d\alpha}\frac{d\alpha}{d\epsilon} && (5.24)\\ &= \frac{2\pi}{N}\frac{\epsilon}{4gJ^2}\frac{1}{\sqrt{1 - \left(\frac{1+g^2}{2g} - \frac{\epsilon^2}{8gJ^2}\right)^2}}. && (5.25) \end{aligned}$$

An example plot of the density of states in ϵ is given in Fig. 5.2. This density of states is singular when

$$\begin{aligned} \frac{\epsilon^2}{8gJ^2} &= \frac{1+g^2}{2g} \pm 1 && (5.26)\\ \Rightarrow \quad \frac{\epsilon}{2J} &= \pm|g \pm 1|. && (5.27) \end{aligned}$$

Here we can discard the negative energy solutions and get the singular points

$$\epsilon = 2J|g \pm 1|. \tag{5.28}$$

This expression is related to the crossover lines in Figure 5.1 in that the crossovers occur when $\epsilon = k_B T = 2J|g \pm 1|$. Let us now assume that N is finite, which means that k is discrete. Then

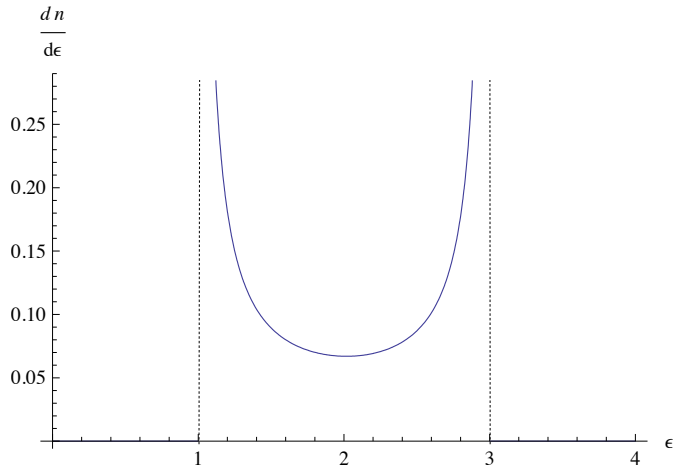

Figure 5.2: Density of states for the case $g = \frac{1}{2}$ and $J = 1$.

the Hamiltonian can be written as

$$\hat{H} = \sum_k \epsilon_k \hat{\gamma}_k^\dagger \hat{\gamma}_k. \tag{5.29}$$

Since we know the energy spectrum, we can calculate the partition function:

$$\begin{aligned} Z &= \sum_{n_1=0}^{1} \sum_{n_2=0}^{1} \cdots \sum_{n_N=0}^{1} e^{-\beta \sum_{j=1}^{N} \epsilon_j n_j} && (5.30)\\ &= \left(\sum_{n_1=0}^{1} e^{-\beta \epsilon_1 n_1} \right) \left(\sum_{n_2=0}^{1} e^{-\beta \epsilon_2 n_2} \right) \cdots \left(\sum_{n_N=0}^{1} e^{-\beta \epsilon_N n_N} \right) && (5.31)\\ &= \left(1 + e^{-\beta \epsilon_1}\right) \cdots \left(1 + e^{-\beta \epsilon_N}\right) && (5.32)\\ &= \prod_{j=1}^{N} \left(1 + e^{-\beta \epsilon_j}\right). && (5.33) \end{aligned}$$

One can easily see that the zeros of this partition function are defined by:

$$\begin{aligned} 1 + e^{-\beta \epsilon_j} &= 0 \qquad \exists j \in \{1, \ldots, N\} && (5.34)\\ \Rightarrow \quad e^{-\beta \epsilon_j} &= -1. && (5.35) \end{aligned}$$

And consequently we get the condition for β:

$$\beta = \frac{i\pi}{\epsilon_j}(2n + 1). \tag{5.36}$$

We can draw two conclusions from this:

- All zeros are purely imaginary in β.
- The zeros form bands with lower limits $\frac{\pi(2n+1)}{\epsilon_{max}}$ and upper limits $\frac{\pi(2n+1)}{\epsilon_{min}}$ on the imaginary axis.

Since there is a direct mapping from the energy bands to the bands of zeros, we can infer the density of zeros from the density of states. We use

$$\Im(\beta) = \beta'' = \frac{\pi}{\epsilon}(2n+1) \tag{5.37}$$

$$= \frac{\pi}{\epsilon} \qquad \text{for the first band.} \tag{5.38}$$

Therefore

$$\frac{dn}{d\beta''} = \frac{dn}{d\epsilon}\frac{d\epsilon}{d\beta''} \tag{5.39}$$

$$= \frac{dn}{d\epsilon}\left(-\frac{\pi}{(\beta'')^2}\right) \tag{5.40}$$

$$= \frac{2\pi}{N}\frac{\pi}{\beta''}\frac{1}{4gJ^2}\frac{1}{\sqrt{1-\left(\frac{1+g^2}{2g}-\frac{\pi^2}{8gJ^2(\beta'')^2}\right)^2}}. \tag{5.41}$$

An example of the shape of the first band of zeros is given in Fig. 5.3.

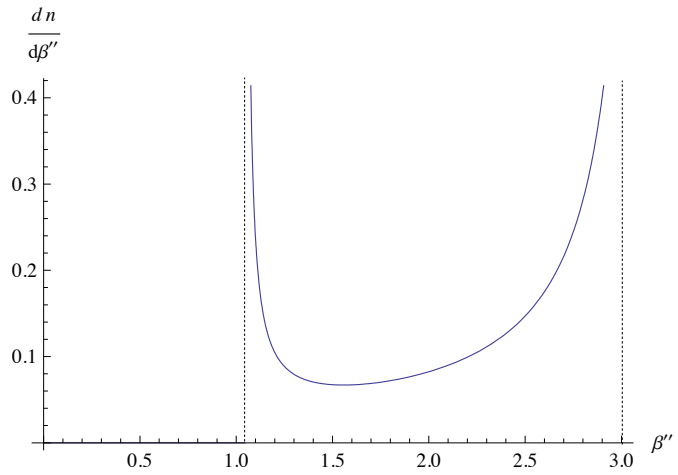

Figure 5.3: Density of zeros for the first band with $g = \frac{1}{2}$ and $J = 1$.

In order to shed more light on the structure of the bands, we calculated under which conditions the bands start to overlap. More precisely, the n^{th} band starts to overlap with the m^{th} band for $m > n$ when

$$\frac{\pi}{\epsilon_{min}}(2n+1) = \frac{\pi}{\epsilon_{max}}(2m+1). \tag{5.42}$$

Since $\epsilon_{min} = g - 1$ and $\epsilon_{max} = g + 1$ (for $g > 1$) we can find the condition for crossing bands in terms of g:

$$g = \frac{n + m + 1}{m - n}. \tag{5.43}$$

A diagram of the crossings of the first few bands is shown in Fig. 5.4.

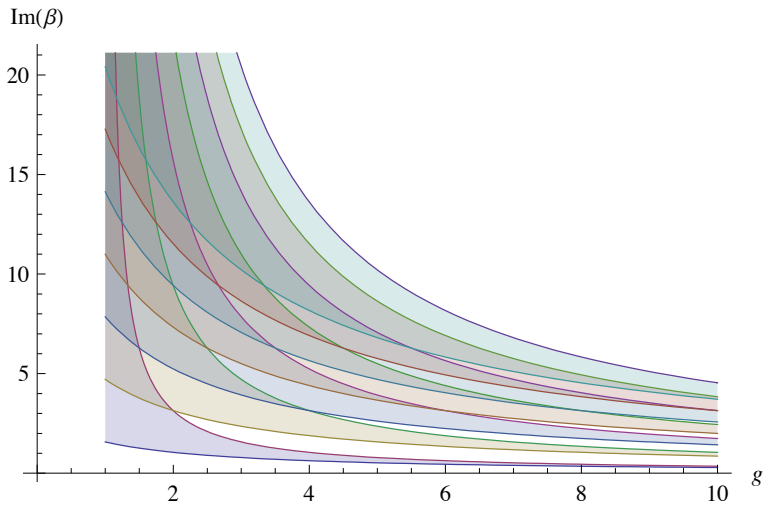

Figure 5.4: Crossings of the first few bands.

We can calculate the density of crossing points between $g = \infty$ and $g = 1+\epsilon$. By rearranging 5.43 we get

$$g - 1 = \frac{2n + 1}{m - n}. \tag{5.44}$$

Looking at the crossing points for the zeroth band with the m^{th} band, we can locate them at

$$g(m) = 1 + \frac{1}{m} \tag{5.45}$$

and calculate the density of crossings:

$$\begin{aligned}
\nu(g) &= \frac{1}{g(m) - g(m+1)} && (5.46)\\
&= \frac{1}{\frac{1}{m} - \frac{1}{m+1}} && (5.47)\\
&= \frac{1}{\frac{m+1-m}{m(m+1)}} && (5.48)\\
&= m(m+1) && (5.49)\\
&\sim m^2 \qquad \text{as } m \to \infty && (5.50)\\
&= (g-1)^{-2}. && (5.51)
\end{aligned}$$

since from (5.45) $g - 1 = \frac{1}{m}$. We are still unsure about how to interpret these partition function zeros. They seem to have a rather different nature than the zeros in the transfer matrix cases and we have no intuition about the impact on the classification of the transition.

Chapter 6

Summary and outlook

In this thesis we have shown that there is density-wave long-range order on and spiral order near the contour of Fisher zeros of the one-dimensional Ising chain. In addition, there is an imaginary "latent heat" associated with crossing that contour (see Chapter 2). These effects remain if we increase the width of the chain and create an Ising ladder (see Chapter 3).

By increasing the width of those ladders, we should be able to see how the contours of zeros approach the thermodynamic limit, i.e. the zeros of the two-dimensional Ising model on a square lattice (see Chapter 3). There seems to be some discrepancy with the results presented in the literature, which is resolved in the way the thermodynamic limit is approached: the results presented in the literature use the partition function *in* the thermodynamic limit in which a lot of the structure that is present as the thermodynamic limit is *approached* can no longer be seen (see Chapter 4). A paper with the results presented in Chapters 2 and 3 is being prepared by myself and my supervisor, Chris Hooley, together with our collaborators Roderich Moessner and Vadim Oganesyan and will hopefully be submitted to Physical Review Letters shortly after the submission of this thesis.

We then move on to calculate the Fisher zeros for frustrated two-dimensional Ising lattices, in particular the triangular and the kagomé lattice (see Chapter 4) as well as the one-dimensional transverse-field Ising model (see Chapter 5). These results are still preliminary since we do not have a suitable interpretation of the results.

If the project continues, it will be interesting to look at the issues that occur when taking the thermodynamic limit more closely, in particular how we can calculate the zeros more consistently. At the moment this is done by taking the partition function in the thermodynamic limit and looking for its zeros on a finite-size lattice.

Another interesting project would be to look at how we can interpret Fisher zeros in models that do not contain sums over the eigenvalues of a transfer matrix, such as in the transverse-field Ising model.

Bibliography

[1] Matthias Vojta. Quantum Phase Transitions. *Rep. Prog. Phys.*, 66:2069, 2003.

[2] R. B. Laughlin, G. G. Lonzarich, P. Monthoux, and David Pines. The Quantum Criticality Conundrum. *Adv. Phys.*, 50:361, 2001.

[3] T.D. Lee and C.N. Yang. Statistical Theory of Equations of State and Phase Transitions. I. theory of Condensation. *Phys. Rev.*, 87(3):404, 1952.

[4] T.D. Lee and C.N. Yang. Statistical Theory of Equations of State and Phase Transitions. II. Lattice Gas and Ising Model. *Phys. Rev.*, 87(3):410, 1952.

[5] F. Mandl. *Statistical Physics*. John Wiley and Sons, 2nd edition, 1988.

[6] H. Eugene Stanley. *Introduction to Phase Transitions and Critical Phenomena*. Oxford University Press, 1971.

[7] Url:. $http://www.its.caltech.edu/\%7eatomic/snowcrystals/ice/h2ophase.gif$. last accessed: 14.04.2009.

[8] R. Kenna, D.A. Johnston, and W. Janke. Scaling Relations for Logarithmic Corrections. *Phys. Rev. Lett.*, 96:115701, 2006.

[9] L. D. Landau. *Collected papers of L.D. Landau*. Oxford: Pergamon Press, 1965.

[10] L. D. Landau and E. M. Lifshitz. *Statistical Physics*, volume 5 of *Course of Theoretical Physics*. Elsevier, 3rd edition, 1980.

[11] Ben Simons. Url: $http://www.tcm.phy.cam.ac.uk/\sim bds10/phase.html$. Lecture notes; last accessed 29.04.2009.

[12] K.G. Wilson. Renormalization Group and Critical Phenomena. I. Renormalization Group and the Kadanoff Scaling Picture. *Phys. Rev. B*, 4:3174, 1971.

[13] J.M. Yeomans. *Statistical Mechanics of Phase Transitions*. Clarendon Press, 1992.

[14] Chris Hooley. Private communication.

[15] L.P. Kadanoff. Notes on Migdal's Recursion Formulas. *Ann. Phys.*, 100:359, 1976.

[16] S. L. Sondhi, S. M. Girvin, J. P. Carini, and D. Shahar. Continuous Quantum Phase Transitions. *Rev. Mod. Phys.*, 69:315, 1997.

[17] L. Zhu, M. Garst, A. Rosch, and Q. Si. Universally Diverging Grüneisen Parameter and the Magnetocaloric Effect Close to Quantum Critical Points. *Phys. Rev. Lett.*, 91:066404, 2003.

[18] J. A. Hertz. Quantum Critical Phenomena. *Phys. Rev. B*, 14:1165, 1976.

[19] S. Chakravarty, B.I. Halperin, and D.R. Nelson. Two-dimensional quantum Heisenberg antiferromagnet at low temperatures. *Phys. Rev. B*, 39:2344, 1989.

[20] A. J. Millis. Effect of a nonzero temperature on quantum critical points in itinerant fermion systems. *Phys. Rev. B*, 48:7183, 1993.

[21] Piers Coleman and Andrew J. Schofield. Quantum Criticality. *Nature*, 433:226, 2005.

[22] D. Belitz, T. R. Kirkpatrick, and Thomas Vojta. Nonanalytic behavior of the spin susceptibility in clean Fermi systems. *Phys. Rev. B*, 55:9452, 1997.

[23] Andrey V. Chubukov and Dmitrii L. Maslov. Nonanalytic corrections to the Fermi-liquid behaviour. *Phys. Rev. B*, 68:155113, 2003.

[24] D. J. W. Geldart and M. Rasolt. Analytical structure of the wave-number-dependent susceptibility of many-fermion systems at low temperature and long wavelength I. *Phys. Rev. B*, 15:1523, 1977.

[25] D. J. W. Geldart and M. Rasolt. Analytical structure of the wave-number-dependent susceptibility of many-fermion systems at low temperature and long wavelength II. *Phys. Rev. B*, 22:4079, 1980.

[26] D. Bitko, T. F. Rosenbaum, and G. Aeppli. Quantum Critical Behaviour for a Model Magnet. *Phys. Rev. Lett.*, 77:940, 1996.

[27] T. Giamarchi, C. Rüegg, and O. Tchernyshyov. Bose-Einstein condensation in magnetic insulators. *Nature Physics*, 4:198, 2008.

[28] Philipp Gegenwart, Qimiao Si, and Frank Steglich. Quantum criticality in heavy-fermion metals. *Nature Physics*, 4:186, March 2008.

[29] Q. Si. Quantum Criticality and Global Phase Diagram of Magnetic Heavy Fermions. *Phys. Status Solidi B*, 247:476, 2010.

[30] G. R. Stewart. Heavy-fermion systems. *Rev. Mod. Phys.*, 56:755, 1984.

[31] D. M. Broun. What lies beneath the dome? *Nature Physics*, 4:170, 2008.

[32] S. V. Kravchenko and M. P. Sarachik. Metal-insulator transition in two-dimensional electron systems. *Rep. Prog. Phys.*, 67:1, 2004.

[33] D. A. Kurtze. *Yang-Lee edge singularities in ferromagnetic systems.* PhD thesis, Cornell University, 1980.

[34] M.E. Fisher. *in: Lectures in Theoretical Physics*, volume VII C. Gordon and Breach, 1964.

[35] T. Asano. Generalization of the Lee-Yang Theorem. *Prog. Theor. Phys.*, 40:1328, 1968.

[36] T. Asano. Generalized Lee-Yang's Theorem. *J. Phys. Soc. Japan*, 25:1220, 1968.

[37] R.B. Griffiths. Rigorous Results for Ising Ferromagnets of Arbitrary Spin. *J. Math. Phys.*, 10:1559, 1969.

[38] M. Suzuki. Theorems on Extended Ising Model with Applications to Dilute Ferromagnetism. *Prog. Theor. Phys.*, 40:1246, 1968.

[39] M. Suzuki. Theorems on the Ising Model with General Spin and Phase Transition. *J. Math. Phys.*, 9:2064, 1968.

[40] O.J. Heilmann. Zeros of the Grand Partition Function for a Lattice Gas. *J. Math. Phys.*, 11:2701, 1970.

[41] D. Ruelle. Some Remarks on the Location of Zeroes of the Partition Function for Lattice Systems. *Commun. math. Phys.*, 31:265, 1973.

[42] M. Suzuki and M. Fisher. Zeros of the Partition Function for the Heisenberg, Ferroelectric and General Ising Models. *J. Math. Phys.*, 12(2):235, 1971.

[43] S. Y. Kim and R. J. Creswick. Fisher zeros of the Q-state Potts model in the complex temperature plane for nonzero external magnetic field. *Phys. Rev. E*, 58:7006, 1998.

[44] M. Biskup, C. Borgs, J. T. Chayes, and R. Kotecký. Partition function zeros at first-order phase transitions: Pirogov-Sinai theory. *J. Stat. Phys.*, 116:97, 2004.

[45] R. G. Ghulghazaryan, K. G. Sargsyan, and N. S. Ananikian. Partition function zeros of the one-dimensional Blume-Capel model in transfer matrix formalism. *Phys. Rev. E*, 76:021104, 2007.

[46] D. Kurtze. The Yang-Lee Edge Singularity in One-Dimensional Ising and N-Vector Models. *J. Stat. Phys.*, 30:15, 1983.

[47] M.E. Fisher. Yang-Lee Edge Singularity and ϕ^3 Field Theory. *Phys. Rev. Lett.*, 40:1610, 1978.

[48] S. Grossmann. *Analytic Properties of Thermodynamic Functions and Phase Transitions*, volume 9 of *Festkörperprobleme*, pages 207–254. Vieweg und Sohn, Braunschweig, 1969.

[49] R. Abe. Critical Behavior of Pair Correlation Function in Ising Ferromagnets. *Prog. Theor. Phys.*, 38:568, 1967.

[50] R. Abe. Logarithmic Singularity of Specific Heat near the Transition Point in the Ising Model. *Prog. Theor. Phys.*, 37:1070, 1967.

[51] R. Abe. Note on the Critical Behavior of Ising Ferromagnets. *Prog. Theor. Phys.*, 38:72, 1967.

[52] R. Abe. Singularity of Specific Heat in the Second Order Phase Transition. *Prog. Theor. Phys.*, 38:322, 1967.

[53] W. Janke and R. Kenna. The Strength of First and Second Order Phase Transitions from Partition Function Zeroes. *J. Stat. Phys.*, 102:1211, 2001.

[54] M.L. Glasser, V. Privman, and L.S. Schulman. Complex-temperature-plane zeros: Scaling theory and multicritical mean-field models. *Phys. Rev. B*, 35:1841, 1987.

[55] M. Suzuki. A Theory on the Critical Behavior of Ferromagnets. *Prog. Theor. Phys.*, 38:289, 1967.

[56] M. Suzuki. A Theory of the Second Order Phase Transitions in Spin Systems. II. *Prog. Theor. Phys.*, 38:1225, 1967.

[57] M. Suzuki. Note on Singularity of Specific Heat in the Second Order Phase Transition. *Prog. Theor. Phys.*, 38:1243, 1967.

[58] W. Janke, D.A. Johnston, and R. Kenna. Critical exponents from general distributions of zeroes. *Computer Physics Communications*, 169:457, 2005.

[59] R. Kenna, D.A. Johnston, and W. Janke. Self-Consistent Scaling Theory for Logarithmic-Correction Exponents. *Phys. Rev. Lett.*, 97:155702, 2006.

[60] M.R. Evans. Phase Transitions in One-Dimensional Nonequilibium Systems. *Brazilian Journal of Physics*, 30:42, 2000.

[61] R.A. Blythe. An introduction to phase transitions in stochastic dynamical systems. *J. Phys.: Conf. Series*, 40:1, 2006.

[62] R.A. Blythe and M.R. Evans. Lee-Yang zeros and Phase Transitions in Nonequilibrium Steady States. *Phys. Rev. Lett.*, 89:08061, 2002.

[63] R.A. Blythe and M.R. Evans. The Lee-Yang Theory of Equilibium and Nonequilibrium Phase Transitions. *Brazilian Journal of Physics*, 33:464, 2003.

[64] C. Flindt and J.P. Garrahan. Trajectory Phase Transitions, Lee-Yang Zeros, and High-Order Cumulants in Full Counting Statistics. *Phys. Rev. Lett.*, 110:050601, 2013.

[65] A. Polkovnikov, K. Sengupta, A. Silva, and M Vengalattore. Colloquium: Nonequilibrium dynamics of closed interacting quantum systems. *Rev. Mod. Phys.*, 83:863, 2011.

[66] M. Greiner, O. Mandel, T. Esslinger, T.W. Hänsch, and I. Bloch. Quantum phase transition from a superfluid to a Mott insulator in a gas of ultracold atoms. *Nature*, 415:39, 2002.

[67] M. Greiner, O. Mandel, T.W. Hänsch, and I. Bloch. Collapse and revival of the matter wave field of a Bose-Einstein condensate. *Nature*, 419:51, 2002.

[68] M. Heyl, A. Polkovnikov, and S. Kehrein. Dynamical Quantum Phase Transitions in the Transvese Field Ising Model. arXiv:1206.2505v2, January 2013.

[69] Wilhelm Lenz. Beitrag zum Verständnis der magnetischen Erscheinungen in festen Körpern. *Phys. ZS.*, 21:613, 1920.

[70] Ernst Ising. Beitrag zur Theorie des Ferromagnetismus. *Z. Phys.*, 31:253, 1925.

[71] T.D Schultz, D.C. Mattis, and E.H. Lieb. Two-Dimensional Ising Model as a Soluble Problem of Many Fermions. *Rev. Mod. Phys.*, 36(3):856, 1964.

[72] M.E. Fisher. On the Dimer Solution of Planar Ising Models. *Journal of Mathematical Physics*, 7(10):1776, 1966.

[73] P.W. Kasteleyn. Dimer Statistics and Phase Transitions. *J. Math. Phys.*, 4:287, 1963.

[74] Lars Onsager. Crystal Statistics. I. A Two-Dimensional Model with an Order-Disorder Transition. *Phys. Rev.*, 65:117, 1944.

[75] S. Beraha and J. Kahane. Is the 4-color Conjecture Almost False. *J. Combin. Theory B*, 27:1, 1979.

[76] S. Beraha, J. Kahane, and N.J. Weiss. Limits of Zeros of Recursively Defined Polynomials. *Proc. Nat. Acad. Sci. USA*, 72:4209, 1975.

[77] S. Beraha, J. Kahane, and N.J. Weiss. *Studies in Foundations and Combinatorics*, volume 1 of *Advances in Mathematics Supplementary Studies*. Academic Press, New York, 1978.

[78] S. Beraha, J. Kahane, and N.J. Weiss. Limits of Chromatic Zeros of Some Families of Maps. *J. Combin. Theory B*, 28:52, 1980.

[79] J. Salas and A. D. Sokal. Transfer Matrices and Partition-Function Zeros for Antiferromagnetic Potts Models. *J. Stat. Phys.*, 135:279, 2009.

[80] Barry M. McCoy. *Advanced Statistical Mechanics*. Oxford University Press, 2010.

[81] H. Nakano and M. Takahashi. Quantum Heisenberg model with long-range ferromagnetic interactions. *Phys. Rev. B*, 50:10331, 1994.

[82] Rudolf Peierls. On Ising's model of ferromagnetism. *Proc. Cambridge Phil. Soc.*, 32:477, 1936.

[83] H.A. Kramers and G.H. Wannier. Statistics of the two-dimensional ferromagnet. Part I. *Phys. Rev.*, 60:252, 1941.

[84] H.A. Kramers and G.H. Wannier. Statistics of the two-dimensional ferromagnet. Part II. *Phys. Rev.*, 60:263, 1941.

[85] P.M. Chaikin and T.C. Lubensky. *Principles of condensed matter physics.* Cambridge University Press, 1995.

[86] P.C. Hohenberg. Existence of Long-Range Order in One and Two Dimensions. *Phys. Rev.*, 158(2):157, 1967.

[87] N.D. Mermin and H. Wagner. Absence of ferromagnetism or antiferromagnetism in one- or two-dimensional isotropic Heisenberg models. *Phys. Rev. Lett.*, 17(22):1133, 1966.

[88] M.E. Fisher. Statistical Mechanics of Dimers on a Plane Lattice. *Phys. Rev.*, 124(6):1664, 1961.

[89] P.W. Kasteleyn. The Statistics of Dimers on a Lattice. *Physica*, 27:1209, 1961.

[90] Buria Kaufman. Crystal Statistics. II. Partition Function Evaluated by Spinor Analysis. *Phys. Rev.*, 76(8):1232, 1949.

[91] Subir Sachdev. *Quantum Phase Transitions.* Cambridge University Press, 1999.

[92] Subir Sachdev. Quantum Criticality: Competing Ground States in Low Dimensions. *Science*, 288:475, 2000.

[93] P. Jordan and E. Wigner. Über das Paulische Äquivalenzverbot. *Z. Phys.*, 47:631, 1928.

[94] E.H. Lieb, T.D Schultz, and D.C. Mattis. Two soluble models of an antiferromagnetic chain. *Ann. Phys.*, 16:407, 1961.

[95] N. N. Bogoliubov. On the theory of superfluidity. *Acad. Sci. USSR J. Phys.*, 11(23), 1947.